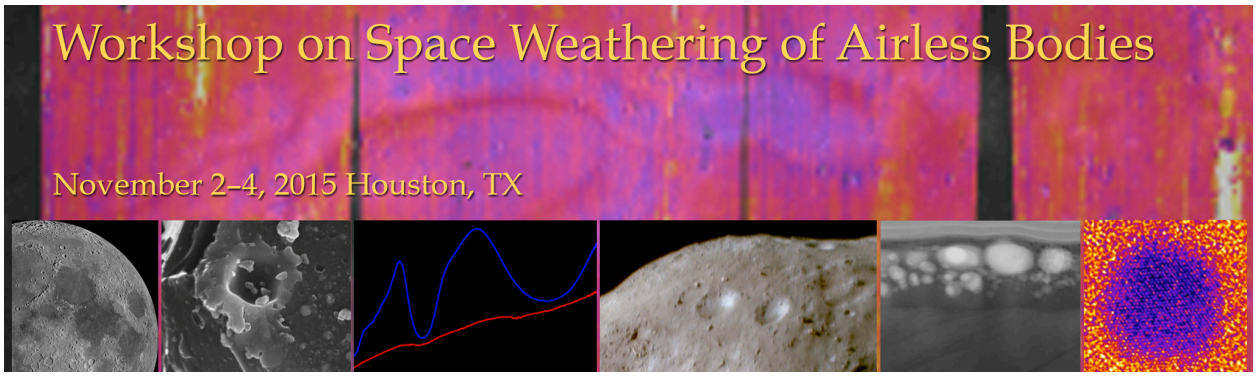

Workshop on
Space Weathering of Airless Bodies

November 2–4, 2015

Program

LPI Contribution No. 1878

LUNAR AND PLANETARY INSTITUTE

USRA

Workshop on Space Weathering of Airless Bodies

November 2–4, 2015 • Houston, Texas

Organizer

Universities Space Research Association

Conveners

Lindsay Keller
NASA Johnson Space Center

Ed Cloutis
University of Winnipeg

Paul Lucey
University of Hawaii

Tim Glotch
Stony Brook University

Scientific Organizing Committee

Lindsay Keller
NASA Johnson Space Center

Ed Cloutis
University of Winnipeg

Paul Lucey
University of Hawaii

Tim Glotch
Stony Brook University

Mark Loeffler
NASA Goddard Space Flight Center

Deborah Domingue
Planetary Science Institute

Roy Christoffersen
Jacobs – NASA Johnson Space Center

Keiko Nakamura Messenger
NASA Johnson Space Center

Sarah Noble
NASA Headquarters

Michelle Thompson
University of Arizona

Abstracts for this workshop are available in electronic format via the workshop website at www.hou.usra.edu/meetings/airlessbodies2015/ and can be cited as Author A. B. and Author C. D. (2015) Title of abstract. In *Workshop on Space Weathering of Airless Bodies,* Abstract #XXXX. LPI Contribution No. 1878, Lunar and Planetary Institute, Houston.

Lunar and Planetary Institute 3600 Bay Area Boulevard Houston TX 77058-1113

Technical Guide to Sessions

Sunday, November 1, 2015

5:00 p.m. – 6:30 p.m.	Great Room	Registration and Reception

Monday, November 2, 2015

8:30 a.m.	Lecture Hall	Moon I
1:30 p.m.	Lecture Hall	Asteroids/Itokawa
5:00 p.m. – 6:30 p.m.	Great Room	Poster Session: Space Weathering of Airless Bodies

Tuesday, November 3, 2015

8:30 a.m.	Lecture Hall	Mercury/Carbonaceous Chondrites Experiments
1:30 p.m.	Lecture Hall	Moon II

Wednesday, November 4, 2015

8:30 a.m.	Lecture Hall	NpFe/Simulants/OuterSS

Program

Monday, November 2, 2015
MOON I
8:30 a.m. Lecture Hall

Chairs: **Lindsay Keller**
Joshua Cahill

8:30 a.m. Pieters C. M. *
The Many Forms of Space Weathering **[#2047]**
Space weathering takes many forms and its alteration products are a direct function of a) location in the solar system, b) composition and texture of the surface, c) mass and magmatic evolution of the body, and d) length of time exposed.

9:00 a.m. Hemingway D. J. * Garrick-Bethell I. Kreslavsky M. A.
Latitudinal Variation in Spectral Properties of the Lunar Maria and Implications for Space Weathering **[#2039]**
The spectral properties of the lunar surface vary systematically with latitude in a way that matches the signature found at lunar swirls. This result could help us to distinguish between the effects of solar wind and micrometeoroid weathering.

9:15 a.m. Jeong M. Kim S. S. Garrick-Bethell I. Park S. M. Sim C. K. * Jin H. Min K. W.
Latitude-Dependence of Median Grain Size in the Lunar Regolith **[#2030]**
We conducted polarimetric observations of the Moon and constructed a grain size map of the lunar regolith. The grain size is found to be larger at higher latitude. This is thought to be a result of reduced space weathering effects at high latitudes.

9:30 a.m. Greenhagen B. T. * Lucey P. G. Song E. Arnold J. A. Lemelin M. Donaldson Hanna K. L. Bowles N. E. Glotch T. D. Paige D. A.
Space Weathering Effects in the Thermal Infrared: Lessons from LRO Diviner **[#2021]**
We quantify the degree to which space weathering affects the thermal infrared Christiansen Feature measured by LRO Diviner, and presents techniques to normalize space weathering effects and enable examination of the underlying composition.

9:45 a.m. Donaldson Hanna K. L. * Bowles N. E. Pieters C. M. Greenhagen B. T. Glotch T. D. Lucey P. G.
Effects of Space Weathering on Thermal Infrared Emissivity Spectra of Bulk Lunar Soils Measured Under Simulated Lunar Conditions **[#2020]**
In this initial study, TIR emissivity spectral measurements are made under lunar-like conditions of two highland soil samples that are similar in composition, but differing maturities to understand the effects of space weathering on TIR spectra.

10:00 a.m. BREAK

10:15 a.m. Cahill J. T. S. * Lawrence D. J. Delen O. Stickle A. Raney R. K. Patterson G. W. Greenhagen B. T.
The Maturely, Immature Orientale Impact Basin **[#2016]**
Examining non-polar highlands regolith maturity from a variety of perspectives.

10:30 a.m. Wang Z. C. Wu Y. Z. Zheng Y. C. Blewett D. T. * Cloutis E. A.
Estimating the Degree of Space Weathering at the Chang'E-3 Landing Site: Radiative-Transfer Modeling of Nanophase Iron Abundance **[#2002]**
Estimating the degree of space weathering at the Chang'E-3 landing site: Radiative-transfer modeling of nanophase iron abundance.

10:45 a.m. Noble S. K. * Keller L. P. Christoffersen R. Rahman Z.
The Microstructure of a Micrometeorite Impact into Lunar Olivine **[#2034]**
Through TEM analysis of the cross-section of a ~20 μm diameter crater into an olivine single crystal we can see first-hand the effects of a single impact, including the creation of nanophase iron in the melt.

11:00 a.m. Thompson M. S. * Zega T. J.
Simulation of Micrometeorite Impacts Through In Situ Dynamic Heating of Lunar Soil **[#2018]**
We simulate micrometeorite impact events using slow and rapid-heating stages inside the TEM. We observe the development of Fe nanoparticles and possible vesiculated textures.

11:15 a.m. Christoffersen R. * Dukes C. A. Keller L. P. Rahman Z. Baragiola R. A.
Problems at the Leading Edge of Space Weathering as Revealed by TEM Combined with Surface Science Techniques **[#2065]**
Analytical field-emission TEM techniques cross-correlated with surface analyses by X-ray photoelectron spectroscopy (XPS) provides a unique two-prong approach for characterizing how solar wind ion processing contributes to space weathering.

11:30 a.m. Keller L. P. * Zhang S.
Rates of Space Weathering in Lunar Soils **[#2056]**
Space weathering effects (both vapor-deposited rims and solar wind amorphized rims) accumulate in 10^6–10^7 y in mature lunar soils based on observed solar flare track densities in individual space-weathered grains.

Monday, November 2, 2015
ASTEROIDS/ITOKAWA
1:30 p.m. Lecture Hall

Chairs: **Roy Christoffersen**
David Blewett

1:30 p.m. Sasaki S. * Okazaki M. Hiroi T. Tsuchiyama A. Miyake A. Matsumoto T.
Space Weathering: From Itokawa to Mercury via the Moon **[#2055]**
A small S-type asteroid Itokawa provided new aspects on space weathering, which are confirmed by experiments using pulse laser. Rocky surface could be weathered as regolith and sulfur would be another key element especially on Mercury.

1:45 p.m. Tsuchiyama A. * Matsumoto T. Uesugi M. Yada T. Shimada A.
Sakurama T. Kadokawa T.
Space Weathering on Itokawa Surface Deduced from Shape and Surface Features of Hayabusa Regolith Particles **[#2046]**
Examination of shape and surface features of Itokawa particles showed that space-weathered rims developed on individual particle surfaces promoted spectral change of Itokawa, while mechanical abrasion and fragmentation suppressed the spectral change.

2:00 p.m. Keller L. P. Berger E. L. * Christoffersen R.
Surface Exposure Ages of Space-Weathered Grains from Asteroid 25143 Itokawa **[#2044]**
The presence of track gradients in the three Hayabusa particles indicates that the regolith in the Muses-C region on Itokawa was relatively stable at mm to cm-depths for the last ~10^5 years, implying little overturn.

2:15 p.m. Matsumoto T. * Tsuchiyama A. Watanabe N. Yasuda K. Miyake A. Nakauchi Y. Okada T.
Abe M. Yada T. Uesugi M. Karouji Y. Nakato A.
Hashiguschi M. Kumagai K.
Systematic Ion Irradiation Experiments to Olivine: Comparison with Space Weathered Rims of Itokawa Regolith Particles **[#2045]**
We performed H and He ion irradiation experiments using olivine fragments, in order to reveal formation time-scales of space weathered rims and formation processes of blisters by solar wind irradiation.

2:30 p.m. Loeffler M. J. * Dukes C. A. Christoffersen R. Baragiola R. A.
Space Weathering of Silicates Simulated by Laser Irradiation **[#2023]**
We present our results from experiments where we have laser irradiated pressed pellets of SiO_2 and two different olivine compositions (Fo_{90} and Fo_{99+}), while monitoring our samples with reflectance and photoelectron spectroscopy.

2:45 p.m. Christoffersen R. * Loeffler M. J. Dukes C. A. Baragiola R. A.
Compositional and Microstructural Evolution of Olivine During Pulsed Laser Irradiation: Insights Based on a FIB/Field-Emission TEM Study **[#2051]**
Field-emission TEM shows multi-layer vapor and melt deposits produced on olivine by pulsed laser irradiation contain abundant nanophase metallic Fe and have some microstructural similarities to melt deposits in micrometeorite impact craters.

3:00 p.m. BREAK

3:15 p.m. Vilas F. * Hendrix A. R.
Seeking Evidence in UV/Blue Reflectance Spectra for Differences in Submicroscopic Iron Created by Space Weathering on Particles from S-Complex Asteroids and the Moon **[#2042]**
Does the UV/blue/Spectrum change with different/Nanophase iron?

3:30 p.m. Blewett D. T. * Denevi B. W. Le Corre L. Reddy V. Schroder S. E. Pieters C. M. Tosi F. Zambon F. De Sanctis M. C. Ammannito E. Roatsch T. Raymond C. A. Russell C. T.
Modeling and Observations of Optical Space Weathering on Vesta **[#2004]**
We use Hapke model spectra to predict the effects of lunar-style space weathering on Vesta, contrast with the effects of mixing with carbonaceous-chondrite material, and to guide interpretation of Dawn multispectral observations of Vesta.

3:45 p.m. Kohout T. * Malina O. Penttilä A. Kröger A. Britt D. Filip J. Muinonen K. Zboril R.
Space Weathering Induced Slope Changes in Pyroxene and Howardite Spectra **[#2022]**
Space weathering laboratory simulations with pyroxene and howardite show lack of reddening over 1 μm region similarly as observed on Vesta. Thus DAWN observations do not contradict space weathering mechanism driven by the presence of $npFe^0$.

4:00 p.m. Stojic A. N. * Pavlov S. G. Markus A. K. Weber I. Morlok A. Hiesinger H.
Experimental Space Weathering: A Coordinated LIBS, TEM, VIS, and NIR/MIR Study **[#2019]**
We pursue an experimental approach simulating space weathering by irradiating analog material and subsequently investigating the altered areas by means of Transmission Electron Microscopy, VIS/NIR, and MIR spectral measurements.

4:15 p.m. Yang Y. Z. * Yuan Y. Wang Z. W. Zhang H. Jin W. D. Hsu W. B.
Mid-Infrared Reflectance Spectra of Pulsed Laser Irradiated Olivine Grains **[#2013]**
To understand the effects of space weathering processes on VNIR and MIR reflectance spectra, we carried out pulsed laser irradiation simulations and reflectance spectroscopic measurements of olivine grains.

4:30 p.m. Libourel G. * Delbo M. Wilkerson J. Ganino C. Michel P.
Effects of Solar Heating on Asteroids **[#2005]**
We will describe laboratory experiments and numerical modelling devoted to study under which conditions solar heating may alter asteroid surfaces.

4:45 p.m. DISCUSSION

Monday, November 2, 2015
POSTER SESSION: SPACE WEATHERING OF AIRLESS BODIES
5:00 p.m. Great Room

Savin D. W. Domingue D. L. Miller K. A.
A Proposed Apparatus to Study the Impact of Solar Wind Ions on the Surfaces of Mercury, the Moon, and Asteroids **[#2007]**
We propose to construct a unique instrument to study the effects of solar wind ion irradiation on the regolith surfaces of Mercury, the Moon, and asteroids. Our approach will overcome many of the limitations of past work.

Yesiltas M. Thieme J. Simos N. Glotch T. D.
Simulation of Space Weathering: Instrumentational Development **[#2012]**
We are designing a series of experiments in order to simulate space weathering in the laboratory and measure its effects on astronomically relevant samples.

Cintala M. J. Keller L. P. Christoffersen R. Hörz F.
Space Weathering in Houston: A Role for the Experimental Impact Laboratory at JSC **[#2061]**
In the highly multidisciplinary field of space weathering, experimentation often is the only means of collecting hard information. The Experimental Impact Laboratory at JSC is capable of supporting a wide array of relevant impact investigations.

Vance A. M. Christoffersen R. Keller L. P.
Evolution of Shock Melt Compositions in Lunar Agglutinates **[#2064]**
A novel compositional spectrum imaging technique reveals the presence of an anomalous Fe-rich component in the shock melt glass matrix in lunar agglutinates.

Malina O. Kohout T. Tucek J. Filip J. Britt D. Zboril R.
Methodology of Space Weathering Simulation and Its Application on Olivine and Pyroxene Samples **[#2029]**
We reported here a new two-step thermal treatment method for the simulation of space weathering process in laboratory. The two-step synthesis method has been used for two different materials (olivine and pyroxene) and spectral changes were compared.

Corley L. M. Gillis-Davis J. J. Lucey P. G.
Comparison of the Temperature Effects on Reflectance Spectra of Fresh and Experimentally Space Weathered Olivine **[#2067]**
Reflectance spectra of fresh and laser irradiated olivine are measured at temperatures between 100–255 K to determine if an anticorrelation between temperature and reflectance in LOLA data is due to the influence of temperature on space weathering.

Esposito V. J. Farrell W. M. Zimmerman M. I.
Solar Wind Hydrogen Implantation and Diffusion in Defect-Rich Regolith on the Moon **[#2038]**
We examine the correlation of retained solar wind hydrogen with crystal defects in the top 100 nm of material.

Wilson J. K. Schwadron N. Jordan A. P. Spence H. E. Looper M. D. Townsend L. W.
Shallow Lunar Hydrogen and Forward-Scattered Albedo Protons **[#2015]**
The CRaTER instrument sees a ~40% higher flux of lunar albedo protons (>65 MeV) at grazing angles compared to the nadir direction. A shallow layer (<10 cm) of hydrated lunar regolith may enhance the yield of forward-scattered albedo protons.

Sim C. K. Kim S. S. Jeong M.
Maturity of the Crater Rim Walls as a Function of the Crater Size **[#2024]**
The median grain size <d> retrieved from ground-based polarimetry and optical maturity (OMAT) of the interior rim walls of ~140 craters of various size. We discuss the relationship between maturation rate and crater size.

Retherford K. D. Liu Y. Hendrix A. R. Greathouse T. K. Gladstone G. R. Mandt K. E. Patrick E. L. Egan A. F. Kaufmann D. E. Hurley D. M. Cahill J. T. S. Pryor W. R.
Lunar Reconnaissance Orbiter LAMP Investigations of Space Weathering **[#2070]**
LRO-LAMP far-UV lunar reflectance measurements are strongly diagnostic of space weathering effects within the top 50–100 nm of the surface.

Penttilä A. Kohout T.
Online Spectral Fit Tool for Analyzing Reflectance Spectra **[#2054]**
The Online Spectral Fit Tool is developed for analyzing Vis-NIR spectral behavior of asteroids and meteorites. Implementation is done using JavaScript/HTML. Fitted spectra consist of spline continuum and gamma distributions for absorption bands.

Kim I. H. Jeong M. S. Sim C. K. Baek K. H. Kim S. S.
Multi-Band Polarimetry of Lunar Regolith Materials in Laboratory **[#2025]**
To understand the polarization characteristics of the lunar regolith, we have carried out multi-band (U, B, V, and R) polarimetric measurements. Powders of SiO_2, Fe_2O_3, Al_2O_3, CaO that are found in the lunar regolith and JSC-1A were considered.

MacLennan E. M. Emery J. P. Lucas M. P. Pinilla-Alonso N.
Assessment and Characterization of Space Weathering Styles on Asteroid Surfaces **[#2033]**
We present preliminary results of a new project aimed at searching for and characterizing differing styles of space weathering among S-complex asteroids and quantifying the dependence on solar wind exposure, grain size, mineralogy, and surface age.

Clark B. E. Barucci M. A. Merlin F. Lantz C. Campins H. Fornasier S. Dotto E. Lauretta D. S.
How to Map Space Weathering on an Asteroid Surface **[#2036]**
Our OSIRIS-REx space weathering map of asteroid 101955 Bennu will be an expression of the probability that each surface facet exhibits space weathering. To each surface facet, we will assign a ranking in: slope, band depth, albedo, and context.

Schriver D. Travnicek P. Domingue D. Helbert J.
Precipitation of Electrons at Mercury's Surface from the Magnetosphere **[#2040]**
Results from a global kinetic simulation of Mercury's magnetosphere will be presented to describe the properties of electron precipitation at Mercury's surface which can result in space weathering of the regolith.

Tuesday, November 3, 2015
MERCURY/CARBONACEOUS CHONDRITES EXPERIMENTS
8:30 a.m. Lecture Hall

Chairs: **Deborah Domingue**
Heather Kaluna

8:30 a.m. Domingue D. L. * Schirver D. Trávní?ek P. M. Helbert J.
Mercury's Weather-Beaten Surface: An Examination of the Relevant Processes Through Comparisons and Contrasts with the Moon and Asteroids **[#2028]**
We examine global color properties of Mercury and their correlations to the predicted trends due to particle bombardment and thermal processing. Color ratio and spectral slope analyzes are interpreted relative to lunar and asteroid studies.

9:00 a.m. Gillis-Davis J. J. * Kaluna H. M. Bradley J. P. Ishii H. A. Lucey P. G.
Darkening of Mercury's Surface by Sulfides and Carbon **[#2041]**
We report on sulfur/sulfide and carbon-bearing composition related spectral effects for materials that have experienced identical simulated space-weathering conditions.

9:15 a.m. Lucey P. G. * Trang D. Kaluna H. M. Lemelin M. T. Gillis-Davis J. Glotch T. Blewett D. T.
Quantitative Modeling of the Optical Effects of Space Weathering **[#2008]**
Models of the optical effects of space weathering are used to derive the abundance of space weathering products.

9:30 a.m. Trang D. * Lucey P. G. Izenberg N. R.
Radiative Transfer Modeling of MESSENGER VIRS Spectra of Mercury: Detection and Mapping of Submicroscopic Iron and Carbon **[#2043]**
We produced maps of the distribution of nanophase iron, nanophase carbon, and microphase iron on the surface of Mercury.

9:45 a.m. Stockstill-Cahill K. R. * Domingue D. L. Cahill J. T. S.
Radiative Transfer Modeling of Near-Infrared Reflectance Data of Airless Planetary Bodies **[#2048]**
We are adapting algorithms developed for the radiative transfer theory of Hapke for application to a broader scope of airless planetary bodies.

10:00 a.m. BREAK

10:15 a.m. Kaluna H. M. * Gillis-Davis J. J. Lucey P. G. Masiero J. R. Meech K. J.
Space Weathering Trends Among Carbonaceous Asteroids and Materials **[#2009]**
We combine observations and experiments to gain a comprehensive view of space weathering trends among carbonaceous asteroids and materials. Our data suggest space weathering trends may allow us to probe the aqueous histories of C-complex asteroids.

10:30 a.m. Lantz C. * Brunetto R. Barucci M. A.
Space Weathering on Primitive Asteroids: Ion Irradiation of Carbonaceous Chondrites **[#2003]**
We simulate space weathering processes on primitive bodies using ion implantation as a simulation of solar wind irradiation. The laboratory analogs we irradiate and analyze with visible to mid-infrared spectroscopy are carbonaceous chondrites.

10:45 a.m. Dukes C. A. * Fulvio D. Baragiola R. A.
Ion-Irradiation Induced Changes in the Surface Composition of Carbonaceous Meteorites **[#2063]**
The effect of weathering on carbonaceous materials remains ambiguous. In this work, we examine in detail the alterations in surface chemistry that result from ion impact on carbonaceous meteorites which accompany the changes in optical reflectance.

11:00 a.m. Keller L. P. * Christoffersen R. Dukes C. A. Baragiola R. A. Rahman Z.
Experimental Space Weathering of Carbonaceous Chondrite Matrix **[#2010]**
Helium ion irradiation of Murchison matrix resulted in amorphization of the matrix phyllosilicates, loss of OH, surface vesiculation, and a significant reduction of the Fe^{3+}/Fe^{2+} ratio in fine-grained phyllosilicates.

11:15 a.m. Helbert J. * Maturilli A. Ferrari S.
Laboratory Studies of Thermal Space Weathering on Airless Bodies **[#2001]**
Thermal space weathering can produce reversible as well as irreversible changes and acts on much shorter timescales than "traditional space weathering." We are going to present a number of examples of thermal space weathering measured at PEL.

11:30 a.m. Orlando T. M. * Fiege K. Bennett C. J. Trieloff M. Srama R.
Space Weathering of Asteroids, Mercury, and the Moon **[#2069]**
We summarize recent laboratory studies on photon, ion, and micrometeorite "weathering" of Mercury and asteroid surface analogs as well as actual lunar regolith samples and present results from linking micrometeorite impacts to energetic irradiation.

Tuesday, November 3, 2015
MOON II
1:30 p.m. Lecture Hall

Chairs: **William Farrell**
Daniel Britt

1:30 p.m. Glotch T. D. * Lucey P. G. Hayne P. O. Bandfield J. L. Greenhagen B. T. Shirley K. A.
Observations of Lunar Swirls by the Diviner Lunar Radiometer **[#2058]**
Diviner observations of lunar swirls show a CF anomaly consistent with abnormal space weathering. Night time cooling and surface roughness models indicate that the finely structured lunar regolith has not been disturbed at swirls.

1:45 p.m. Kramer G. Y. *
Space Weathering Effects in the Visible-IR Dominated by Solar Wind at Earth-Moon Distance **[#2068]**
Which of you changes/Airless body surfaces?/"Aye, it is I", said the Sun.

2:00 p.m. Farrell W. M. * Hurley D. M. Esposito V. J. Loeffler M. J. McLain J. L. Orlando T. M. Hudson R. L. Killen R. M. Zimmerman M. I.
The Role of Crystal Defects in the Retention of Volatiles at Airless Bodies **[#2037]**
The nature of defects in the crystal determines the retention properties of volatiles, like solar wind-implanted hydrogen.

2:15 p.m. McLain J. L. * Sarantos M. Johnson N. M. Keller J. W. Nuth J. A. Farrell W. M.
Thermal Desorption Kinetics of Volatiles on Silicate "Smokes:" Analog to Micrometeoric Impact Vapor Condensates **[#2053]**
Laboratory measurements of the thermal desorption kinetics of Ar, H_2O and other common lunar volatiles on silicate smokes will be presented, with a focus on comparing the desorption energies and surface chemistry with other regolith analogs.

2:30 p.m. Kuhlman K. R. * Kvit A. V. Baba K. Poplawsky J. D. Hiroi T. Isheim D.
Correlative Microscopy and Visible/Near-Infrared Spectral Analysis of Simulated Solar Wind Implanted Olivine **[#2060]**
Here we present the results of the first atom probe tomography (APT) and scanning transmission electron microscopy study (STEM) of San Carlos olivine (Fo90.1) exposed to simulated solar wind-based space weathering due to hydrogen (~1keV/amu).

2:45 p.m. Jordan A. P. * Wilson J. K. Stubbs T. J. Izenberg N. R. Schwadron N. A. Spence H. E.
The Space Weathering Implications of Dielectric Breakdown in Lunar Polar Regolith **[#2014]**
Solar energetic particles may cause dielectric breakdown in the lunar polar regolith. This breakdown weathering may significantly affect the regolith and may occur on other airless bodies in the solar system.

3:00 p.m. BREAK

3:15 p.m. Spence H. E. * Schwadron N. A. Wilson J. K. Jordan A. P. Winslow R. Joyce C. Looper M. D. Case A. W. Stubbs T. J. Zeitlin C. Blake J. B. Kasper J. C. Mazur J. E. Smith S. S. Townsend L. W.
Particle Radiation Environments and Their Effects at Planetary Surfaces of Airless Bodies: Remote Sensing Lessons Learned at the Moon by LRO/CRaTER and Extension to Other Planetary Objects **[#2006]**
We summarize the physics of GCR and SEP interactions with the Moon's surface and quantify how these same processes operate at similar airless objects throughout the solar system, including at Mercury, Mars' moons, asteroids, and the Pluto system.

3:30 p.m. Wetteland C. J. * Sickafus K. E. McSween H. Y. Jr. Taylor L. A.
The Earliest Solar System Weathering: Mega-Solar-Wind Effects in Early Solar System Silicates **[#2027]**
Early solar materials may be exposed to large fluxes of high-energy protons during stellar evolution. Experimental results indicate that small fragments of minerals may be melted, and low Z atoms can be transmuted to exotic isotopes.

3:45 p.m. Wang X. * Schwan J. Hsu H. W. Horanyi M.
Laboratory Investigations of Electrostatic Dust Transport on Airless Bodies and Its Effects on Space Weathering **[#2031]**
We present new laboratory experimental results of electrostatic dust transport and its mechanisms, and discuss its possible effects on the space weathering on the surface of airless bodies.

4:00 p.m. Britt D. T. * Schelling P. K. Blair R.
The Chemistry and Physics of Space Weathering **[#2057]**
Local chemistry and the nature of the energy input drive space weathering. Weathering products are not random, but the predictable outcome of reactions that depend on chemical feedstock, mineral kinetics, catalytic components, and energetic inputs.

4:15 p.m. Blair R. G. * Schelling P. K. Britt D. T.
Aspects of Space Weathering via Mechanically Initiated Chemistry **[#2059]**
The high energies or transient pressures developed during an impact event can open up reaction pathways that are not accessible at standard conditions. Reactive intermediates bind and transform surfaces producing weathering and redox chemistry.

4:30 p.m. DISCUSSION

Wednesday, November 4, 2015
NPFE/SIMULANTS/OUTERSS
8:30 a.m. Lecture Hall

Chairs: **Michelle Thompson**
Charles Hibbitts

8:30 a.m. Cahill J. T. S. * Blewett D. T. Nguyen N. V. Lawrence S. J. Denevi B. W.
Optical Constants of Iron and Nickel Metal from the Far-Ultraviolet to the Near-Infrared **[#2050]**
New iron and nickel far-ultraviolet to near-infrared optical constants are reported as well as models demonstrating their utility for modeling of airless bodies.

8:45 a.m. Legett C. IV * Glotch T. D. Lucey P. G.
VNIR Effects of Space Weathering: Modeling Strong Absorbers in a Scattering Matrix **[#2071]**
We use the Multiple Sphere T-Matrix Model to examine a shift from darkening and reddening to just darkening of VNIR spectra of space weathered material. We will also present laboratory work using aerogel in combination with iron and carbon powders.

9:00 a.m. Hendrix A. R. * Vilas F. Retherford K. D. Mandt K. E. Greathouse T. K. Cahill J. T. S.
Lunar Space Weathering Effects in the Ultraviolet **[#2049]**
Ultraviolet/Observations of the Moon/Weathering effects!

9:15 a.m. Thompson M. S. * Zega T. J. Keane J. T. Becerra P. Byrne S.
The Oxidation State of Nanophase Fe Particles in Lunar Soil: Implications for Space Weathering **[#2017]**
The oxidation state of individual Fe nanoparticles is measured using electron energy-loss spectroscopy. The results indicate increasing oxidation state with increasing soil maturity.

9:30 a.m. Burgess K. D. * Stroud R. M. Dyar M. D. McCanta M. C.
Understanding Space Weathered Material Using STEM-EELS: Fe Oxidation State Measurements **[#2011]**
Measurements of Fe oxidation state using EELS in an aberration-corrected STEM show that experimental silicate glasses are heterogeneous at sub-micron spatial scales. Similar measurements on lunar soils will analyze oxidation states of npFe grains.

9:45 a.m. Penttilä A. * Väisänen T. Kohout T. Muinonen K.
Explaining Space-Weathering Effects on Spectra with Light-Scattering Simulations **[#2035]**
Space-weathering introduces changes to spectra of asteroid surfaces. We study these changes with controlled samples and laboratory measurements of the spectra. Measurements are modeled and explained using light-scattering theory and simulations.

10:00 a.m. BREAK

10:15 a.m. Taylor L. A. * Pieters C. M.
Lunar Soil Simulants Cannot Reproduce Apollo Lunar Soils with Many Space Weathering Products **[#2032]**
Apollo lunar samples are not available for most In-Situ Resource Utilization (ISRU) studies. Therefore, there have been many lunar soil simulants produced that are inadequate, but not appreciated as such. We will address this issue.

10:30 a.m. Schelling P. K. * Britt D. T. Quadery A. H. Tucker W. C. Blair R.
Atomic-Scale Modeling and Theory of Space Weathering Processes: Mechanisms and Surface Properties **[#2052]**
We apply atomic-scale simulation to describe space weathering, including point-defect migration and surface properties. Distinct differences are reported between olivine and orthopyroxene. Surface properties including adhesion are described.

10:45 a.m. Poston M. J. * Blacksberg J. Brown M. Carey E. Carlson R. Ehlmann B. L. Eiler J. Hand K. Hodyss R. Mahjoub A. Wong I.
Visible and Infrared Spectra of Weathered Solar System Ices **[#2066]**
Laboratory simulation of the weathering experienced by an icy object starting in the Kuiper Belt and migrating to the Trojan cloud.

11:00 a.m. Hibbitts C. A. * Paranicas C.
Space Weathering of the Non-Ice Material on Europa **[#2062]**
The Jovian magnetosphere will alter the non-ice material on the surface of Europa in many ways. Although the drivers of that alteration are known, the nature of that alteration is not well understood and should be characterized in the laboratory.

11:15 a.m. Scipioni F. * Schenk P. Tosi F.
Space Weather in the Saturn System **[#2026]**
We analyze the effect of space weather acting on the Saturn satellites Mimas, Enceladus, Tethys, Dione, and Rhea from the spectroscopic point of view. We will show results from the analysis of spectra returned by VIMS instrument onboard Cassini.

NOTES

CONTENTS

ASPECTS OF SPACE WEATHERING VIA MECHANICALLY INITIATED CHEMISTRY R.G. Blair[1], P. K. Schelling[1], and D.T. Britt[1] [1]University of Central Florida Department of Physics, P.O. Box 162385, Orlando FL 32816-2385, Richard.Blair@ucf.edu

Introduction: The weathering of terrestrial minerals is largely dictated by chemical and thermal conditions. In space, weathering chemistry is dictated by surface interactions. Solar or mechanical forces must provide energy to drive these processes. Solar heating may dominate close to the sun, but solar input falls off rapidly and heating becomes minimal at modest distances. Sputtering and macroscopic impacts can both induce chemical weathering. Sputtering produces high energy, low-pressure impacts and macroscopic impacts are lower in energy, but produce much higher transient pressures.

Experimental simulations of sputtering are well established. In the mechanochemical field experimental work involving micrometeorite impacts has lagged behind sputtering investigations due to lack of equipment capable of producing impacts in the desired velocity range (1.0-80 km s^{-1}). Experimental success has been realized in the production impacts by bodies with these velocities.[1] However, the chemical consequences of lower velocity impacts have been largely ignored. These could be from ejecta falling back to a body's surface or low velocity interactions between small airless bodies. At lower impact energies chemical reaction not ionization or vaporization are favored (1.0-90 m s^{-1}). In fact, this energy regime overlaps nicely with conditions produced during mechanochemical reactions. Little overlap exists between the space weathering and mechanochemical communities as well as technological challenges have limited investigations in this area.

Work in the Blair group has sought to bridge disciplinary boundaries for investigation of cross-reaching application of mechanochemistry. We have developed specialized mechanochemical reactors capable of operating from deep vacuum to 10 bar with absolute control of the internal atmosphere, temperature, and energies. For example, carbon monoxide can be easily hydrogenated to a variety of reactive compounds such as formic acid. Under the high transient pressures realized these compounds can interact with mineral surfaces and enhance the weathering. As such a combined chemical and mechanical process can lead to faster and unique weathering under space conditions.

Previous work has shown that mechanical forces applied to minerals similar to those found in asteroids and the moon can produce hydrogen.[2, 3] In addition to hydrogen, reactive intermediates that can form small molecules are present. The high energies or transient pressures developed during an impact event can open up reaction pathways that are not otherwise accessible at standard conditions. Radicals and ionic intermediates chemically bind and transform the surface of the mineral producing weathering and redox chemistry.[4] Additionally, weathering products such as serpentines become highly active in the presence of mechanical force and water or simple alcohols.[5] In order to fully understand weathering in space, the distribution of small molecules, weathering products, and energy input must be known.

References: [1] C.J. Bennett, C. Pirim, T.M. Orlando, Chem. Rev. (Washington, DC, U. S.), 113 (2013) 9086-9150.
[2] J. Kameda, K. Saruwatari, H. Tanaka, F. Tsunomori, Earth Planet Sp, 56 (2004) 1241-1245.
[3] I. Kita, S. Matsuo, H. Wakita, Journal of Geophysical Research: Solid Earth, 87 (1982) 10789-10795.
[4] S. Mohammadnejad, J.L. Provis, J.S.J. van Deventer, Journal of Colloid and Interface Science, 389 (2013) 252-259.
[5] G. Kaupp, CrystEngComm, 11 (2009) 388-403.

MODELING AND OBSERVATIONS OF OPTICAL SPACE WEATHERING ON VESTA. D.T. Blewett[1,*], B.W. Denevi[1], L. Le Corre[2], V. Reddy[2], S.E. Schröder[3], C.M. Pieters[4], F. Tosi[5], F. Zambon[5], M.C. De Sanctis[5], E. Ammannito[5,6], T. Roatsch[3], C.A. Raymond[7], and C.T. Russell[6]. [1]Planetary Exploration Group, Johns Hopkins University Applied Physics Laboratory, Laurel, MD, 20723, USA; [2]Planetary Science Institute, Tucson, USA. [3]Institute of Planetary Research, German Aerospace Center (DLR), Berlin, Germany. [4]Dept. of Earth, Environmental and Planetary Sciences, Brown University, Providence, USA. [5]Istituto di Astrofisica e Planetologia Spaziali, INAF, Rome, Italy. [6]Institute of Geophysics and Planetary Physics, University of California, Los Angeles, USA. [7]Jet Propulsion Laboratory, California Institute of Technology, Pasadena, USA. (*david.blewett@jhuapl.edu)

Introduction: High-reflectance crater rays on the Moon fade with time in response to macroscopic lateral and vertical impact mixing and also because of space weathering, the processes associated with ion and micrometeoroid bombardment of the surface. The well-known optical effects of lunar-style space weathering (LSSW) are a decrease in reflectance, weakening of mineralogical absorption bands, and an increase in reflectance with increasing wavelength ("reddening") [e.g., 1]. These changes in lunar spectra are caused by nanometer- to micrometer-sized blebs and coatings of iron metal (collectively called nanophase iron, $npFe^0$, or submicroscopic metallic iron, SMFe) on and within regolith grains [e.g., 2, 3] resulting from vaporization and reduction of Fe^{2+} in silicates to Fe^0 by ion sputtering or implantation and/or micrometeoroid impacts. Asteroids exhibit a range of space-weathering effects that differ from LSSW. In the case of Vesta, regolith evolution involves darkening and diminished mafic mineral absorption bands without reddening [4]; this is attributed to impact mixing of exogenic carbonaceous chondrite-like material (CC) [e.g., 5, 6]. Vesta's apparent lack of LSSW ($npFe^0$ production) is interesting, because S-type asteroids are thought to undergo reddening linked to solar-wind exposure ([e.g., 7]) and hence production of $npFe^0$ is likely to be taking place on ordinary chondrite asteroids. Questions about the relative importance of ion vs. micrometeoroid bombardment in LSSW also apply to asteroids, so it is important to explore the effects of space weathering in different regions of the Solar System and on bodies of differing composition.

Model Spectra and *Dawn* Data: The goals of this work [8] are to: A) Explore the effects of LSSW in the presence of CC-mixing, using radiative-transfer model spectra computed with Hapke's model [3]. This will help to evaluate the extent to which the presence of low-reflectance material on Vesta could be masking the effects of LSSW. B) Survey space weathering in a wide range of vestan terrains. We employ *Dawn* Framing Camera (FC) multiband image mosaics (seven narrow wavelength bands between 438 and 965 nm) to provide high spatial resolution (pixel dimension of ~60 m), and use spectral parameters as indicators of space weathering style.

Separating LSSW and CC-Mixing: To represent typical vestan material, we constructed model spectra for a howardite mineral assemblage. To evaluate LSSW in such material, $npFe^0$ was added in abundances of zero, 0.1, 0.7, 1.0 and 5.0 parts per thousand (ppt, by weight). Using a spectrum of the Murchison meteorite as the CC component, we next created model spectra with zero, 1, 3 and 5 wt.% CC content, both with and without the five levels of $npFe^0$ abundance.

Spectral parameter plot. A plot of the 438-nm/555-nm ratio vs. the 749-nm reflectance (Fig. 1) shows that the spectral effects of LSSW and CC-mixing can be separated. We use this plot as a guide to evaluate observed trends on Vesta. All cases examined are consistent with CC-mixing or have special circumstances not linked to LSSW. Thus, $npFe^0$ is not detected in our analysis, and its production via space weathering is likely to be extremely limited if not absent on Vesta.

References: [1] E. Fischer and C. Pieters (1994), *Icarus 111*, 475. [2] C. Pieters et al. (2000), *MPS 35*, 1101. [3] B. Hapke (2001), *JGR 106*, 10039. [4] C. Pieters et al. (2012), *Nature 491*, 79. [5] V. Reddy et al. (2012), *Icarus 221*, 544. [6] M.C. De Sanctis et al. (2012), *Ap. J. Lett. 758*, L36. [7] E. Nakamura et al. (2012), *PNAS 109*, E624. [8] D. Blewett et al. (2015) *Icarus*, in revision.

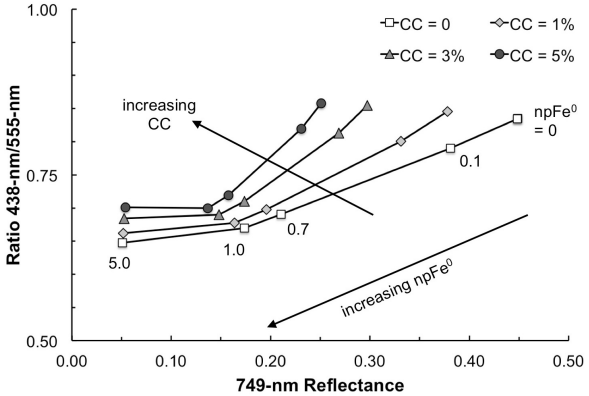

Fig. 1. Visible ratio-reflectance plot for model spectra computed to explore the combined effects of LSSW and CC mixing on howardite material.

THE CHEMISTRY AND PHYSICS OF SPACE WEATHERING. D.T. Britt[1], P. K. Schelling[1], and R. Blair[1]
[1]University of Central Florida Department of Physics, P.O. Box 162385, Orlando FL 32816-2385, britt@physics.ucf.edu.

Introduction: Space weathering is a generic term for the effects on atmosphereless solid bodies in the solar system from a range of processes associated with direct exposure to the space environment. These include impact processes (shock, vaporization, fragmentation, heating, melting, and ejecta formation), radiation damage (from galactic and solar cosmic rays), solar wind effects (irradiation, ion implantation, and sputtering), and the chemical reactions driven by these processes (reduction, formation of carbon compounds, catalysis). The classic example of space weathering is the formation of the lunar spectral red slope associated with the production of nanophase Fe ($npFe^0$) in the dusty lunar regolith [1,2]. Similar $npFe^0$ has been recovered from asteroid 25143 Itokawa and some asteroid classes do exhibit modest spectral red slopes [3]. This impressive array of processes makes it difficult to see the "forest for the trees" in the overall driving forces behind space weathering. What we propose is a simple theory of space weathering

A Conceptual Roadmap for Space Weathering: Space weathering is, in its most basic form, the response of surface materials to: (1) the local chemistry, and (2) energetic inputs. The surfaces of airless bodies can be viewed as a chemical system frozen in disequilibrium with the current surroundings. Extreme vacuum, solar wind implanted hydrogen, extreme low oxygen fugacity, sputtering, radiation damage, generation of catalytic components, and the physical admixture of mutually reactive species provide high potential for reactions. What prevents these reactions from moving forward is the energy required to push these reactants out their current energy well. Weathering occurs when sufficient energy becomes available to initiate reactions. The energy delivery along with the subsequent reactions can occur at any scale, but the scale and intensity of the energy inputs also affect reactions and reaction products.

Another factor in weathering is presence of catalytic materials. A catalytic surface is initiated in the space environment via the production of point-defects and the generation of catalytic species such as $npFe^0$ due to surface reduction. The overall result is to reduce energy barriers for chemical reactions, hence increase the reaction rate with even modest energy inputs. In this picture, weathering encompasses not only physical reaction processes (i.e. sputtering, vapor deposition, and radiation damage), but also chemical reactions that occur due to compositional evolution with relatively modest energy inputs.

Weathering processes and products depend on:

Chemistry:

- The initial chemistry at the surface which is driven by the bedrock mineralogy plus any accreted or implanted materials such as solar wind.
- The evolution of the surface due to space weathering, including point defects, surface reduction, and morphological evolution.
- The presence of an available feedstock of reactive components.

Energy:

- The nature and scale of the energy input. Larger and/or more concentrated energy inputs produce a different array of products and final states.

An example would be the response of olivine to lunar versus asteroidal energy inputs. On average micrometeorite impact velocities on the Moon are over double those of asteroids, so the energy input per micrometeorite impact is over four times greater. The surface chemistry in this narrow case is similar, i.e. olivine in extreme low oxygen fugacity with the highly reducing environment of solar wind implanted hydrogen. On asteroids the lower energy input would heat grains, resulting in the sub-solidus reduction of the grain rims and the production of $npFe^0$ [e.g. 4]. The much higher lunar energy input would tend to vaporize the target material, again producing reduction of the silicates and $npFe^0$, but the form would be as vapor deposited glassy rims because of the higher energy input. The actual weathering pattern of the Moon and most asteroids is complicated by the fundamental mineralogical differences between the feldspar normative lunar materials and olivine normative chondritic materials, but the basic idea is that the surface chemistry and the energy inputs determine the weathering products.

Conclusions: Local chemistry and the nature of the energy input drive weathering, thus determining weathering products. The weathering products are not random, but the predictable outcome of reactions that depend on the chemical feedstock, mineral kinetics, catalytic components, and energetic inputs. The theoretical and experimental tools developed by materials science physics, catalytic chemistry, and mechano-chemistry can provide substantial insight into space weathering.

References: [1] Chapman, C.R. (2004) Annual Review of Earth & Planet. Sci. 32, 539-567. [2] Pieters, C.M., et al. (2000) MAPS 35, 1101-1107. [3] Noguchi, T. (2011) Science 333, 1121-1125. [4] Kohout T. et al. (2015) Workshop on Space Weathering.

UNDERSTANDING SPACE WEATHERED MATERIAL USING STEM-EELS: FE OXIDATION STATE MEASUREMENTS. K. D. Burgess[1], R. M. Stroud[2], M. D. Dyar[3], and M. C. McCanta[4], [1]ASEE Postdoc, Naval Research Laboratory, Washington, DC 20375 USA (kate.burgess.ctr@nrl.navy.mil); [2]Naval Research Laboratory, Washington, DC 20375 USA; [3]Mount Holyoke College, South Hadley, MA 01075 USA; [4]Tufts University, Medford, MA 02155 USA.

Introduction: Space-weathered materials exhibit a wide range of complex nanometer-scale features, such as nanophase iron metal particles (npFe^0) and complex amorphous rims. The amount of space weathered material in a soil is linked to other measures of maturity, such as spectral reddening and darkening [1,2]. Analysis of such materials requires specialized techniques, and the development of electron energy-loss spectroscopy (EELS) in the aberration-corrected scanning transmission electron microscope (STEM) is leading to significant improvement in both the spatial and energy resolution available for the analysis of space-weathered materials. Aberration-corrected STEM has here been used to examine a number of samples with varying Fe^{2+} and Fe^{3+} contents including synthetic silicate glasses, ferriolivine, and high-Ti lunar soils.

Methods: We prepared specimens by microtome, crushing, or focused ion beam (FIB). FIB preparation allows for site-specific analysis to focus on the weathered rims of the lunar samples. To collect EELS and EDS data, we use PRISM, the NION UltraSTEM at the Naval Research Laboratory equipped with a Gatan Enfinium ER EEL spectrometer (0.3 eV energy resolution) and a Bruker SSD-EDS detector. We used a range of conditions including 200 kV and 0.01-1.5 nA.

Results: Fe L-edges in EELS spectra are caused by the excitation of inner shell (2p) electrons to the unoccupied 3d orbitals. EEL spectra of Fe^{2+}- and Fe^{3+}- bearing minerals show distinct edge shapes and chemical shifts that depend on the oxidation state and the symmetry and coordination of the atom site. The well-characterized (e.g., using microprobe, x-ray diffraction, Mössbauer, x-ray absorption spectroscopy) synthetic glass samples were designed to provide end-member datasets for calibrating valence state measurements on samples of interest using "bulk" techniques. However, the experimental glasses were found to be heterogeneous on a sub-micrometer scale (Fig. 1), and spectra from the samples show a large range in oxidation state when quantified using published methods [3,4]. We are able to test for damage to the samples by the electron beam using a range of beam currents and repeated measurements in the same location. We see increasing oxidation with electron dose in many cases, but this does not account for the variability in oxidation state within each sample. Differences in oxidation state in a single region correlated with thickness variations indicate some surface oxidation during sample preparation. EDS data show diffusion of cations other than Si away from regions where the beam dwells for >1 s. Crystalline samples are more resistant to damage, and damage is apparent only at relatively high dose rates.

Lunar soils 71061, 71501, and 79221 are high-Ti mare basalts and range from immature to mature. Recent work by [5] has shown variation in the oxidation state of individual Fe-rich nanoparticles in lunar soils, with more mature soils having more oxidized particles. The soils we will study have all been previously analyzed by the Lunar Soil Characterization Consortium, and our data will be able to add further very-high-resolution understanding of the samples to an existing framework.

References: [1] Keller, L. P., and D. S. McKay (1997) *Geochim Cosmochim Acta, 61*, 2331-2341. [2] Pieters, C. M., et al. (2000) *Meteorit Planet Sci, 35*, 1101-1107. [3] Calvert, C. C., et al. (2005) *J Electron Spectrosc, 143*, 173-187. [4] Van Aken, P., and B. Liebscher (2002) *Phys Chem Mineral, 29*, 188-200. [5] Thompson, M. S., et al. (2015) *LPSC, 46*, Abstract #2932.

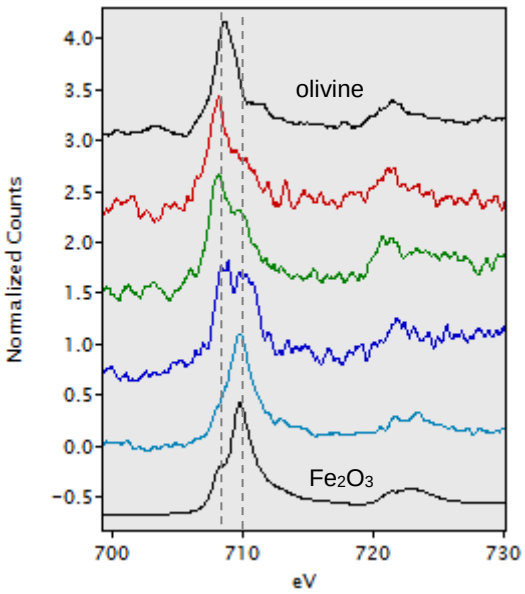

Figure 1. Fe L-edge spectra from IW-basalt3 sample showing variable oxidation state in different sub-micrometer regions in the same sample. San Carlos olivine (all Fe^{2+}) and Fe_2O_3 (all Fe^{3+}) spectra are included for comparison.

OPTICAL CONSTANTS OF IRON AND NICKEL METAL FROM THE FAR-ULTRAVIOLET TO THE NEAR-INFRARED. J.T.S. Cahill[1], D.T. Blewett[1], N.V. Nguyen[2], S.J. Lawrence[3], B.W. Denevi[1]. [1]Johns Hopkins University Applied Physics Laboratory, Laurel, MD, 20723. [2]National Institute of Standards and Technology, Gaithersburg, MD. [3]Arizona State University, Tempe, AZ. (Joshua.Cahill@jhuapl.edu).

Introduction: The opaque metals Fe and Ni, which are also found in nature as Fe,Ni-alloys have lacked for precise accounting during modeling and interpretation of reflectance spectra for airless bodies such as the Moon, Mercury, and asteroids. These metals are often found as native components in meteorites and on planetary surfaces in the form of grains significantly larger than the wavelength of the incident light. However, submicroscopic iron metal grains are also a key by-product of space weathering [1-6] and introduce confounding effects on ultraviolet (UV), visible (VIS), and near-infrared (NIR) spectra as seen in laboratory and spacecraft data for airless bodies (e.g., Clementine, M^3, LRO LAMP & WAC, Kaguya SP, Dawn, Hayabusa, and MESSENGER). Preliminary laboratory evidence has also been presented to suggest that submicroscopic Ni (SMNi) and Fe,Ni (SMFe,Ni) metal could play a role as a space-weathering byproduct [7]. Therefore, knowledge of the optical properties of these metals is necessary for effective spectral characterization and theoretical modeling analysis of mixtures containing these constituents.

The reflectance and absorption of light by a material are governed by the complex index of refraction $n_c = n + ik$; n and k are also known as the optical constants. Measured optical constants of iron [8-11] and nickel [8, 9, 11, 12] are presently available in the literature, however data for both of these metals have various drawbacks with respect to use in planetary reflectance modeling. For example, spectral resolution and range of wavelength coverage are less than ideal, and the extent to which the metals were exposed to the atmosphere is poorly documented. *Cahill et al.* [5] recently obtained new measurements of the optical constants of iron using a novel approach that involved ellipsometric measurement through a fused-silica prism. *Cahill et al.* [5] reported values for the UV, VIS, and a portion of the NIR (~160 to 1700 nm). Use of the prism avoided difficulties related to oxidation of the iron. The presence of a thin layer of iron oxide, not visible to the eye, will significantly alter the optical properties of the iron metal. Oxidation of bare films was found to occur with even modest exposure to the ambient terrestrial atmosphere, minutes to hours [5].

Here we use the same measurement technique and report the optical constants of iron deeper into NIR, as well as new nickel metal optical constants in the UV, VIS, and NIR wavelengths.

Measuring Optical Constants: Our method for measuring optical constants involves vacuum-depositing a high-purity metal film on one surface of a fused-silica prism in an electron-beam evaporator. The measurement of n and k is done within the prism, such that fused silica is the ambient medium. The light interacts only with the "inside" surface of the metal film in contact with the prism, which is not exposed to the atmosphere. For comparison, we also measured the optical constants of bare metal films that were exposed to the atmosphere of the laboratory. Measurements from 160 to 1700 nm were performed for nickel with a variable angle spectroscopic ellipsometer (VASE). We have now made additional measurements with an IR VASE to determine the optical constants to ~3600 nm for both iron and nickel. This long-wavelength limitation is imposed by the transmission of the fused-silica prism.

Use in Radiative-Transfer Models: We have used these new data to simulate varying degrees of space weathering on reflectance spectra for a variety of common airless body minerals and mixtures (olivine, pyroxene, and plagioclase). The modeling was performed using Hapke's equations [3, 13] and accounts for nano-, micro-, and macrophase metal constituents in an approach detailed by [14]. The effect of oxidation of the Fe and Ni film is apparent by the overall lower reflectance of the spectrum computed with the air-exposed optical constants compared to that with the protected (prism) values. This spectral difference between ambient oxidized and unoxidized metal appears to continue to increase with increasing wavelength into the near-infrared; however oxidize metal measurements were not made in the near-infrared.

Preliminary spectral weathering models of 286 mineral assemblages with similar amounts and ratios of nanophase to microphase Fe particles as compared to Ni particles were performed. Results show SMNi to weather the continuum slope of an assemblage more rapidly. However, 1-μm band depth appears to be attenuated at a rate similar to that caused by SMFe.

References: [1] Keller and McKay (1997) GCA, 61, 2331. [2] Pieters et al. (2000) MaPS, 35, 1101. [3] Hapke (2001) JGR, 106, 10039. [4] Noble et al. (2007) Icarus, 192, 629. [5] Cahill et al. (2012) GRL, 39, L10204. [6] Trang et al. (2013) JGR, 118, 708. [7] Gillis-Davis et al. (2015) LPSC, 46, #1607. [8] Johnson and Christy (1974) PR, 9, 5056. [9] Ordal et al. (1985) AO, 24, 4493. [10] Deeter and Sarid (1989) AO, 28, 2911. [11] Paquin, *Handbook of Optics, Volume II,* 1995. [12] Palik, *Handbook of Optical Constants of Solids II*, 1991, 1. [13] Hapke, *Theory of Reflectance and Emittance Spectroscopy*. 2012. [14] Lucey and Riner (2011) Icarus, 212, 451.

THE MATURELY, IMMATURE ORIENTALE IMPACT BASIN. J. T. S. Cahill[1], D. J. Lawrence[1], O. Delen[1], A. Stickle[1], R.K. Raney[2], G.W. Patterson[1], and B.T. Greenhagen[1]. [1]The Johns Hopkins University Applied Physics Laboratory (Joshua.Cahill@jhuapl.edu), [2]Unaffiliated.

Introduction: Lunar surface maturity is consistently examined using the NIR optical maturity parameter (OMAT) [1]. However, the NIR only provides a perspective of the upper microns of the lunar surface. Recent studies of Lunar Prospector (LP) and Lunar Reconnaissance Orbiter data sets are now demonstrating additional measures of maturity with sensitivities to greater depths (~2 m) in the regolith. These include thermal infrared, S-band radar, and epithermal neutron data sets [2-4].

Previous Work: Interestingly, each of these data sets measured parameter or abundance is directly comparable to OMAT despite each measuring slightly different aspects of the regolith. This is demonstrated by *Lawrence et al.* [3] where LP-measured non-polar highlands epithermal neutrons trend well with albedo, OMAT, and the Christensen Feature (CF). *Lawrence et al.* [3] used these data to derive and map highlands hydrogen (H) which is dominantly a function of H-implantation. With this in mind, areas of enriched-H are mature, while areas of depleted H are immature.

Study Presented Here: Surface roughness as measured by S-band radar [4], also provides a measure of maturity. In this case, the circular polarization ratio (CPR) is high when rough and immature, and low when smooth and mature. Knowing this, one can recognize areas in the non-polar lunar highlands that show contradictory measures of maturity. For example, while many lunar localities show consistently immature albedo, OMAT, CF, CPR, and H concentrations (e.g., Tycho), others do not. Orientale basin is the most prominent example, shown to have immature CPR, CF, and H concentrations despite a relatively mature albedo and OMAT values as well as an old age determination (~3.8 Ga; **Figure 1**).

Summary: To better understand how the lunar regolith is weathering in the upper 1-2 m of regolith with time we examine the Orientale basin relative to other non-polar highlands regions (~35 localities).

References: [1] Lucey P.G. et al. (2000) JGR-Planets, 105, 20377-20386. [2] Lucey P.G. et al. (2013) Lunar and Planetary Science Conference, XXXXIV, 2890. [3] Lawrence D.J. et al. (2015) Icarus, j.icarus.2015.01.005. [4] Neish C.D. et al. (2013) Journal of Geophysical Research-Planets, 118, 2247-2261.

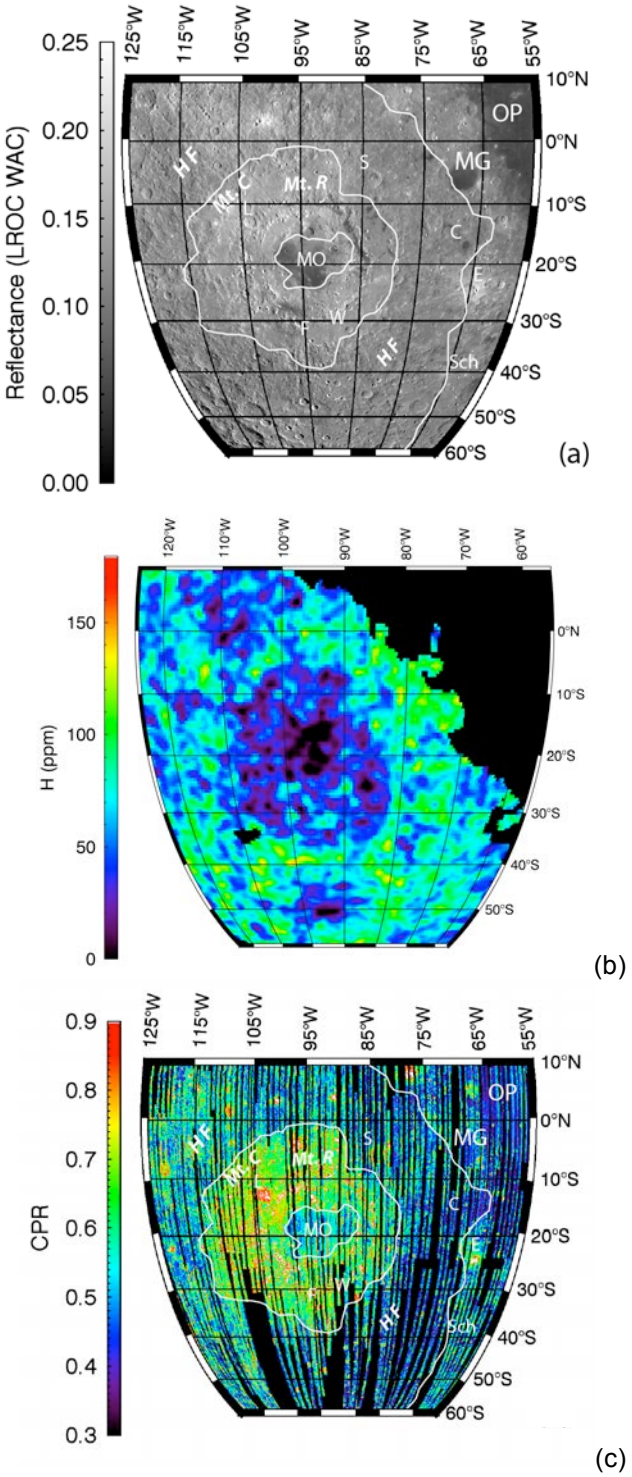

Figure 1*: Orientale impact basin in (a) LROC WAC monochrome, (b) Lunar Prospector derived Hydrogen, and (c) Mini-RF derived CPR maps at 2 ppd.*

PROBLEMS AT THE LEADING EDGE OF SPACE WEATHERING AS REVEALED BY TEM COMBINED WITH SURFACE SCIENCE TECHNIQUES. R. Christoffersen[1], C. A. Dukes[2], L.P. Keller[3], Z. Rahman[1], and R. A. Baragiola[2,†], [1]Jacobs, NASA Johnson Space Center, Mail Code XI, Houston, TX 77058, USA, (roy.christoffersen-1@nasa.gov), [3]NASA JSC, Houston, TX, 77058, USA, [3]University of Virginia, Laboratory of Atomic and Surface Physics, Charlottesville, VA 22904, USA, [†]deceased.

Introduction: Both transmission electron microscopy (TEM) and surface analysis techniques such as X-ray photoelectron spectroscopy (XPS) were instrumental in making the first characterizations of material generated by space weathering in lunar samples [1,2]. Without them, the nature of nanophase metallic Fe ($npFe^0$) correlated with the surface of lunar regolith grains would have taken much longer to become recognized and understood. Our groups at JSC and UVa have been using both techniques in a cross-correlated way to investigate how the solar wind contributes to space weathering [e.g., 3]. These efforts have identified a number of ongoing problems and knowledge gaps. Key insights made by UVa group leader Raul Baragiola during this work are gratefully remembered.

Threshold Fluences for Solid-State Amorphization by the Solar Wind. Early application of TEM to the Apollo samples showed that solar wind ions produced partial to completely amorphous "rims" up to ~150 nm thick on regolith mineral grains [1]. Later TEM work revealed additional layers of vapor or sputter deposited material adding to the complexity of rim formation processes [4]. The width of the ion-processed portions of the rims can be developed as one type of "exposure clock" for measuring how long a given grain has been completely uncovered on the regolith surface [5]. This development, however, is hindered by incomplete experimental calibration of the critical ion fluences for amorphization of key minerals under solar wind irradiation conditions. We will review why past experimental design has played a role in keeping this knowledge gap open.

Depth Evolution of Surface Composition Changes Produced by The Solar Wind: During in-situ ion irradiation under solar wind conditions in the XPS, surface reduction occurs in Fe-bearing silicates and oxides (e.g., ilmenite) [6,7]. This is typically interpreted to occur by the preferential sputtering of oxygen [6]. High-resolution field-emission TEM (FE-STEM) indeed confirms that a layer of surface-correlated $npFe^0$ grains a few nm thick is produced as part of the process [3]. What FE-STEM also shows, however, is that as the outer ~100 nm of some irradiated minerals amorphizes and/or become more ion processed, compositional gradients deepen and become complex to a degree not so easily explained by preferential sputtering alone [7]. In ilmenite in particular, the gradients show a significant resemblance to those in irradiated grain rims on natural lunar ilmenite [8]. Currently, these observations frame a knowledge gap regarding how the solar wind actually creates the integrated thickness of the $npFe^0$-bearing, optically-active layers on space weathered grains over time.

Solar Wind Sputter Erosion. Solar wind sputter erosion can potentially remove layers of space weathered material from grain and rock surfaces. We used XPS in-situ surface analysis, combined with ex-situ FE-STEM, to track changes in microstructure and bulk surface composition of mature lunar mare soil 10084 under step-wise in-situ ion irradiation by 4 kV He^+ and Ar^+ [3]. XPS showed surface major element ratios changing from a unique surface mono-layer composition towards the bulk composition of space weathered grain rims in the soil [3]. FE-STEM found no evidence of sputtering removing or altering existing grain rims in the sample even up to He^+ fluences equivalent lunar surface exposure times of 10^4-10^5 years. The results point to a surface "cleaning" effect of the solar wind, but not to significant sputter erosion of rims over the exposure lifetime of lunar grains.

Solar Wind Sputter Deposition. Solar wind sputter deposition has been proposed to deposit dark optically-active surfaces layers on regolith grains [9]. We repeated the famous "Hapke experiment" [9] using a mm-scale lunar orthopyroxene substrate cantilevered over a homogeneous lunar glass sputtering target [10]. Sputtering by 5 keV Ga^+ ions produced a 70 nm-thick amorphous sputter deposit on the orthopyroxene. FE-STEM analyses show that the deposit is completely amorphous, contains no $npFe^0$, and is compositionally homogeneous with no significant element enrichments/depletions relative to the sputtered source. It does not resemble the $npFe^0$ surface deposits on lunar grain rims, suggesting sputter deposition may not play a significant role in the latter's formation.

References: [1] Dran J. C. et al. (1970) *EPSL* 9, 391. [2] Housley R. M. and Grant R. W. (1975) *Proc. 6th Lunar Sci. Conf.*, 3269. [3] Christoffersen R. et al. (2012) *MAPS Suppl.*, 5341. [4] Keller, L. P. and McKay, D.S. (1997) GCA, 61, 2331. [5] Christoffersen R. et al. (2015) 46th LPSC, #2084 [6] Loeffler, et al. (2009) JGR 114, 3003. [7] Christoffersen R. et al. (2010) 41st LPSC, #2010. [8] Zhang, S. et al. (2010) 41st LPSC, #1432, [9] Hapke B. (2001) JGR, 106(E5), 10039. [10] Christoffersen et al. (2012) 43rd LPSC, #2614.

COMPOSITIONAL AND MICROSTRUCTURAL EVOLUTION OF OLIVINE DURING PULSED LASER IRRADIATION: INSIGHTS BASED ON A FIB/FIELD-EMISSION TEM STUDY

R. Christoffersen[1], M. J. Loeffler[2], C. A. Dukes[3] and R. A. Baragiola[3,†], [1]Jacobs, NASA Johnson Space Center, Mail Code XI, Houston, TX 77058, USA, (roy.christoffersen-1@nasa.gov), [2]NASA GSFC, Greenbelt, MD 20771, USA, [3]University of Virginia, Laboratory of Atomic and Surface Physics, Charlottesville, VA 22904, USA, [†]deceased.

Introduction: The use of pulsed laser irradiation to simulate the short duration, high-energy conditions characteristic of micrometeorite impacts is now an established approach in experimental space weathering studies [1, 2]. The laser generates both melt and vapor deposits that contain nanophase metallic Fe ($npFe^0$) grains with size distributions and optical properties similar to those in natural impact-generated melt and vapor deposits [3]. There remains uncertainty, however, about how well lasers simulate the mechanical work and internal (thermal) energy partitioning that occurs in actual impacts [4]. We are currently engaged in making a direct comparison between the products of laser irradiation and experimental/natural hypervelocity impacts. An initial step reported here is to use analytical TEM is to attain a better understanding of how the microstructure and composition of laser deposits evolve over multiple cycles of pulsed laser irradiation.

Experimental Methods: We irradiated pressed-powder pellets of San Carlos olivine (Fo_{90}) with up to 99 rastered pulses of a GAM ArF excimer laser. The irradiated surface of the sample were characterized by SEM imaging and areas were selected for FIB cross sectioning for TEM study using an FEI Quanta dual-beam electron/focused ion beam instrument. FIB sections were characterized using a JEOL2500SE analytical field-emission scanning transmission electron microscope (FE-STEM) optimized for quantitative element mapping at <10 nm spatial resolutions.

Results: In the SEM the 99 pulse pressed pellet sample shows a complex, inhomogeneous, distribution of laser-generated material, largely concentrated in narrow gaps and larger depressions between grains. Local concentrations of $npFe^0$ spherules 0.1 to 1 μm in size are visible within these deposits in SEM backscatter images. Fig. 1 shows bright-field STEM images of a FIB cross-section of a one of these deposits that continuously covers the top and sloping side of an olivine grain. The deposit has 3 microstructurally distinct sub-layers composed of silicate glass with varying modal fractions and size distributions of $npFe^0$ spherules, along with nanocrystalline silicate material (Fig. 1). A relatively thin (50-300 nm) topmost surface layer has a high-concentration of $npFe^0$ spherules 5-20 nm in size (Fig. 1a). Element mapping shows the layer to be enriched in Fe by a factor of 2.5 relative to the olivine substrate, with Mg and Si depleted by 20% and 10%

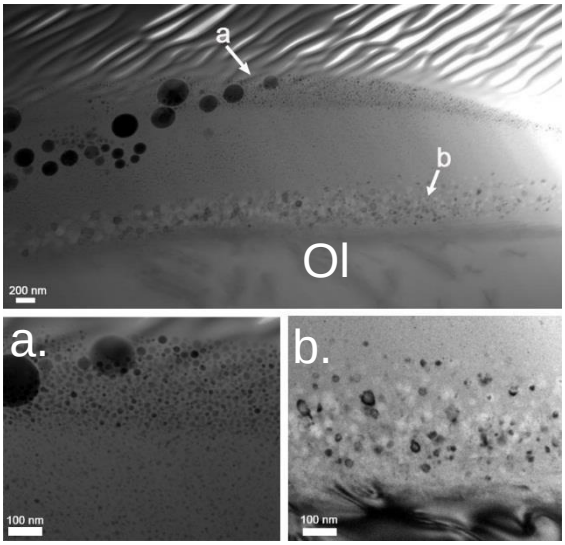

Fig. 1. Bright-field FE-STEM image of layers of laser-deposited material on Fo_{90} olivine grain (Ol).

respectively. This is compositionally complementary to the underlying, middle layer of the deposit that is depleted in Fe, enriched in Mg and has a much lower $npFe^0$ concentration. A third layer of nanocrystalline olivine occurs at the substrate interface.

Discussion: The FE-STEM results suggest the topmost layer is a vapor deposit, underlain by a thicker microstructurally complex melt-generated layer. The compositional relations suggest the melt layer was partially vaporized, preferentially losing more volatile elements (e.g., Fe). The vaporized material recondensed to form the thin, $npFe^0$-rich surface deposit during or immediately after the scan cycle. Nanocrystalline olivine that grew within the melt layer as it formed and cooled is similar in volume and microstructure to what we have observed in the impact melt lining of a micrometeorite impact crater in olivine [5]. This suggest the time-temperature relations attained in the laser sample may not be too different from a micrometeorite impact. Our TEM observations, however, do not show evidence for the same level of mechanical damage (e.g., fracturing) seen around the natural micrometeorite crater [5].

References: [1] Moroz L.V. et al. (2014) *Icarus* 235, 187. [2] Sasaki S. et al. (2001) *Nature* 410, 555. [3] Brunetto R. et al. (2007) *Icarus* 191, 381. [4] Gault, D. E. and E. D. Heitowit (1963) Proc. Hy. V. Impact Sym, NASA, 25. [5] Noble, S.K. et al. (2015) this conference.

SPACE WEATHERING IN HOUSTON: A ROLE FOR THE EXPERIMENTAL IMPACT LABORATORY AT JSC: M.J. Cintala[1] (Mark.J.Cintala@nasa.gov), L.P. Keller[1], R. Christoffersen[2], and F. Hörz[3]. [1]Code XI3, ARES NASA JSC [2]Jacobs/JETS Contract, Code XI2, NASA JSC, [3]LZ Technology, all in Houston, TX 77058.

Introduction: The effective investigation of space weathering demands an interdisciplinary approach that is at least as diversified as any other in planetary science. Because it is a macroscopic process affecting all bodies in the solar system, impact and its resulting shock effects must be given detailed attention in this regard. Direct observation of the effects of impact is most readily done for the Moon, but it still remains difficult for other bodies in the solar system. Analyses of meteorites and precious returned samples provide clues for space weathering on asteroids, but many deductions arising from those studies must still be considered circumstantial. Theoretical work is also indispensable, but it can only go as far as the sometimes meager data allow. Experimentation, however, can permit near real-time study of myriad processes that could contribute to space weathering. This contribution describes some of the capabilities of the Johnson Space Center's Experimental Impact Laboratory (EIL) and how they might help in understanding the space-weathering process.

Laboratory Overview: The EIL comprises three separate, distinct accelerators: a 5.56-mm (bore diameter) light-gas gun (LGG), a 40-mm flat-plate accelerator (FPA), and a vertical gun that can use a variety of barrels, depending on an experiment's requirements. The LGG and FPA are mounted horizontally. Each of the three is equipped with a vacuum system and an impact chamber that can support an almost unlimited variety of target configurations. All sequencing and real-time data collection are performed through PCs with LabVIEW software.

Target vaporization appears to be a critically important requirement for some aspects of nanophase Fe ($npFe^0$) generation [1]. The shock stresses required for wholesale vaporization of most relevant geological materials [2], unfortunately, are beyond the capability of almost all laboratory accelerators on the planet. The LGG and FPA, however, are easily capable of inducing impact melting, and even the vertical gun has generated impact melts in fragmental gabbro targets [3]. Liquid-nitrogen-based systems are available for cooling targets in both the FPA and vertical-gun to temperatures below -100°C in vacuum, and a similar capability is planned for the LGG. Brief descriptions of the three accelerators follow.

The Light-Gas Gun: Projectiles ranging from around 3 mm to 1 μm in diameter can be launched with the LGG to speeds on the order of 7 km s^{-1}. All projectiles are confined in a four-piece sabot, and the smaller ones are "shotgunned" to assure multiple impacts on the target. A sample-containment assembly is under construction that will allow retention and subsequent collection of almost all shocked target material from a given impact. It will include mounts for aerogel coupons that will decelerate and trap high-speed ejecta, if desired.

The Flat-Plate Accelerator: High stresses are obtained with the FPA through a shock-reverberation process [4]: the sample material is encased in a solid-metal container, and the impact of a flat "flyer plate" onto the surface of the container generates a planar shock front that passes through the metal and into the target. It then reflects off the backing metal and through the sample again. This continues until the decompression front passes through the flyer plate and enters the sample holder; each passage of the shock through the sample raises the stress level. Provided the flyer plate is sufficiently thick, the final stress will equal the metal-on-metal shock pressure. The shocked sample can then be recovered for any of a wide range of analyses, including petrographic, e-beam, calorimetric, spectral, etc. Because the peak-shock stress is attained in a stepwise manner (*i.e.*, through the reverberations), the entropy increase suffered by the sample is typically less than that acquired by passage of a single shock of the same peak stress level. Therefore, the result of an FPA experiment must be treated as the minimum that would be induced by an impact generating that peak shock stress. This method was used, for example, to investigate the shock melting of an ordinary chondrite [5].

The Vertical Gun: Like the FPA, the vertical gun uses simple gunpowder as a propellant; its speed ceiling is thus around 2.8 km s^{-1}. Nevertheless, it is easily capable of six to eight experiments per day (depending on the time required for target setup). This, along with its ability to launch projectiles over a wide range of diameters, compositions, and masses, makes it a very useful tool for studies such as those involving laboratory-generated "regoliths" [3,6].

References: [1] Keller and McKay (1993) *Science* **261**, 1305. [2] Ahrens and O'Keefe (1972) *The Moon* **4**, 214. [3] Hörz *et al.* (1985) *PLPSC 15* in JGR **89**, C183. [4] Gibbons and Ahrens (1971) *JGR* **76**, 5489. [5] Hörz *et al.* (2005) **MAPS** *40*, 1329. [6] Cintala *et al.* (2015), in preparation.

HOW TO MAP SPACE WEATHERING ON AN ASTEROID SURFACE. B.E. Clark[1], M.A. Barucci[2], F. Merlin[2], C. Lantz[2], H. Campins[3], S. Fornasier[2], E. Dotto[4], D.S. Lauretta[5], [1]Ithaca College (bclark@ithaca.edu), [2]Paris Observatory, [3]University of Central Florida, [4]Osservatorio Astronomico di Roma, [5]University of Arizona.

Introduction: The OSIRIS-REx asteroid mission science team will create a map of the surface manifestations of space weathering when we reach our target asteroid, 101955 Bennu, a dark B-class object, in 2019.

Background: Space weathering alters the structure and composition of the surface material in such a way that it affects the optical properties in the visible and infrared spectral region. The effect of space weathering on large absorption bands can produce a depth variation of 20-30% or as little as a few % on small absorption features of a dark primitive surface. The reflectance slope can vary up to 10-15% for minerals. Development of nanophase iron is an important effect of space weathering on the lunar surface, while it seems to be largely absent on the weathered soil of Vesta (the Dawn spacecraft data shows that weathered soil on Vesta does not exhibit nanophase metal).

Visible and infrared spectroscopic data collected by OSIRIS-REx will allow us to investigate the initial composition of our target and the effect of space weathering on its surface. This information, together with imaging (cratering rate and structure), will allow us to study the surface age and evolution (dating disruption or resurfacing events), as well as constrain the mechanical and physical processes that govern space weathering on the surface of our target.

Methods: Our space weathering map will be an expression of the probability that each surface facet exhibits space weathering. To each surface facet, we will assign rankings in each of the metrics listed here: continuum slope, band depth, albedo, crater proximity, boulder proximity, slope of location, particle size at location, and proximity to regolith regions. These rankings should place each facet on a likelihood scale according to each metric. For example, if a facet is in a highly sloping location on the shape, then it is more likely to show surface composition that is less space weathered. If a facet exhibits a spectral continuum slope that is distinctly different (by 3 sigma) from the average continuum slope of the surface, then it is more likely to represent a surface that is more space weathered. If a facet exhibits an albedo that is distinctly different from the average albedo of the surface, then it is more likely to represent high space weathering, etc.. So the algorithm for each metric is a relative ranking of each facet according to the range of values exhibited in the data set for each metric.

Asteroid Bennu is so dark that albedo and spectral variations are not likely to be of very high amplitude. It will thus be critical to bring together as many of the indicators as possible in a statistical study of how well they correlate with surface features related to surface processes (such as cratering, downslope movement, scarp stability, etc.).

We want to place limits on our ability to detect space weathering, if it exists, at the surface of Bennu. In order to place these limits, we need to account for all other possible explanations of the indicators, and thereby to estimate the probability that each indicator is associated with true space weathering. Other possible explanations for indicators include mineralogical variations, soil texture variations, crater association variations, and regolith mobility variations. We may be able to validate our approach if we identify young terrain (e.g., landslide, crater) that shows a clear difference in one or more of these parameters.

Our planned method will be presented and opened for discussion.

References: Our proposed mapping relies on the study and publication of space weathering effects, e.g. as in the following partial list of papers:

[1] Hiroi et al. (2006) *Nature, 443,* 56-58. [2] Lantz et al. (2015) *Astronomy and Astrophysics, submitted*. [3] Lantz et al. (2013) *Astronomy and Astrophysics,* 554, A138. [4] Brunetto et al. (2014) *Icarus,* 200, 323. [1] Hapke et al. (2001) *JGR, 106,* 10039. [1] Pieters et al. (2000) *Meteoritics and Planetary Science, 35,* 1101.

COMPARISON OF THE TERMPERATURE EFFECTS ON REFLECTANCE SPECTRA OF FRESH AND EXPERIMENTALLY SPACE WEATHERED OLIVINE. L. M. Corley[1], J. J. Gillis-Davis[1], and P. G. Lucey[1], [1]Hawai'i Institute of Geophysics and Planetology, University of Hawai'i at Mānoa, 1680 East-West Road, Honolulu, HI 96822, USA (lmc44@hawaii.edu).

Introduction: Temperature has a significant effect on near-infrared spectra of common rock forming minerals. Increased reflectance at 1064 nm is measured in permanently shadowed regions (PSRs) by the Lunar Orbiter Laser Altimeter (LOLA) [1,2], areas that feature extremely low temperatures. Laboratory experiments [3-6] showed that the width, area, and placement of absorption bands in mafic silicates change in relation to temperature. The temperature effect for lunar soils is much less than that of pure mafic silicate minerals, suggesting that space weathering masks the temperature effects on reflectance [6]. We test the hypothesis that an anticorrelation between temperature and reflectance in LOLA data may be due to the influence of temperature on space weathering. We measured the reflectance of fresh and laser irradiated olivine at temperatures between 100-255 K and under vacuum. Temperature effects on unaltered olivine are inactive at 1064 nm [6]; therefore, any influence that space weathering has on temperature effects at 1064 nm would be obvious.

Methods: Fo_{89} olivine, separated from green sand and powdered to <45 μm, was irradiated with a 1064-nm, 6-8 nsec (20-Hz) pulsed laser, simulating micrometeorite impacts on the Moon. Irradiation was performed under vacuum pressure of 10^{-6} mbar at ambient temperature. The 0.85g sample was irradiated for 40 min at 1-min intervals.

We measured the reflectance of the fresh and irradiated olivine at temperatures between ambient temperature and 100 K, under vacuum pressure of 10^{-7} mbar. Samples were placed in the same thermal chamber used by [6], which uses liquid nitrogen for cooling. Silicon diode sensors mounted on the cold-plate and thermal shield measured temperature.

Reflectance measurements were taken with an Analytical Spectral Devices Inc. FieldSpec 4 spectrometer, which measures reflectance from the UVVIS to NIR (0.35-2.5 μm). We used an 850-nm long pass filter to reduce radiative heating from the light source. The incidence and emissions angles are 10.5° and the phase angle is 21.0°. Reflectance was measured relative to Spectralon standards at ambient temperature.

Results: Unaltered olivine shows a narrowing of the 1-μm absorption band with decreasing temperature (Fig. 1a), consistent with the results of [3-6]. In comparison, the band of the irradiated olivine (Fig. 1b) narrows to a lesser degree. Albedo at 1064 nm of unaltered olivine does not systematically change, while the altered olivine shows a 7% decrease in albedo. The altered olivine is brighter at wavelengths >1500nm and has more spectral contrast than the unaltered olivine.

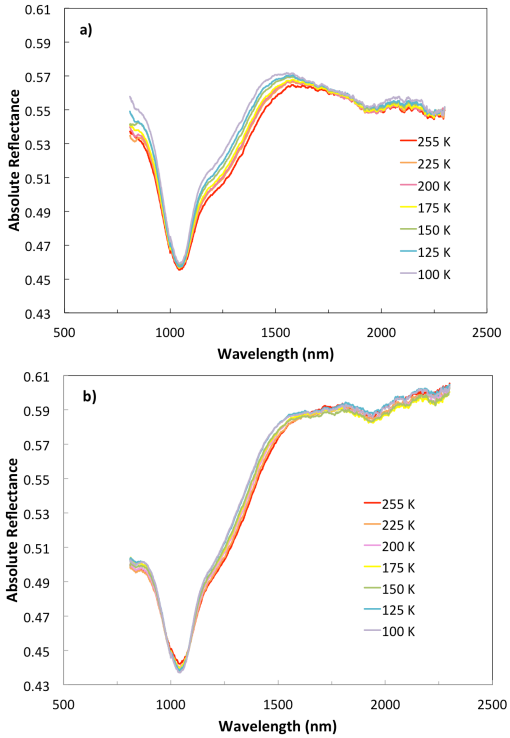

Figure 1: Absolute reflectance of fresh (a) and laser irradiated (b) olivine at temperatures from 100 K to 255 K.

Discussion: Our results indicate that space weathering masks the temperature effects on spectral properties, likely due to submicroscopic iron (SMFe) as was suggested by [6]. Weathered olivine becomes darker at 1064 nm with decreasing temperature, suggesting that the effect of low temperature on albedo is not responsible for increased brightness in PSRs. Our working hypothesis is that extremely low temperatures of PSRs reduce the melting and development of SMFe. Decreased production of SMFe due to lower temperatures in PSRs could cause material to be brighter, and could contribute to increased reflectance measured by LOLA. We plan to test this hypothesis by performing laser irradiation at ~80 K.

References: [1] Zuber M. T. et al. (2012) *Nature, 486(7403),* 378-381. [2] Lucey P. G. et al. (2014) *JGR, 119,* 1665-1679. [3] Roush T. L. (1984) *Effects of temperature on remotely sensed mafic mineral absorption features,* Master's Thesis, University of Hawaii. [4] Singer R. B. and Roush T. L. (1985) *JGR, 90, B14,* 12434-12444. [5] Roush T. L. and R. B. Singer (1986) *JGR. 91, B10,* 10301-10308. [6] Hinrichs J. L. and Lucey P. G. (2002) *Icarus, 155,* 169-180.

MERCURY'S WEATHER-BEATEN SURFACE: AN EXAMINATION OF THE RELEVANT PROCESSES THROUGH COMPARISONS AND CONSTRASTS WITH THE MOON AND ASTEROIDS. D. L. Domingue[1], D. Schriver[2], P.M. Trávníček[3], Jörn Helbert[4], [1]Planetary Science Institute (1700 East Fort Lowell Road Suite 106, Tucson, AZ 85719-2395; domingue@psi.edu), [2]Department of Physics and Astronomy (University of California, Los Angeles, CA 90095; dave@igpp.ucla.edu), [3]Space Sciences Laboratory, University of California, Berkeley, CA (pavel@ssl.berkeley.edu), [4]Institute for Planetary Research (DLR, Rutherfordstrasse 2, 12489 Berlin, Germany; joern.helbert@dlr.edu)

Introduction: The physical, chemical, and mineralogical properties of the regoliths of atmosphere-free planetary bodies are altered by a set of processes collectively termed space weathering. These processes include bombardment by micrometeorites, solar wind ions and electrons (or where applicable magnetospheric ions and electrons), thermal processing, and irradiation by photons [e.g. 1, 2]. Intimate mixing of fine-grained constituents has been added to the list of possible processes to explain Vesta's spectral properties [3]. The resulting physical, chemical, and mineraologic changes affect the remote sensing observations (namely color and spectral observations) of these bodies.

Sample returns from the lunar surface, and now from asteroid Itokawa [4, 5], have provided insights into the nature of these alterations. Based on the paper by Domingue et al. (2014) we review the potential role of the major space weathering processes and their application to the surface of Mercury.

Micrometeorite Bombardment. The flux of impactors on Mercury is at least 5.5 times that for the lunar surface, with a mean impact velocity that is 30 – 60 % higher [6, 7]. This results in enhanced melt and vapor production, greater material reduction and devolatilization, and an environment condusive to the added production of nanophase materials compared to either the lunar or asteroidal scenarios [2]. This environment supports the production of thicker rims on grains due to impact melt and vapor deposition in addition to the formation of a greater abundance of agglutinates [2].

Ion and Electron Bombardment. This process both sputters and implants material into the regolith. The net results are to destroy the crystalline lattice of the upper grain layers (thus creating an amorphous rim), premote the production of nanophase material, migrate volatiles within the regolith, and foster the migration of materials within grain centers to grain exteriors [e.g.2]. Mercury's magnetic field operates as an imperfect shield to solar wind and magnetospheric charged particles [8, 9], creating latitudinal variations in surface irradiation (Fig. 1).

Thermal Processing. Mercury experiences large temperature fluxuations due to its proximity to the Sun. Examination of temperature cycling of relevant sulfides [10] has demonstrated spectral changes strongly affect remote determinations of surface composition.

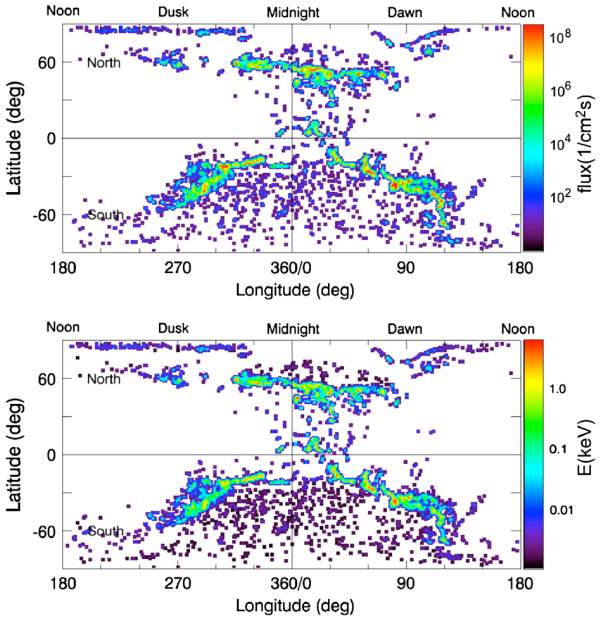

Fig. 1. Taken from Schriver et al. (2011) and Domingue et al. (2014), these graphs show the electron precipitation flux (top) and the electron precipitation energy (bottom) simulation correlating to MESSENGER's first flyby of Mercury. Longitude is a function of local time and not geographic longitude.

Mercury Global Properties. We present examination of global color properties and their correlations to the predicted trends due to particle bombardment and thermal processing. We examine color ratios and color slope analyses commensurate with lunar and asteroid weathering studies as applied to Mercury.

References: [1] Hapke (2001) J. Geophys. Res. 106, 10039. [2] Domingue, D. L. et al. (2014) *Space Sci. Rev., 181,* 121-214. [3] Pieters et al. (2012) Nature 491, 79. [4] Noguchi et al. (2011) Science 333, 1121. [5] Noguchi et al. (2014) Meteorit. Planet. Sci. 49, 188. [6] Cintala (1992) J. Geophys. Res. 97, 947. [7] Borin et al. (2009) Astron. Astrophys. 503, 259. [8] Benna et al. (2010) Icarus 209, 3. [9] Schriver et al. (2011) Planet. Space Sci. 59, 2026. [10] Helbert et al. (2013) Earth Planet. Sci. Lett. 369, 233

EFFECTS OF SPACE WEATHERING ON THERMAL INFRARED EMISSIVITY SPECTRA OF BULK LUNAR SOILS MEASURED UNDER SIMULATED LUNAR CONDITIONS. K. L. Donaldson Hanna[1,2], N.E. Bowles[1], C. M. Pieters[2], B. T. Greenhagen[3], T. D. Glotch[4], and P. G. Lucey[5], [1]Atmospheric, Oceanic and Planetary Physics, University of Oxford, Oxford, UK (Kerri.DonaldsonHanna@physics.ox.ac.uk), [2]Dept. of Earth, Environmental and Planetary Sciences, Brown University, Providence, RI, USA, [3]Johns Hopkins University Applied Physics Laboratory, Laurel, MD, USA, [4]Dept. of Geosciences, Stony Brook University, Stony Brook, NY, USA, and [5]Hawaii Institute of Geophysics and Planetology, University of Hawaii, Honolulu, HI, USA.

Introduction: Understanding the spectral effects of space weathering on thermal infrared (TIR) observations of the lunar surface is an important consideration for the interpretation of current and future remote sensind datasets as the entire lunar surface has experienced some degree of space weathering. A study of TIR reflectance measurements of a suite of plagioclase feldspars demonstrated that the vitrification process does not affect the position of the Christensen feature (CF), an emissivity maximum in TIR spectra indicative of mineralogy and composition[1-3]. This led many to believe that effects on TIR emissivity spectra due to space weathering would not be observed. However recent work by Lucey et al. [4] has demonstrated that space weathering does strongly influence the position of the CF as observed in observations by the Diviner Lunar Radiometer Experiment (Diviner) onboard NASA's Lunar Reconnaissance ORbiter.

In this initial characterization of Apollo bulk soil samples, TIR emissivity spectral measurements are made under Earth-like (ambient) and lunar-like conditions of two highland soil samples that are similar in composition, but differing maturities in an effort to better understand the effects of space weathering on TIR spectra.

Experimental Setups and Samples: TIR spectral emasurements were made in the Asteroid and Lunar Environment Chamber (ALEC), a vacuum chamber at Brown University designed to simulate the space environment experienced by the near-surface regolith of the Moon and asteroids. The design details of the vacuum chamber have previously been discussed [5]. ALEC is connected to a Thermo Nicolet 870 Nexus FTIR spectrometer which allows laboratory emissivity spectra to be collected at a resolution of 4 cm^{-1} over the ~400 – 2000 cm^{-1} spectral range.

Bulk lunar soils measured in this initial study include Apollo samples requested from NASA's CAPTEM as a part of the Thermal Infrared Emission Studies of Lunar Surface Compositions Consortium (TIRES-LSCC). The two highlands bulk lunar soil samples included in this study, 66031 and 67701, have similar soil chemistries and normalized modal contents [6-8], but different maturities (I_s/FeO = 102 and 39, respectively) [9].

Results: Spectral measurements of both soils under Earth-like or ambient conditions have similar CF positions (8.11 μm versus 8.10 μm), but the spectrum of immature soil 67701 has greater contrast in spectral features at wavelengths longer than the CF than the spectrum of mature soil 66031. However under simulated lunar conditions, two observations are made: (1) the CF position of immature soil 67701 has shifted to shorter wavelengths when compared to the CF position of mature soil 66031 (7.93 μm versus 8.02 μm) and (2) the spectral contrast between the CF and the reststrahlen bands (RB) is much greater in the immature, higher albedo soil sample (Figure 1). These initial results suggest that space weathering has observable effects on TIR emissivity spectra measured under simulated lunar conditions these effects are similar to those observed in the Diviner TIR observations of immature locations like crater ejecta rays and the more mature surface locations the ejecta deposits are emplaced on [4].

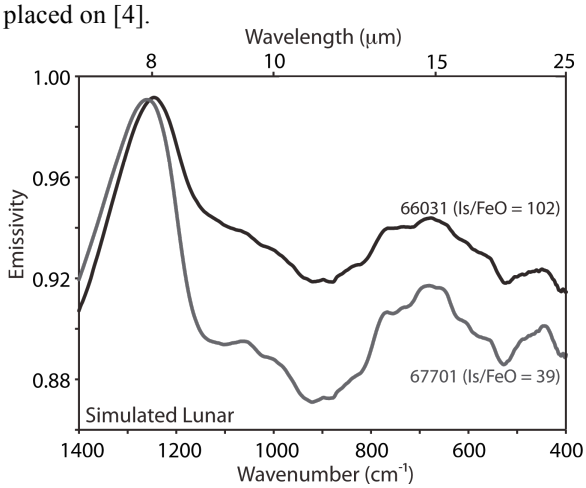

Figure 1. Lunar-like spectral measurements of mature lunar soil 66031 and immature lunar soil 67701.

References: [1] Nash D. B. and Salisbury J. W. (1991) *GRL, 18,* 1151–1154. [2] Nash D. B. et al. (1993) *JGR, 98*, 23,535-23,552. [3] Lyon R. J. P. (1964) *NASA Rep. CR-100*, 264 pp. [4] Lucey P. G. et al. (2015), *Icarus, In submission*. [5] Donaldson Hanna K. L. et al. (2013) *LPS XXXXIV*, Abstract #2225. [6] Rose H. J. et al. (1975) *LSC VI*, 1363-1373. [7] Korotev R. L. (1982) *LPS XIII*, A269-278. [8] Taylor G. J. et al. (2012) *LPS XLIII,* Abstract #2316. [9] Morris R. V. (1978) *LSC IX*, 2287-2297.

ION-IRRADIATION INDUCED CHANGES IN THE SURFACE COMPOSITION OF CARBONACEOUS METEORITES. C.A. Dukes[1] , D. Fulvio[2], and R.A. Baragiola[1†], [1]Laboratory for Astrophysical and Surface Physics, University of Virginia, Charlottesville, VA 22904 (cdukes@virginia.edu), [2]Pontifical Catholic University of Rio de Janeiro, Departamento de Física, 22451-900 Gávea, Rio de Janeiro, Brazil (dfu@oact.inaf.it), †deceased.

Introduction: While the optical effects of space weathering on Fe-bearing minerals has been widely investigated and the resulting darkening and reddening appears consistent for both observed planetary surfaces and laboratory investigations, the effects of weathering on carbonaceous materials remain ambiguous. Laboratory experiments simulating solar wind impact on the parent bodies of carbonaceous chondrites (CCs) generally measure the overall change in reflectance (albedo), the change in slope in the UV-visible region, as well as any variation in the near-IR region. The results for ion impact are mixed, with optical changes (brightening/darkening; reddening/bluing) varying widely with ion type, energy, and meteoritic composition [1,2]. Similar optical variation occurs with laser impact [3,4]. In this work, we examine in more detail the alterations in surface chemistry that result from ion impact on carbonaceous meteorites which accompany the changes in optical reflectance.

Experiments: Irradiations and *in situ* X-ray photoelectron spectroscopic (XPS) measurements were taken in two different ultra-high vacuum (< 5 x 10^{-9} Torr) systems. The first series of experiments measured the surface elemental composition of pressed powder pellets from the CC Tagish Lake meteorite (hereafter TL). Measurements were taken as a function 4 keV He ion fluence and composition was measured *in situ,* without exposure to atmosphere, using a PHI 560 XPS/SAM system [5,6]. A low energy electron flood gun was used during both irradiation and surface analysis to minimize surface charge. Vis-NIR reflectance spectra were taken *ex situ* before and after irradiation.

Chemical maps of TL samples were taken with a PHI Quantera SXM Scanning XPS Microprobe. Samples were prepared by sprinkling ground and sieved powder on C-tape atop Ta substrates. 4 keV Ar ions used for irradiation and 400 x 350 micron^2 images were acquired as a function of ion fluence, by scanning Al X-rays across the meteorite surface with a spot size of 18 microns. The surface charge was neutralized during data acquisition using low energy electrons and ions.

Results and Discussion: Elemental atomic concentrations for the surface of TL as a function of He ion fluence are shown in Fig.1. We find that the primary effect of ion irradiation is to deplete carbon from the surface, which can explain the brightening reported by Vernazza et al. [1]. However, silicates are known to *darken* under ion irradiation as a result of oxygen loss and formation of metallic Fe, seen in XPS. Thus, the net effect of solar wind irradiation on an asteroid will depend on the relative fraction of carbon (whose removal brightens the surface) and silicates (which darken upon irradiation).

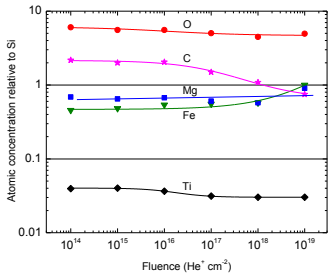

Fig. 1. *Atomic concentrations relative to Si vs. fluence*

Coordinated elemental maps for Si, C, Mg, and Fe on the TL loose powder surface after removal of adventitious carbon but prior to 4 keV Ar ion irradiation are shown in Fig.2. High spatial resolution offers the first opportunity for comparative studies on the surface chemical effects of space weathering of multi-component meteorite grains.

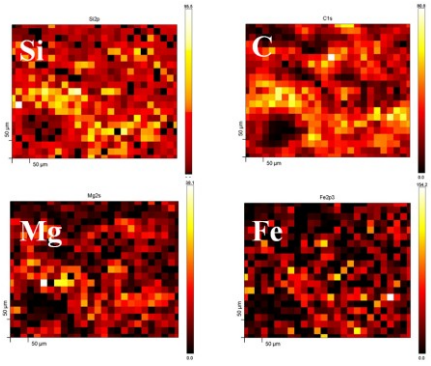

Fig. 2. *TL meteorite elemental surface maps.*

References: [1] Vernazza, P., Fulvio, D., Dukes, C.A. et al. (2013) Icarus 225, 517. [2] Lantz, C. et al. (2015) A&A 577, A41. [3] Gillis-Davis, J.J. et al. (2013) LPSC 44, Abstract #2494. [4] Matsuoka, M. et al. (2015) Icarus 254, 135. [5] Dukes, C. A.et al. (1999) JGR 104, 1865. [6] Loeffler, M. J., Dukes, C. A., Baragiola, R. A. (2008) JGR E 114, E03003.

SOLAR WIND HYDROGEN IMPLANTATION AND DIFFUSION IN DEFECT-RICH REGOLITH ON THE MOON, V. J. Esposito[1], W. M. Farrell[2], M. I. Zimmerman[3], 1. NASA/GSFC Intern Program, Greenbelt MD and Univ. of South Carolina, 2. NASA/GSFC, Greenbelt, MD (William.M.Farrell@nasa.gov); 3. JHU/Applied Physics Laboratory, Laurel MD.

Motivation: The solar wind bombards the surfaces of airless bodies near 1 AU with a flux of protons near 2 x 10^{12}/m^2-s. As illustrated in the figure, some of these protons are reflected at or near the surface, some implant in the surface but quickly diffuse back out as H or H_2, and some implant in the surface but get trapped by defects in the crystal lattice to become delayed in their diffusive exit. It is the trapped and delayed component that can create an enhancement in the near-surface OH.

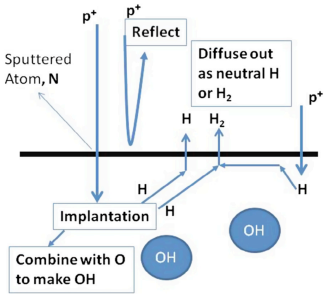

H Interactions. Starukhina [1] described vacancy defect sites as locations possessing a large activation energy, U, that reduced mobility of the implanted atom. Since H retention times vary as ~ exp(U/T) (where T is the surface temperature in eV), at locations with large activation energies (U > 1 eV), the implanted hydrogen could dwell for substantially longer than a lunation. In contrast, if the surface has an intact crystal lattice, the U values remain low (U < 0.3 eV) and the hydrogen dwell times are seconds or less.

Fink et al [2] compared the implantation of energetic protons into silicon and silica and found that the presence of unsatisfied O bonds in the silica added a delayed component to the H diffusion. The H interactions with the unbounded O could form a very loose temporary OH structure. They derived an 'effective' activation energy of U ~ 0.5 eV. Thus unlike silicon, in silica there were three classes of diffusion: Defect-free, vacancies, and O-interactions.

TRIM Model Runs. In order to ascertain the effect of solar wind protons on silicon dioxide, we used the Transport of Ions in Matter (TRIM) code that provided the vacancy locations, implantation locations, and vacancy per incident proton. We found that the implantation depth for the proton/H was approximately a factor of 1.5 - 2 deeper than the layer where the vacancies resided. Thus, any implanted H has to diffuse through a layer of damaged lattice sites to exit. For 1 keV protons, there were typically 2 vacancies created per ion, but the vacancy number dropped with decreasing ion energy, being 0.2 vacancies/proton at 0.2 keV.

Bulk Damage Model. TRIM damage is not accumulated. Instead, each incident proton is considered independent and assumed entering a perfect crystal. We thus developed a bulk damage model that accumulated the vacancies and interstitials from solar wind over time. The model also considers the case where interstitial Os and Sis become so numerous that they encroach on the vacancy space, effectively reducing or eliminating true vacancies over time. After long times, the model shows that interstitial atoms (or, we now call these non-crystal atoms) dominate the near-surface layer creating an amorphous structure.

Hydrogen Diffusion. Given a model of the evolution of the crystal structure over time, we can run an H-diffusion code [3] to derive the formation of OH and H release as a function of temperature. For N implantation sites, we create 3 normal distributions: (1) a distribution with U < 0.2 that have quick diffusion paths for undamaged crystal regions, (2) a distribution at intermediate U values centered near 0.5 eV that represent the H interactions with interstitial Os, and (3) a distribution centered at large U > 1.2 eV representative of implantations that encounter vacancy defects.

The output from the bulk damage code then determined the relative dominance of the three distributions. At early times when the crystal is mostly undamaged, distribution (1) dominates, but at long times, when the crystal becomes amorphous, (2) dominates.

Application to a Lunar Magnetic Anomaly. We used the surface solar wind flux and energy at a model magnetic anomaly [4]. In regions where the B-field was strong and horizontal, far fewer solar wind protons are incident with the surface, and those that do get to the surface are of low energy (< 0.2 keV). As such, there is little damage. Given the more pristine crystalline structure, any implanted H can quickly diffuse from the surface – little is retained for long periods. This result is similar to M^3 observations [5] where there was less OH found in the flanks of the swirl mag anomaly regions. Our modeling suggests that without vacancies and interstitials, implanted H will not be delayed in its fast diffusion from the surface.

References: [1] Starukhina, L, V., Adv. Space Res., 37, 50, 2006; [2] Fink, D. et al., Appl. Phys. A, 61, 381, 1995; [3] Farrell, W. M., et al., Icarus, 55, 116, 2015; [4] Zimmerman, M. I. et al., J. Geophys. Res., submitted, 2015. [5] Kramer, G. Y., et al., J. Geophys. Res., 116, E00G18, 2011.

THE ROLE OF CRYSTAL DEFECTS IN THE RETENTION OF VOLATILES AT AIRLESS BODIES. W. M. Farrell[1], D. M. Hurley[2], V. J. Esposito[3], M. J. Loeffler[1], J. L. McLain[4], T. M. Orlando[5], R. L. Hudson[1], R. M. Killen[1], M. I. Zimmerman[2], 1. NASA/Goddard SFC, Greenbelt, MD (William.M.Farrell@nasa.gov); 2. JHU/APL, Laurel MD; 3. NASA/GSFC Summer Intern, Greenbelt, MD; 4. University of Maryland, College Park, MD; 5. Georgia Institute of Technology, Atlanta, GA;

Motivation: Over long times, the surfaces of exposed oxide-rich rocky bodies get weathered by the harsh elements of the space environment, including processes like sputtering by the solar wind plasma, impacting by micro-meteoroids, and irradiation by galactic cosmic rays and solar energetic particles.

These exposed surfaces develop a set of defects (vacancies and interstitials) having local sites with relatively higher trapping potentials or high activation energy, U, for implanted volatile movement. The nature of the defects are revealed in part as the amorphous rims [Keller and McKay, 1997]. Such weathered surfaces have effects on any implanted atoms or molecules.

In this presentation, we will describe a set of examples where crystal defects play clear roles in volatile retention. Some of the examples are from NLSI/SSERVI DREAM2 team studies and others are from close SSERVI collaborators. As a set, the examples reveal just how critical a defected surface becomes in retaining volatiles.

Solar Wind H Retention. The role of defects on solar wind proton/H implantation and retention was described by Starukhina [1] who considered vacancy defect sites as locations possessing large activation energy, U. Since H retention times vary as ~ exp(U/T) (where T is the surface temperature in eV), at locations with high U, the implanted hydrogen could dwell for substantially longer than a lunation. In contrast, if the surface had a near-perfect crystal, the U values are low and the hydrogen dwell times would be seconds or less.

Pieters et al. [2] found that the Moon possessed an OH veneer likely due to solar wind H implantation. The surfacial H may also display a diurnal effect [3] with H being removed at the warmer local noon. A possible explanation for this behavior is the consideration of a distribution of implantation sites with a statistical spread in U values (a distribution of defects of various potency), with sites at intermediate U values between 0.3 eV and 0.7 eV capable delaying H diffusion in cold surfaces but releasing H in warmed surfaces [4].

Migrating Water Retention. NLSI/SSERVI Investigators at APL and Georgia Tech have found that surface-migrating water molecules are retained on surfaces with defects. Using Temperature-Programmed Desorption (TPD) analysis, Poston et al. [5] mapped out the tail of the distribution of activation energies on surfaces of albite and JSC simulant, and found a population of activation energies for water retention above 1 eV. Thus, migrating water on the surface of any airless body will get trapped and become 'delayed' on defect-rich surfaces with large U values.

The Two-Beam Defect Study. As part of DREAM2, we are building a system to irradiate samples (including eventually lunar samples) with high-energy argon ions near 1 MeV to purposely create surface defects. In the same chamber and under the same vacuum, we then will follow this initial beam with a low energy 1 keV proton or D beam to consider the effect these new defects have on H/D retention and OH/OD formation. We will briefly describe the motivation and development of this laboratory work.

Conclusions. While temperature appears to be a controlling variable in volatile retention, NLSI/SSERVI work indicates that the crystal defect structure plays possibly a larger role than T. We demonstrate that the temperature variations are only revealed in solar wind H retention due to the dominance of sites with activation energies at intermediate values that are susceptible to H release > 200K. However, if hypothetically the surface distribution of defects was different (with the dominant values >> 1 eV, for example) the dependence of temperature would be lost.

As a set, the examples are designed to stimulate discussion for a greater connection of detailed surface defect studies to volatiles retention and emission studies– connecting missions like LADEE to the asteroid & lunar sample analysis community.

References: [1] Starukhina, L, V., Adv. Space Res., 37, 50, 2006; [2] Pieters, C. M., et al., Science, 326, 568, 2009; [3] Sunshine et al., Science, 326, 565; [4] Farrell, W. M., et al., Icarus, 55, 116, 2015; [5] Poston, M. J. et al., J. Geophys. Res., 118, 105, 2013.

DARKENING OF MERCURY'S SURFACE BY SULFIDES AND CARBON. J. J. Gillis-Davis[1], H. M. Kaluna[1], J. P. Bradley[1], H. A. Ishii[1], P. G Lucey[1]. [1]Hawaii Institute of Geophysics and Planetology, University of Hawaii at Manoa, 1680 East West Road, Honolulu, Hawaii 96822, U.S.A.

Introduction: Space weathering darkens and reddens the spectra of airless bodies of the inner Solar System [1]. Comparisons of albedo and continuum slope reflect not only degree of space weathering [2], but also minor element chemistry [3]. For instance Mercury's albedo is lower than the Moon [4]. The differing space-weathering environment at Mercury – with greater fluxes of both protons and micrometeorites, higher impact energies, and higher temperatures – complicates the interpretation of spectra. Moreover, recent compositional data of Mercury reveals some key differences between the two bodies. MESSENGER X-ray data indicate that Mercury's surface is enriched by up to 4 wt.% sulfur [5,6] and potentially up to 3 wt.% carbon [7]. We examine sulfur/sulfide and carbon-bearing composition related spectral effects for materials that have experienced identical simulated space-weathering conditions.

Methods: A pulsed laser was used to simulate the micrometeorite component of space weathering – 1064 nm wavelength, pulse duration of 6-8 nanoseconds to simulate timescales of micrometeorite dust impacts [8], and with an incident energy of 30mJ per pulse. Samples were irradiated as uncompressed powers with grain sizes of <75 µm. The first suite of samples was a mixture of olivine with various amounts of elemental S (0, 2 4, and 8wt.%). The second sample mixed Stillwater Anorthosite with the same four weight fractions of S. The third sample was a natural mixture of ~3% siderite ($FeCO_3$), 23% pyrite (Fes2) and 74% cronstedtite ($Fe_2^{2+}Fe^{3+}(SiFe^{3+})O_5OH_4$). Three aliquots of each sample were irradiated under vacuum, 10^{-5} to 10^{-6} mbar, for intervals that totaled 30 minutes. Spectra were measured *ex situ* with an Analytical Spectral Device spectrometer, with the standard 30° phase angle illumination.

Results: After 30 minutes of laser irradiation, plagioclase with 0% wt.% S darkened by 13% compared to 27% darkening for the sample 2 wt.% S (Fig. 1). The continuum slope of the 0 wt.% S composition increased by 34%, while the 2 wt.% S composition increased by 92%. There are diminishing effects above 2% sulfur. Samples with >2 wt.%. sulfur only became slightly darker/redder. Olivine mixtures exhibited similar darkening and reddening effects. The cronstedtite/pyrite /siderite sample is not an analog to Mercury other than it contains sulfide and carbon-bearing phases. The spectra of sample became darker and bluer with laser irradiation. TEM analysis of this sample reveals submicroscopic blebs of carbon material (SMC) in the melt rims (Fig 2), which as a spectrally neutral opaque would darken and flatten spectra. This result is similar to [9] but without production of carbon bearing agglutinates.

Conclusions: Spectra of compositions containing S, and by inference sulfides, are modified by laser weathering to a greater degree than compositions with none. Hence objects with greater sulfide composition would exhibit more darkening than bodies with less sulfide yet similar Fe compositions [3]. SMC-driven spectral darkening and flattening are consistent with VIS/NIR data of low-reflectance materials on Mercury as measured in MESSENGER MDIS and MASCS data [10].

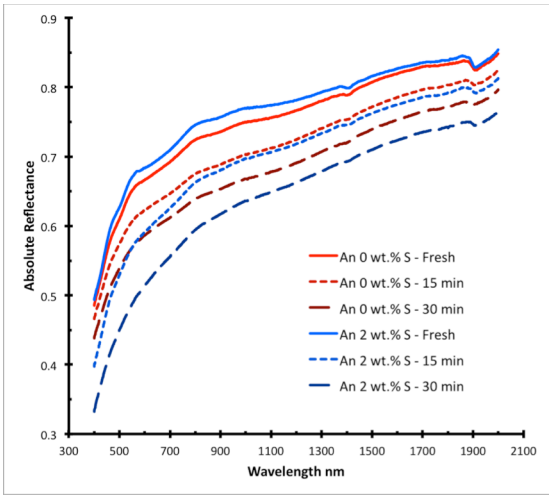

Fig 1. Comparison of laser weathered anorthosite without sulfur and with 2wt.% S.

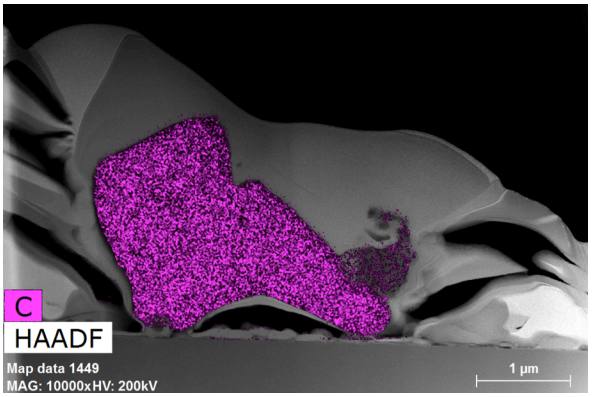

Fig 2. Merged HAADF gray-scale image with EDX map for carbon, carbon is >50wt% in magenta area.

References: [1] Hapke B., 2001, *JGR* 106, 10039–10073; [2] Lucey, P. G., et al., 2001, *JGR* 105, 20297-20305; [3] Gillis-Davis, J. J., E. R. D. Scott, 2014, LPSC 45, #1189 [4] Denevi, B. W., M. S. Robinson, 2008, *Icarus* 197, 239-246; [5] Nittler, L. R. et al., 2011, *Science* 333, 1847-1850; [6] Weider, et al., 2015, *EPSL 416*, 109-120; [7] Peplowski, et al., 2015, *Planet. Space Sci., 108*, 98-107; [8] Yamada et al., 1999, *Earth Planet. Sci.* 51, 1255-1265; [9] Syal, et al. 2015, *Nat. GeoSci.*, NGEO2397; [10] Murchie et al., *Icarus* 254 (2015) 287–305.

OBSERVATIONS OF LUNAR SWIRLS BY THE DIVINER LUNAR RADIOMETER: EVIDENCE FOR MAGNETIC FIELD STANDOFF BY THE SOLAR WIND. T. D. Glotch[1], P. G. Lucey[2], P. O. Hayne[3], J. L. Bandfield[4], B. T. Greenhagen[5], and K. A. Shirley[1]. [1]Stony Brook University, Stony Brook, NY 11794-2100 timothy.glotch@stonybrook.edu, [2] Hawaii Institute of Geophysics and Planetology, University of Hawaii at Manoa, [3]Jet Propulsion Laboratory, [4]Space Science Institute, [5]Applied Physics Laboratory

Introduction. Lunar swirls are high albedo features on the Moon associated with local magnetic fields. Hypotheses for their formation include (1) standoff of the solar wind [1] by the magnetic field leading to abnormal space weathering dominated by micrometeoroid bombardment [2], (2) scouring of the lunar surface by a comet/asteroid swarm impact vapor plume, leading to albedo and photometric property variations [3-4], (3) lofting and transport of finely particulate feldspar-enriched dust [5], and (4) a "hybrid" model that requires both regolith disturbance and dust lofting [6]. In this work, we argue that Diviner Lunar Radiometer measurements of lunar swirls are inconsistent with formation mechanisms that require alteration of the regolith structure, either through sorting, or scouring. This suggests that solar wind standoff by local magnetic fields is chiefly responsible for the formation of the lunar swirls.

Diviner Lunar Radiometer CF Measurements. Recent observations by the Diviner Lunar Radiometer Experiment show that swirls exhibit a Christiansen Feature (CF) anomaly consistent with surfaces that are spectrally immature compared to the surrounding terrains [7]. The CF anomalies, and Diviner's sensitivity to space weathering in general, is likely due to variable thermal gradients in the swirls and surrounding terrains caused by visible albedo differences. Laboratory measurements under simulated lunar conditions of quartz with variable amounts of carbon black added to reduce the sample's visible albedo show a correlation between CF position and visible albedo (Figure 1).

Roughness and Night-time Cooling Models from Diviner Temperature Measurements. Modeling of the night-time cooling of Reiner Gamma shows that temperature differences between the swirl and surrounding terrains can be completely explained by the swirl's higher albedo [7]. The addition of a 2 mm thick layer of material with a thermal inertia 50% of the standard regolith model [8] results in swirl temperatures that are much too cold. This result suggests that dust transport resulting in a mm-scale or thicker low thermal inertia layer is not a likely mechanism to form the Reiner Gamma swirl. Recent ground-based observations of Reiner Gamma during lunar eclipse confirm that any layered structure, if present, must be less than 1 mm in thickness [9].

We have also used Diviner data to calculate the roughness on and off the Reiner Gamma and Airy swirls. The Diviner data indicate that both swirls have an RMS slope distribution of 25-30 degrees at mm to cm scales, which is indistinguishable from typical lunar regolith. The finely structured lunar regolith at these swirls place tight constraints on the swirl's formation, and requires a formation mechanism that will not substantially disturb the regolith at cm scales.

Analysis of the Diviner data is ongoing, and we will present detailed spectral analysis, roughness, and night-time cooling models for other swirls, including those at Descartes, Firsov, Gerasimovich, Hopmann, Mare Ingenii, Mare Marginis, Moscoviense, and Rima Sirsalis. Preliminary spectral analysis of these swirls indicates that each shows a CF anomaly relative to the surrounding terrain, although the magnitude of the anomaly varies. Detailed thermophysical modeling of each of the swirls will further constrain their origins and allow us to determine if they share a common formation mechanism.

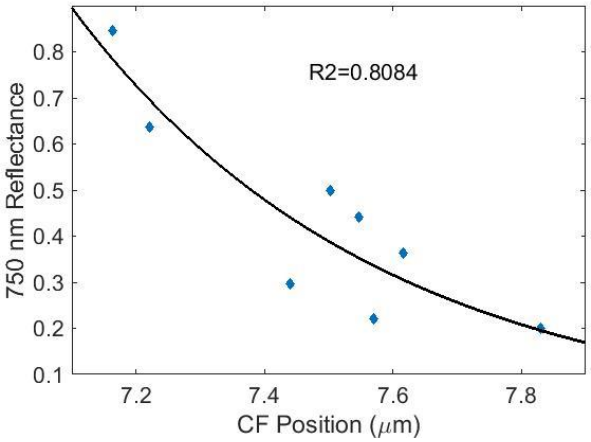

Figure 1. 750 nm reflectance vs CF position measured in a simulated lunar environment for quartz samples darkened using amorphous carbon black. CF position is dependent on the visible albedo of the sample.

References: [1] Hood, L. L., and G. Schubert (1980), *Science*, 208, 49-51. [2] Kramer, G. Y. et al. (2011), *J. Geophys. Res*., 116, E04008. [3] Schultz, P. and L. J. Srnka (1980), *Nature*, 284, 22-26. [4] Starukhina, L. V. and Y. G. Shkuratov (2004), *Icarus*, 167, 136-147. [5] Garrick-Bethell, I. et al. (2011), *Icarus*, 212, 480-492. [6] Pieters, C. M. et al. (2014), *Lunar Planet. Sci. XLV*, abstract 1408. [7] Glotch, T. D. et al. (2015), *Nat. Comm.*, 6, 6189, doi:10.1038/ncomms7189. [8] Vasavada, A. R. et al. (2012), J. Geophys.Res., 117, E00H18. [9] Hayne, P. O. et al. (2015), *Lunar Planet. Sci. XLVI*, abstract 1997.

SPACE WEATHERING EFFECTS IN THE THERMAL INFRARED: LESSONS FROM LRO DIVINER.
B. T. Greenhagen[1], P. G. Lucey[1], E. Song[3], J. A. Arnold[4], M. Lemelin[2], K. L. Donaldson Hanna[4], N. E. Bowles[4], T. D. Glotch[5], and D. A. Paige[6], [1]Johns Hopkins Applied Physics Laboratory, [2]University of Hawaii at Manoa, [3]Jet Propulsion Laboratory, [4]University of Oxford, [5]Stony Brook University, [6]University of California, Los Angeles.

Introduction: Before the launch of the Lunar Reconnaissance Orbiter (LRO), it was suggested that thermal infrared spectroscopy would be a unique tool for lunar compositional remote sensing in part because evidence indicated this technique was less susceptible to the known optical effects of lunar surface exposure to space [1] than the more widely used visible and near-infrared wavelengths [e.g. 2, 3]. However, with global data from the LRO Diviner Lunar Radiometer (Diviner), it quickly became evident that the Christiansen Feature (CF; a mid-infrared compositional indicator) on the lunar surface was affected by space weathering [4, 5]. Young features such as interiors, ejecta and ray deposits of the craters Tycho and Jackson show CF positions at systematically shorter wavelengths than their more space weathered surroundings, as do deposits of the other young rayed craters. Lunar swirls, commonly thought to form as a result of inhibition of the space weathering process, also show shorter CF positions than their surrounding terrains [6].

This presentation quantifies the degree to which space weathering affects the CF, and presents techniques for normalization of space weathering effects to enable examination of the underlying composition. We will also present and discuss hypotheses for the unanticipated space weathering dependence revealed by Diviner.

Datasets: We used calibrated radiances from Diviner's three 8 μm-region channels to calculate effective emissivity and then fit the three emissivity values with a parabola. The wavelength maximum of the parabola is the estimated CF wavelength [5]. Our data were "photometrically" corrected by projecting the data onto a topographic grid, calculating photometric geometry, and applying an empirical correction methodology [*after* 5]. Diviner data were binned at 32 pixel per degree to produce global maps of CF values for latitudes below 60 degrees (Figure 1 - top). We compare the CF to the Clementine-derived optical maturity (OMAT) parameter (Figure 1 – middle) [7].

Results: Here we revisit the correction of [4], which showed that a properly scaled independent measure of extent of space weathering may be successful at freeing the CF measurement from space weathering influences, and update its parameters. We elected to subtract an offset from the sum of CF+OMAT to make the central peak of Jackson equal to its minimum value (~7.9 microns). We also limit the minimum OMAT value to 0.3 everywhere prior to correction, which minimizes the tendency for OMAT to overestimate space weathering effects on the least weathered surfaces (e.g. Giordano Bruno). The final correction is

$$CF_{Adjusted} = CF + (OMAT > 0.3) - 0.285$$

The CF map adjusted for space weathering is presented in Figure 1 - bottom.

Conclusions: The near-IR derived OMAT parameter can be used to correct the CF data for the space weathering effect, but the results can be further improved upon. Comparisons of CF and OMAT at high resolution suggest that in the least weathered areas the two parameters diverge in their response to space weathering and the proposed correction is less effective in the lunar maria. Future work will focus on adjustments that could improve it, such as imposing a composition-dependent scale factor, and evaluating hypotheses for the CF-space weathering dependence.

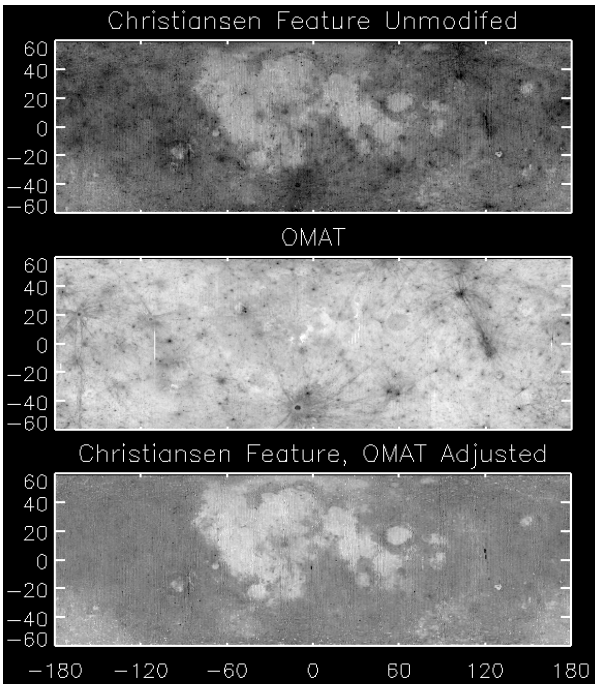

Figure 1. Demonstrating the use of OMAT to correct space weathering effects from Diviner CF data.

References: [1] Nash et al. (1993) *JGR*, *18*, 1151-1154, [2] Pieters et al. (2000) *MPS*, *35*, 1101-1107, [3] Hapke (2001) *JGR*, *106*, 10039-10073, [4] Lucey et al. (2010) *LPSC XLI*, #1600, [5] Greenhagen et al. (2010) *Science*, *329*, 1507, [6] Glotch et al. (2015) NatComm, *6*, 6189, [7] Lucey et al. (2000) *JGR*, *105*, 20377-20386.

Laboratory studies of thermal space weathering on airless bodies. J. Helbert[1], A. Maturilli[1] and S. Ferrari[1], [1]Institute of Planetary Research, DLR, Rutherfordstrasse 2, 12489 Berlin, Germany (joern.helbert@dlr.de).

Introduction: Deriving the surface composition of Mercury from remote sensing hyper spectral data is a challenging task. Mercury's surface has a low iron abundance, which complicates the application of "traditional" space weathering approach. In addition the high temperatures on Mercury lead to previously unseen changes in the spectral characteristics, which we call "thermal space weathering".

The Planetary Emissivity Laboratory (PEL) at DLR in Berlin was setup specifically to study the effects of high temperatures on the spectral characteristics of planetary analog materials. It allows characterizing "thermal space weathering" and adds temperature as another important factor for the creation of spectral libraries.

Thermal space weathering can produce reversible as well as irreversible changes in the spectral characteristics of materials. In comparison to "traditional space weathering" it acts on much shorter timescales. We are going to present a number of examples for thermal space weathering effects in the visible as well as infrared spectral range.

The PEL instrumental setup: The PEL facility in Berlin is currently equipped with three Bruker Fourier Transform Infrared-Spectrometers (FTIR) as well as a portable XRD/XRF instrument. All spectrometers can be operated under vacuum to remove atmospheric features from the spectra. In addition PEL has extensive sample handling, preparation and storage facilities.

Two Bruker VERTEX 80V spectrometers are equipped with external chambers to measure emissivity. One spectrometer is optimized for the spectral range from 1 to 100 µm with an extension to 0.6 µm currently ongoing. A newly installed second VERTEX 80V is optimized for the spectral range from 0.2 to 1 µm, covering the very important UV range.

An external evacuable chamber allows measuring emissivity for sample temperatures from 50°C to higher than 800°C [1,2]. An innovative induction heating system allows heating the samples uniformly suppressing thermal gradients. For sensitive samples the chamber can also be purged with nitrogen during the measurements. An iron buffer is placed in the chamber to trap excess oxygen. Several temperature sensors allow characterizing the thermal environment precisely while a webcam can monitor the sample during the heating experiments.

A second emissivity chamber for measurements at low to moderate temperatures can be cooled down to 0°C. Samples can be heated from room temperature to 150°C in a purging environment.

A Bruker A513 accessory can be used in both spectrometer to obtain biconical reflectance with variable incidence angle i and emission angle e between 13° and 85° at room temperature, under purge or vacuum conditions. The combination of both spectrometers allows covering the spectral range from 0.2 to 100 µm in reflectance. Samples can be measured before and after exposure to high temperatures in reflectance to characterize irreversible changes in the spectral characteristics.

Examples of thermal space weathering: We have obtained reflectance spectra in the visible spectral range of magnesium, calcium and manganese sulfides before and after thermal processing at Mercury dayside temperatures in vacuum conditions as analog for the hollow forming material [2]. The spectral contrast of all samples is strongly affected by the heating. Both the spectral slope and the color observed before and after thermal processing showed significant changes. We attribute the spectral changes in the visible to an annealing of samples' color centers.

Focusing on the thermal infrared spectral range we could show for the first time experimentally and numerically, how the thermal emissivity spectra of an Mg-rich olivine significantly change as a function of temperature [3]. The temperature variation during Mercury daytime modifies the olivine spectrum shifting in wavelength its emissivity features, simulating the spectrum of an olivine strongly enriched in iron (a Fa abundance increase from 8% to 23%).

Based on the elemental composition of Mercury's surface, provided by the NASA MESSENGER spacecraft we studied a range of terrestrial komatiites as well as a synthetic komatiite at PEL [4]. Our measurements show that spectral changes between fresh and thermally processed samples occur in in the visible and the thermal infrared, but are stronger in the visible range, with reddening affecting all the samples, while darkening is more selective. The synthetic sample, which is nearly iron-free, is most strongly affected. We attribute the spectral changes in the visible again to a removal of samples' color centers.

References: [1] Helbert, J. et al. 2013. *Earth and Planetary Science Letters* 371:252-257. [2] Helbert J, Maturilli A, D'Amore M (2013) Earth Planet Sci Lett 369-370:233–238. doi: 10.1016/j.epsl.2013.03.045 [3] Helbert J, Nestola F, Ferrari S, et al. (2013) Earth Planet Sci Lett 371-372:252–257. doi: 10.1016/j.epsl.2013.03.038 [4] Maturilli A, Helbert J, St. John JM, et al. (2014) Earth Planet Sci Lett 398:58–65. doi: 10.1016/j.epsl.2014.04.035

LATITUDINAL VARIATION IN SPECTRAL PROPERTIES OF THE LUNAR MARIA AND IMPLICATIONS FOR SPACE WEATHERING. D. J. Hemingway[1] (djheming@ucsc.edu), I. Garrick-Bethell[1,2], and M. A. Kreslavsky[1], [1]University of California, Santa Cruz, Department of Earth & Planetary Sciences, 1156 High Street, Santa Cruz, CA, 95064, [2]School of Space Research, Kyung Hee University, Yongin, South Korea.

Observations: Based primarily on Clementine mosaics, we report a previously unrecognized systematic latitudinal variation in the near-infrared spectral properties of the lunar surface, and in particular, within the maria [1]. The effect is not immediately obvious because the spectra are also strongly affected by composition, which varies considerably across the surface. However, when we account for variations in composition, the latitudinal trends emerge (Fig. 1).

Regions near the equator tend to be darker and have higher 950 nm/750 nm band ratios than high-latitude regions of equal composition (Fig. 1A). These latitudinal trends persist across a wide range of compositions but are especially strong and consistent within the maria (Fig. 1B). We show that highlands contamination cannot be responsible for the latitudinal trends and a comparison with constant-phase-angle LOLA reflectance data (Fig. 2) helps to confirm that the trends are not artifacts of phase angle biases.

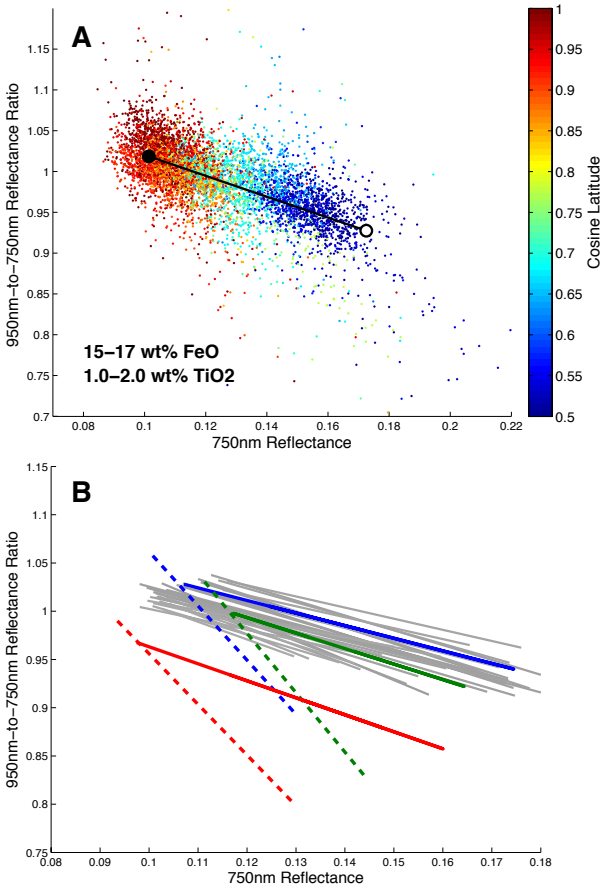

Figure 1: (A) Spectral characteristics of pixels corresponding to one example composition, color-coded by cosine latitude (equatorial pixels in red; high latitude pixels in blue). (B) Latitudinal trends (grey lines) for 28 distinct compositional bins across the lunar maria in comparison with the trends associated with swirls (solid colored lines) and impacts (dashed lines) at Reiner Gamma, Ingenii, and Marginis (red, green, and blue lines, respectively).

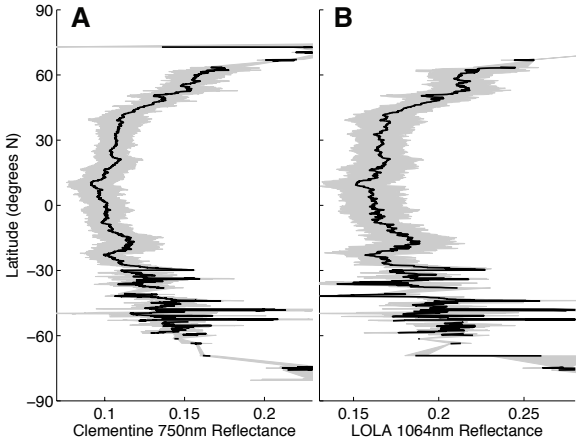

Figure 2: Mean (black lines) and standard deviation (grey bands) of (A) Clementine 750 nm, and (B) LOLA 1064 nm [5] reflectance across the lunar maria. Refelectance tends to be low near the equator and higher at high latitudes.

Discussion: The slopes of the latitudinal color trends (-1.5±0.3) are unlike those associated with impacts (-5.7±0.5) but statistically equivalent to those observed at lunar swirls (-1.6±0.2), suggesting a common mechanism (Fig. 1B). We propose that reduced solar wind flux, which should occur both with increasing latitude (due to the increasing incidence angle), and at swirls (where magnetic fields may be partially shielding the surface from the impinging solar wind [2,3]), is the most likely common mechanism [4]. Our observations lead us to propose a model in which freshly exposed materials initially experience rapid changes in color until reaching a solar wind flux-dependent equilibrium, followed by a more gradual period of optical maturation driven mainly by micrometeoroid impacts.

References: [1] Hemingway et al. (2015) *Icarus*. [2] Hood & Schubert (1980) *Science* **208**, 49–51. [3] Hemingway & Garrick-Bethell (2012) *JGR* **117**. [4] Hapke (2001) *JGR* **106**, 10039–10073. [5] Lucey et al. (2014) *JGR* **119**, 1665–1679.

LUNAR SPACE WEATHERING EFFECTS IN THE ULTRAVIOLET. A. R. Hendrix[1], F. Vilas[1], K. D. Retherford[2], K. E. Mandt[2], T. K. Greathouse[2], J. T. S. Cahill[3], [1]Planetary Science Institute, Tucson, AZ (arh@psi.edu), [2]Southwest Research Institute, San Antonio, TX, and [3]The Johns Hopkins University Applied Physics Laboratory (JHU/APL).

The ultraviolet is an ideal region of the spectrum in which to study space weathering processes and effects because the UV senses largely surface scattering, proportional to Fresnel reflectance, rather than volume scattering. That is, the measured reflectance is directly related to the index of refraction [1]. The index of refraction of many materials increases with decreasing wavelength, so that they become brighter at shorter wavelengths. In the surface scattering regime, absorption (high k) can produce a reflectance maximum. Furthermore, since UV radiation is less penetrating than visible radiation, short wavelengths are more sensitive to thin coatings on grains that may be the result of weathering processes.

Our previous work [2] provided evidence, based on lunar samples and S-class asteroids, that space weathering manifests itself at near-ultraviolet wavelengths (~200-400 nm), 'bluing' the spectrum (i.e., creating a negatively-sloped spectrum), in contrast with the spectral reddening (with a positively-sloped spectrum) that is seen at visible to near-infrared wavelengths (VNIR). UV spectra of lunar soils are bluer than spectra of crushed lunar rocks [2][3][4]. This bluing was further linked to weathering [2] by noting the near-UV spectral behavior of iron (modeled as inclusions in grains) and that the addition of submicroscopic iron (SMFe), likely specifically in the grain rims, would tend to mask the typical Fe^{3+} UV/blue IVCT (intervalence charge transfer) absorption edge (near 300-400 nm) of silicates. Furthermore, it was noted that the effects of space weathering at UV wavelengths tend to appear with less weathering than do the longer-wavelength effects, suggesting that the UV wavelength range is a more sensitive indicator of weathering, and thus age [2][7].

Our more recent work shows that the UV bluing effects extend into the far-ultraviolet (100-200 nm), as confirmed using data from the Lyman Alpha Mapping Project (LAMP) onboard the Lunar Reconnaissance Orbiter (LRO). LAMP data show that the Moon in general is UV blue, consistent with early results from IUE [5]. In the LAMP data, mare regions rise steadily in reflectance from 190 nm down to 130 nm while the highlands regions are spectrally flat between ~160 and 190 nm and rise with a blue slope shortward of 160 nm. Maria are bluer than highlands regions due to greater abundances of opaques such as ilmenite and some pyroxenes.

LAMP data also demonstrate significant spectral differences between mature and immature terrains. Immature terrains (such as visibly-bright crater rays) are somewhat spectrally blue and are significantly *darker* than mature terrains. This could be related to the opaque content: regions of greater opaque concentration (maria and also weathered regions, higher in SMFe) are brighter in the FUV than regions more abundant in silicates (immature regions and some highlands terrains). It could also be related to effects of gardening.

We have also used LAMP data to study the magnetically-anomalous lunar swirl regions [6]. Because swirls are likely regions that are magnetically shielded from the solar wind (e.g. [8]), the spectral differences between swirls and mature terrains can tell us about effects of micrometeoroid bombardment compared to the effects of solar wind processing. We find that these regions, which show VNIR and near-UV [9] evidence of being immature, are spectrally very different from immature terrains at FUV wavelengths: they are not dark like immature regions, but are also not very spectrally blue (if at all). Thus, our initial results suggest that micrometeoroid bombardment – important at swirls - brightens the surface in the UV via gardening of the regolith; the lack of the blue/SMFe signature in the swirls suggests that solar wind particles are primarily responsible for production of SMFe (in non-swirl regions).

Overall, we judge that immature soils are FUV dark due to a relative lack of gardening and are somewhat spectrally blue, the result of a limited amount of solar wind bombardment. Mature soils are relatively FUV bright due to increased gardening and greater SMFe content (the result of solar wind and/or micrometeoroids); mature soils are also bluer than immature soils due to more SMFe. The abundance of ilmenite (and some pyroxenes) can also contribute to spectral blueness in the FUV [5].

References: [1] Henry et al. 1976, *Moon*, 15, 51. [2] Hendrix and Vilas 2006, *Astron. J.*, 132, 1396-1404 [3] Hapke, Wagner, Cohen 1978, *LPSC IX,* 456-458. [4] Wagner, Hapke, Wells 1987, *Icarus,* 69, 14–28. [5] Wells and Hapke 1980, *B.A.A.S.* 12, 660. [6] Hendrix et al. 2015, Far-UV characteristics of lunar swirls, *Icarus, submitted*. [7] Vilas and Hendrix 2015, *Astron. J.* 150, 64-78. [8] Blewett et al. 2011, *J. Geophys. Res.,* 116, E02002, doi:10.1029/2010JE003656. [9] Denevi et al. 2014, *J. Geopys. Res.,* 119, doi: 10.1002 /2013JE004527.

Space Weathering of the NonIce Material on Europa. C.A. Hibbitts[1], C. Paranicas[1], [1]JHU-APL, 11100 Johns Hopkins Rd., Laurel, Md., 20723.; karl.hibbitts@jhuapl.edu; chris.paranicas@jhuapl.edu;

Introduction: The surface of Europa is covered by amorphous water ice and a hydrated nonice material [1,2] that are both constantly bombarded by energetic ions and electrons from the Jovian magnetosphere. This nonice material is either primordial or may be a product of chemical processing of implanted Ionian sulfur ions from the Jovian magnetosphere [e.g. 3]. We propose that the nonice material has an endogenic origin but is subsequently processed, or space weathered, by bombarding particles that were trapped in the Jovian magnetosphere.

Discussion: The chemical and physical expression of the ion bombardment of the nonice material on Europa's surface will have spectral signatures. While much is known about the environment of Europa and there is a basic understanding of the composition and distribution of the nonice material over its surface, the understanding of how the Europan environment alters and weathers the nonice material on its surface is even less mature. Laboratory measurements can address some of these unknowns.

The infrared spectral characteristics of the nonice material informs us that it is likely a hydrated sulfate or sulfuric acid with chemically bound waters of hydration and containing cations of Mg, Ca, and/or Na [e.g. 1, 4]. The space weathering environment at Europa's surface, dominated by protons, sulfur ions, oxygen ions, and electrons that make up the corotating Jovian plasma, will alter this material. In addition, micrometeroid gardening will mix the upper centimeters of the surface burying weathered and altered material while exposing both fresh material and previous altered material [e.g. 5]. In a simple picture, uncharged Iogenic grains that reach Europa's orbit would impact Europa's leading hemisphere, to primarily garden it, whereas the plasma is primarily bombarding the trailing hemisphere (Figure 1). Charged nanograins from Io probably impact the trailing and grains from other sources further complicate the picture. This bombardment of the trailing hemisphere is considered the source of the UV S=O stain and sulfuric acid hydrate on the trailing hemisphere [e.g. 6, 3].

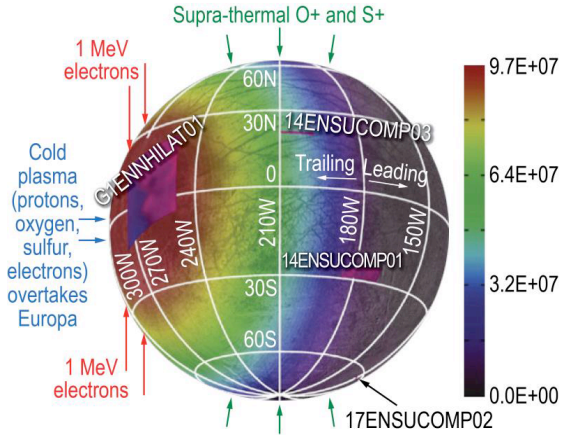

Figure 2. Bombardment of Europa by energetic particles from Dalton et al. (PSS 2013).

The relative rate of sputtering at different locations on the surface has been studied [7] and may be correlated with the amount of exposure of deeper layers and their related constituents. Ion bombardment will also destroy mineral crystallographic structure, which may diminish the strength of related absorption features, such as molecular and lattice vibrational bands and the intensity of crystal field bands. Ion bombardment may also preferentially sputter more weakly bound components of the nonice minerals and thereby may be responsible for the non-oxygen components, such as Na, that have been detected in the exosphere [8]. The nonice material may be depleted in Na due to this process and the reflectance spectrum of the material could change accordingly [9]. The irradiation of organics in the presence of water, such as associated with the hydrated nonice material itself, has been shown theoretically to enable a plethora of reaction pathways producing a large number of simple to complex organic compounds [e.g. 10] and will have spectral signatures distinct from the nonice hydrated material [11].

References: [1] McCord, T.B. et al., (1998), J. Geophys. Res., 103, 8603-8626; [2] Hansen,G.B. and T.B. McCord, (2004), J. Geophys. Res. 109, E01022, doi:10.1029/2003JE002149; [3] Carlson, R.W. et al., (1999), Science, 286, 97, doi: 10.1126/science.286.5437.97; [4] Dalton, J.B. et al., (2005), Icarus, 177, 472-490. [5] Moore et al., 2009, in Pappalardo, R.T., McKinnon, K., Khuran, K (eds), Europa, Univ. Ariz., pp. 329-352. [6] Cassidy, T.A. et al., (2013), Planet. & Space Sci., 77, 64-73; [7] Lane , A. L. et al., (1981), Nature, 292, 38-39. [8] Brown, M.E. and R.E. Hill, (1996), Nature, 380, 229-231; [10] Delitsky, M.L. and A.L. Lane, (1998), J. Geophys. Res., doi: 10.1029/1998JE900020; [11] Dalton, J.B., and K.M. Pitman, (2012), J. Geophys. Res., 117, E09001, doi: 10.1029/2011JE004036;

Acknowledgements: This work has been supported by the OPR Grant NNX10AB83G.

LATITUDE-DEPENDENCE OF MEDIAN GRAIN SIZE IN THE LUNAR REGOLITH. Minsup Jeong[1,2], Sungsoo S. Kim[1], Ian Garrick-Bethell[1,3], So-Myoung Park[1], Chae Kyung Sim[1], Ho Jin[2], Kyoung Wook Min[4], and Young-Jun Choi[2], [1]Dept. of Astronomy & Space Science, Kyung Hee University, Korea, [2]Korea Astronomy and Space Science Institute, [3]Dept. of Earth and Planetary Sciences, University of California, Santa Cruz, USA, and [4]Dept. of Physics, Korea Advanced Institute of Science and Technology, Korea.

Introduction: We have conducted multi-band (U, B, V, R, and I) polarimetric observations of the whole near-side of the Moon with a spatial resolution of 1.1 km. A median grain size map of the near-side regolith of the Moon has been constructed using our polarimetry and albedos. We find that median grain size <d> is a monotonically increasing function of selenographic latitude. At the same latitude, <d> is larger in the maria than in the highlands. The former is thought to be a result of reduced space weathering effects at high latitudes, where the flux of weathering agents such as micrometeoroids is smaller.

Observations and data: We perfomed multi-band polarimetric observation of the whole near-side of the Moon at Lick Observatory using a 15-cm reflecting telescope. The phase angle coverage ranges between 37° and 121°. Polarimetric measurements were made with a polarization filter at 0°, 45°, 90°, and 135° ange at U, B, V, R, and I passbands of Johnson-Cousins filter system. The pixel scale of the images on the Moon corresponds to 1.1 km at the center of the lunar disk.

From our observations, we obtained the degree of linear polarization, P, for each phase angle (α) and passband. Then we constructed a map of polarization maximum, P_{max}, by fitting the observed $P(\alpha)$ to the empirical phase curve obtained by [1]. We also constructed albedo (A) maps for each passband using the Clementine data as calibrators.

Median grain size: We constructed a <d> map for the entire near-side of the lunar disk from our V band A and P_{max} values as suggested by [2] (see Fig. 1). Fig. 2 shows median <d> values at four latitude bins for mare and highland regions. It clearly shows that (1) <d> is a monotonically increasing function of latitude, and (2) at the same latitude, <d> is larger in the maria than in the highlands.

(1) is thought to be a result of reduced space weathering effects at high latitudes, where the flux of weathering agents such as micrometeoroids is smaller. (2) probably indicates that the regolith material in the maria is more resistant to comminution by space weathering than is the material in the highlands. (1) is in agreement with the latitudinal variation in spectral propoerties of the lunar maria found by [3].

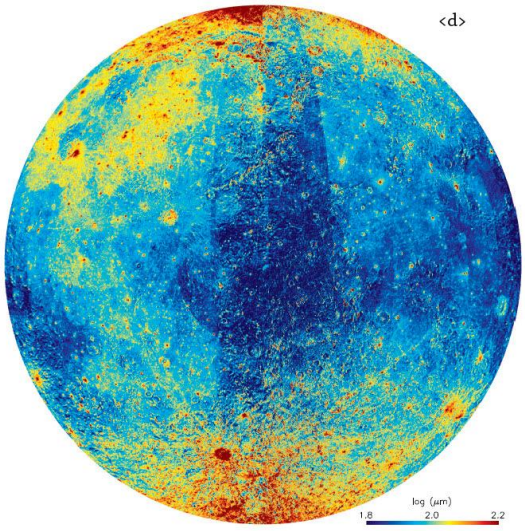

Fig. 1. Median grain size (<d>) map of the near-side of the Moon.

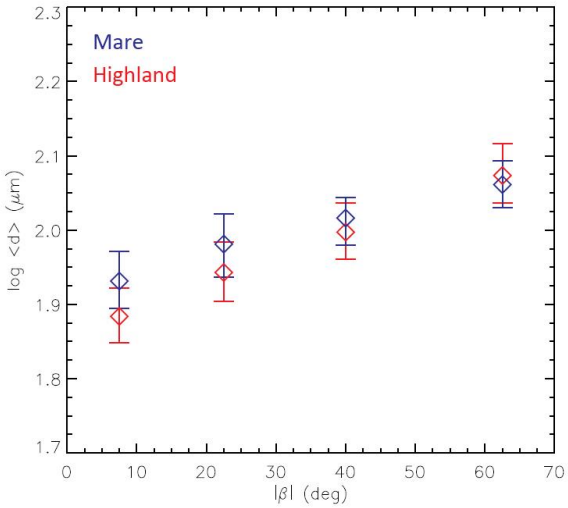

Fig. 2. Medians of the median grain size (<d>) for mare (blue) and highland (red) in the near size of the Moon for four latitude (β) regions.

References: [1] Korokhin V. V. & Velikodsky Yu. I. (2005) *SoSyR, 39*, 45. [2] Dollfus A. (1998) *Icarus, 136*, 69. [3] Hemingway D. J. et al. (2015) *Icarus, in-press*, doi:10.1016/j.icarus.2015.08.004.

THE SPACE WEATHERING IMPLICATIONS OF DIELECTRIC BREAKDOWN IN LUNAR POLAR REGOLITH. A. P. Jordan[1,2], J. K. Wilson[1,2], T. J. Stubbs[3,2], N. R. Izenberg[4], N. A. Schwadron[1,2], H.E. Spence[1,2], [1]EOS Space Science Center, University of New Hampshire, Durham, NH (first author email address: a.p.jordan@unh.edu), [2]Solar System Exploration Research Virtual Institute, NASA Ames Research Center, Moffett Field, California, USA, [3]NASA Goddard Space Flight Center, Greenbelt, MD, [4]The Johns Hopkins University Applied Physics Laboratory, Laurel, MD 20723.

Introduction: A form of space weathering that commonly affects spacecraft has only recently been applied to understanding the airless bodies in the Solar System. Energetic particles in a planet's radiation belt can penetrate electrical insulators, or dielectrics, on spacecraft and cause deep dielectric charging. The charging creates internal electric fields, which, if they become strong enough, can cause dielectric breakdown, or sparking. Breakdown is the leading causing of spacecraft anomalies in Earth's magnetosphere [1], and even Voyager 1 suffered 42 such events when passing through Jupiter's radiation belts [3].

Similarly, solar energetic particles (SEPs) can deep dielectrically charge the regolith of airless bodies. SEPs are sporadically accelerated in solar flares and coronal mass ejections and can penetrate ~1 mm into regolith, which is an effective dielectric. On the Moon, regolith in permanently shadowed regions (PSRs) is so cold (≤50 K) [4] that it has a discharging timescale on the order of weeks—much longer than an SEP event [2]. Consequently, very large SEP events appear capable of charging the regolith so much that the subsurface electric fields are strong enough to cause dielectric breakdown [5]. Recent work indicates that gardened regolith in PSRs has experienced ~10^6 SEP events capable of causing breakdown. Two such events have been detected by the Cosmic Ray Telescope for the Effects of Radiation (CRaTER), aboard the Lunar Reconnaissance Orbiter (LRO) [6]. We build on this previous work to suggest how this breakdown weathering might affect the regolith in the lunar polar regions and on other airless bodies in the Solar System.

Possible Effects of Breakdown Weathering: We find that breakdown weathering may vaporize and melt PSR regolith at a rate of 1.8-3.4 x 10^{-7} kg m^{-2} yr^{-1} [7]. Consequently, breakdown weathering may have affected ~10-25% of gardened regolith—comparable to meteoritic weathering [7]. This suggests that breakdown weathering may significantly affect how PSRs evolve.

Breakdown weathering may therefore affect comminution in PSRs (Figure 1). We use a statistical approach to estimate how breakdown weathering may evolve the distribution of PSR grain sizes. We also consider what fraction of a typical grain may be melt or vapor deposits created by breakdown. We can thus estimate the fraction of grains in the upper ~1 mm that may have experienced breakdown during the two large SEP events detected by LRO/CRaTER. This initial modeling motivates and informs planned future experiments about how breakdown weathering affects comminution and the regolith's optical properties.

Better understanding breakdown weathering may also help interpret remote sensing data from other airless bodies. We briefly discuss whether breakdown weathering might affect Mercury, which has PSRs with temperatures <100 K [8] and is exposed to a higher SEP fluxes than is the Moon [e.g., 9]. Furthermore, many asteroids, such as Vesta, have obliquities that keep a pole in shadow for roughly half an orbit [10, 11], thus making the regolith cold enough [e.g., 12] for breakdown, despite experiencing lower fluxes of SEPs.

References: [1] H. C. Koons et al. (1998), 6th Spacecraft Charging Technology, 7–11, Hanscom AFB, MA. [3] P. Leung et al. (1986), *J. Spacecraft, 23*, 323-330. [4] D. A. Paige, et al. (2010), *Science, 330*, 479-482. [5] A. P. Jordan et al. (2014), *JGR-Planets, 119*, 1806-1821. [6] A. P. Jordan et al. (2015), *JGR-Planets, 120*, 210-225. [7] A. P. Jordan et al. (under review), "Implications of the rate of dielectric breakdown weathering of lunar regolith in permanently shadowed regions," submitted to *Icarus*. [8] A. R. Vasavada et al. (1999), *Icarus, 141*, 179-193. [9] M. A. Dayeh et al. (2010), *Space Weather, 8*, S00E07. [10] A. Kryszczyńska et al. (2007), *Icarus, 192*, 223-237. [11] C. Lhotka et al. (2013), *Astron. Astrophys., 556*, A8. [12] T. J. Stubbs and Y. Wang (2012), *Icarus, 217*, 272-276.

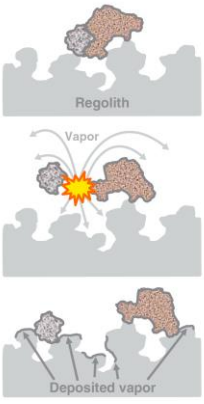

1) Grain at regolith's surface

2) Breakdown vaporizes some of grain's material and splits grain

3) Grain fragments move, changing regolith's porosity; some of vaporized material is deposited on surrounding regolith

Figure 1. Cartoon showing how dielectric breakdown could affect regolith (from [6]).

SPACE WEATHERING TRENDS AMONG CARBONACEOUS ASTEROIDS AND MATERIALS. H. M. Kaluna[1], J. J. Gillis-Davis[1], P. G. Lucey[1], J. R. Masiero[2], K. J. Meech[3]. [1]Hawai'i Institute for Geophysics and Planetology, University of Hawai'i, Honolulu-HI-96822. [2]Jet Propulsion Laboratory, Caltech, Pasadena-CA. [3]Institute for Astronomy, University of Hawai'i, Honolulu-HI.

Introduction: Space weathering effects are difficult to identify on C-complex asteroids due to their low albedos and shallow absorption features [1,2]. Recent observational studies indicate that C-complex asteroids do experience space weathering, but the results show contrasting trends. One study find the spectral slopes decrease with exposure age [3], whereas another finds the slopes increase (i.e. redden) [4]. Combining observations of C-complex asteroids and laboratory experiments on carbonaceous chondrite (CC) materials is a useful approach to investigate the discrepancy in C-complex space weathering trends.

Observational Methods: We use visible spectroscopic and albedo data to search for space weathering trends among the 2.3 Gyr old [5] Themis and < 10 Myr old [6] Beagle C-complex asteroid families. The young Beagle family formed from the breakup of a Themis family member, thus providing a unique tool to assess C-complex space weathering trends while minimizing the effects of composition. We compare slope and albedo data of Themis and Beagle to the young C-complex Veritas asteroid family to assess if mineralogical differences affected the spectral trends found in previous studies [3,4].

Observational Results: The slope and albedo variations between Themis and Beagle families indicate C-complex asteroids become redder and darker in response to space weathering. Although similar in age, the Veritas asteroids exhibit significantly different spectra than the Beagle asteroids. The Veritas family asteroids also appear darker than the Beagle asteroids.

Experimental Methods: Using pulsed laser irradiation, we simulate micrometeorite bombardment-induced space weathering of two phyllosilicates, cronstedtite ($Fe_2^{2+}Fe^{3+}(SiFe^{3+})O_5OH_4$) and lizardite ($(Mg_3Si_2O_5)(OH_4)$), and compare the results to weathered olivine. Each mineral was crushed and dry-sieved to <75 μm and irradiated with a 1064 nm wavelength, pulsed laser. Laser spot size on the sample is 0.25 mm with an incident energy of 30mJ per pulse. A 6-8 nanosecond pulse duration simulates timescales of real micrometeorite dust impacts [7]. The samples were irradiated at various intervals for a total of 40 minutes at 20Hz. Three 0.5g aliquots of each mineral were irradiated. Samples were irradiated as uncompressed powers and under vacuum pressures of 10^{-5} to 10^{-6} mbar. Following each irradiation, the samples were removed from the vacuum chamber for spectral measurement (Figure 1).

Experimental Results: Lizardite spectra became redder at visible wavelengths, but show a slight bluing at near-IR wavelengths with increased irradiation. Cronstedtite initially reddens then become bluer as irradiation time increases in both the visible and near-IR. Lizardite shows little to no changes in albedo, whereas cronstedtite experiences a decrease in both the visible and near-IR wavelengths.

Conclusions: Our laboratory experiments on cronstedtite and lizardite samples yield different spectral responses to laser simulated space weathering. On this basis, both spectral reddening and blueing can be expected in C-complex asteroid families. Modal mineralogy of CCs show a progression from cronstedtite to Mg-serpentines as aqueous alteration progresses [8,9]. Our observational data suggest the Themis and Beagle asteroids have a mineralogy that experiences reddening in response to space weathering. Together these data suggest space weathering trends may depend on the aqueous alteration histories of asteroid parent bodies and may provide a tool to further probe the aqueous histories of C-complex asteroids.

References: : [1] Hapke B. (2001) *JGR, 106,* 10039-10074. [2] Chapman C. R. (2004) *Annual Review of Earth and Planetary Science, 32,* 539-567. [3] Nesvorny D. et al. (2005) *Icarus, 173,* 132-152. [4] Lazzarin M. et al. (2006) *ApJ, 647,* L179-182. [5] Marzari R. et al. (1995) *Icarus*, *113,* 168. [6] Nesvorny D. et al. (2008) *ApJ, 679,* L143. [7] Yamada M. et al. (1999) *Earth, Planets and Space, 51,* 1255. [8] Howard K. T. et al. (2009) *Geochim. Cosmochim. Acta, 73,* 4576-4589. [9] Howard K. T. et al. (2011) *Geochim. Cosmochim. Acta, 75,* 2735-2751.

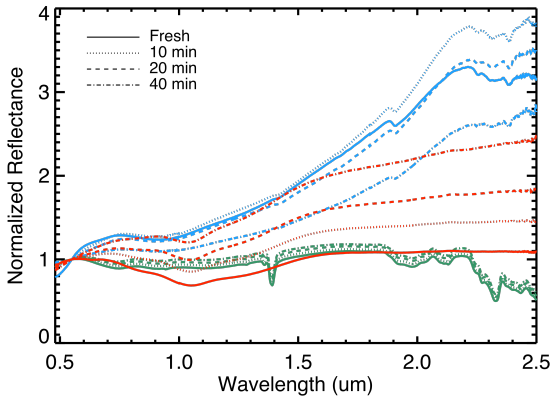

Figure 1: Reflectance spectra of cronstedtite (blue), lizardite (green) and olivine (red), normalized to 0.55μm.

RATES OF SPACE WEATHERING IN LUNAR SOILS. L. P. Keller[1] and S. Zhang[2]. [1]ARES, Code XI3, NASA/JSC, Houston, TX 77058 (Lindsay.P.Keller@nasa.gov). [2]Texas Materials Institute, Univ. Texas, Austin, TX 78712.

Introduction: Lunar soil grains record the combined effects of several regolith processes related to the impact and irradiation history. In fine size fractions of mature soils, pristine (unaltered) surfaces are rare, nearly all silicate surfaces are amorphous with at least some nanophase Fe metal inclusions. It is these fine size fractions of lunar soils that dominate the bulk optical properties of a soil. The amorphous silicate surfaces are not all the same, and include high-T melts, solar wind amorphized crystals and impact-generated vapor deposits. A major unanswered question is the rate at which space weathering effects are acquired in lunar reglith materials. Here we use the accumulation of solar flare particle tracks in individual lunar grains to estimate their exposure age – we then use electron microscope techniques to measure the space weathered rim thickness and composition to determine its formation process.

Materials and Methods: We analyzed <20μm anorthite grains in microtome thin sections from several different soils showing a range of maturity: 67701 10084 and 62231. The microtome thin sections were analyzed using a JEOL 2500SE scanning and transmission electron microscope (STEM) equipped with a Thermo-Noran thin window energy-dispersive X-ray (EDX) spectrometer. We used the recent calibration of the solar flare track production rate in lunar anorthite determined by [1] to estimate exposure ages.

Results and Discussion: Two physically and chemically distinct grain rim types are common in lunar soils. *Solar wind amorphized rims* on anorthite are amorphous, lack inclusions, and are compositionally similar to the host grain. The *vapor-deposited rims* on anorthite are also amorphous, but are compositionally different from the host, and have inclusions of nanophase Fe metal throughout their width. Previous work has shown that the two rim types are equiabundant in mature soils [2], but it is also common to observe vapor-deposited material on top of a solar wind damaged layer. Over 90% of the grains we measured have solar flare track exposure ages <10 My.

The width of *vapor-deposited rims* on anorthite shows no correlation with exposure age suggesting that the deposition occurred in a single or only a few events during the grain's lifetime (Fig. 1). The width of *solar wind amorphized rims* on anorthite increases as a smooth function of exposure age until it levels off at ~180 nm after ~20 My (Fig. 1). Solar wind damage can only accumulate if the grain has a direct line of sight to the Sun, whereas solar flare particles can penetrate mm of regolith. Thus, tracks can accumulate while the particle is not directly exposed at the lunar surface. To assess whether the track density accurately predicts surface exposure, we measured the amorphized rim width and track density in anorthite from the surface of rock 64455 [1] that was never buried, and has a well constrained surface exposure age of 2 My based on isotopic measurements [3]. The 60-70 nm rim width from 64455 plots within error of the well-defined trend for solar wind amorphized rims in Fig. 1, indicating that the measured solar flare track densities are accurately reflecting the surface exposure of the grains. This result however, is 2-3 orders of magnitude longer than the rapid (~10^3-10^4 y) development of amorphized layers predicted by numerical models [4, 5]. The source of this discrepancy is not known.

Conclusions: Space weathering effects (both vapor-deposited rims and solar wind amorphized rims) accumulate in 10^6-10^7 y in mature lunar soils based on observed solar flare track densities in individual space-weathered grains.

References: [1] Berger, E. L. and Keller, L. P. (2015) *LPS XLVI*, #1543. [2] Keller, L. P. and McKay, D.S. (1997) *GCA* 61, 2331. [3] Blanford, G. E. *et al.* (1975) *PLPSC 6th*, 3557. [4] Loeffler, M. J. *et al.* (2009) *JGR-Planets* 144, 3003. [5] Christoffersen, R. & Keller, L. P. (2015) *LPS XLVI*, #2084.

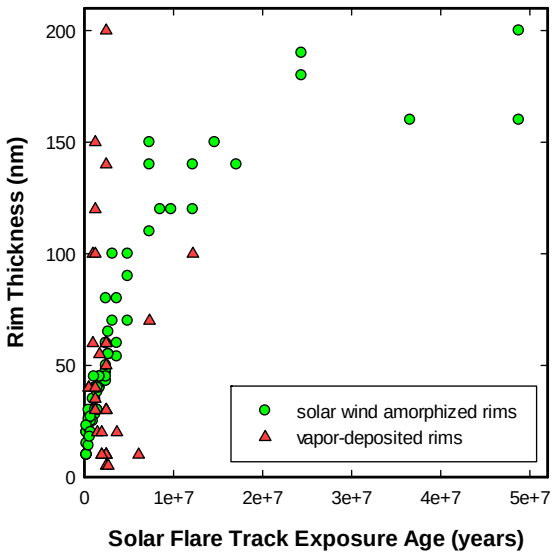

Figure 1. A plot of rim thickness versus solar flare track exposure age for solar wind amorphized and vapor-deposited rims on lunar anorthite.

SURFACE EXPOSURE AGES OF SPACE-WEATHERED GRAINS FROM ASTEROID 25143 ITOKAWA. L. P. Keller[1], E. L. Berger[2] and R. Christoffersen[3]. [1]ARES, Code XI3, NASA/JSC, Houston, TX 77058 (Lindsay.P.Keller@nasa.gov). [2] Geocontrol Systems, Jacobs JETS contract, NASA/JSC, Houston, TX 77058.

Introduction: Space weathering processes such as solar wind ion irradiation and micrometeorite impacts are widely known to alter the properties of regolith materials exposed on airless bodies. The rates of space weathering processes however, are poorly constrained for asteroid regoliths, with recent estimates ranging over many orders of magnitude [e.g., 1, 2]. The return of surface samples by JAXA's Hayabusa mission to asteroid 25143 Itokawa, and their laboratory analysis provides "ground truth" to anchor the timescales for space weathering processes on airless bodies.

Materials and Methods: Itokawa particles RAQD02-0211 (0211) and RA-QD02-0125 (0125) were allocated by JAXA; particle RA-QD02-0192 (0192) was allocated by NASA. Multiple electron transparent thin sections of each of these samples were prepared via a hybrid ultramicrotomy-focused ion beam (FIB) technique using an ultramicrotome and a FEI Quanta 3D dual-beam FIB-SEM [3]. Transmission electron microscope (TEM) analyses were acquired with a JEOL 2500SE 200kV field emission STEM.

Results: Itokawa particles 0211, 0192, and 0125 are all olivine-rich (Fo_{70}) and contain minor Fe-sulfides. They have continuous solar wind damaged rims that are structurally disordered, nanocrystalline, and compositionally similar to the cores of the grains. All three particles have adhering mineral grains and melt particles, as well as solar flare particle tracks (tracks). Compared to lunar soil grains with a similar exposure history, the Itokawa grains are notable for a relative lack of abundant melt spherules and vapor deposits. Interestingly, the track densities and rim thicknesses vary across all three particles. Particle 0211 exhibits a track density gradient across the grain that correlates with the rim thickness. The widest solar wind damaged rim (~80 nm) is on the side of the particle with the highest track density (3.4×10^9 tracks/cm^2), while the thinnest rim (~40 nm) is on the opposite side of the particle (track density: 9.2×10^8 tracks/cm^2). Particle 0192 also shows a track density gradient (2.9×10^9 to 1.1×10^9 tracks/cm^2) and has similar rim widths to particle 0211. Particle 0125 shows a track density of 1.1×10^9 tracks/cm^2) and a solar wind damaged rim thickness of ~50 nm. Applying the track production rate calibration of [4] to the Itokawa particles gives surface exposure ages of ~80,000 years for 0211, ~70,000 years for 0192, and ~25,000 years for 0125.

Discussion: Based on the solar flare particle track production rate in olivine at 1AU, the Itokawa grains recorded solar flare tracks over timescales of $<10^5$ years. Interestingly, the preservation of well-defined solar flare track gradients in all three particles indicates that they maintained a relatively stable orientation at mm to cm depths for ~10^4–10^5 years in the Itokawa regolith. Plots of track density vs. depth for the particles showing track gradients reveal no changes or breaks in slope suggesting the particles experienced little or no erosion of their surfaces.

Over timescales of a few 10^3 years, interaction with the solar wind produces ion-damaged rims on the outer ~100 nm of grains that are exposed on the uppermost surface of lunar and asteroidal regoliths. The damaged rims on Itokawa grains are predicted to become amorphous and reach a steady state thickness of 80–100 nm within a few thousand years [5]. As the rims are not amorphous and portions are thinner than 60–70 nm, this suggests their direct exposure to the sun was less than ~10^3 years. Although rims are generally continuous around the grain circumference, their thickness varies in a manner suggesting different sides of the grain had different solar wind exposure times. This indicates the Itokawa regolith was sufficiently dynamic for the grains to rotate, but not so dynamic that the grains become lost to space.

Conclusions: Space weathering of regolith particles on airless bodies results in a number of morphological changes, including cosmic ray exposure tracks, solar flare particle tracks and solar wind damaged rims. Each of these space weathering effects yields information about particle histories at different depths and over multiple timescales. Together, they give us information about the regolith dynamics on asteroid Itokawa. The presence of track gradients in the particles indicates that the regolith in the Muses-C region on Itokawa was relatively stable at mm to cm-depths for the last ~10^5 years, implying little overturn. We conclude that only late in their history ($<10^3$ years) were the particles directly exposed to the solar wind. The continuous nature of the damaged rims on the Itokawa particles however, requires grain movement on the uppermost surface of Itokawa in order to expose all sides of the particles to the solar wind.

References: [1] Willman, M. *et al*. (2010) *Icarus*, 208, 758. [2] Vernazza, P. *et al*. (2009) *Nature*, 458, 993. [3] Berger, E. L. & Keller, L. P. (2015) *Microscopy Today*, 23, 18. [4] Berger, E. L. & Keller, L. P. (2015) *LPS XLVI*, #1543. [5] Christoffersen, R. & Keller, L. P. (2015) *LPS XLVI*, #2084.

EXPERIMENTAL SPACE WEATHERING OF CARBONACEOUS CHONDRITE MATRIX. L. P. Keller[1], R. Christoffersen[2], C. A. Dukes[3], R. A. Baragiola[3], and Z. Rahman[2]. [1]ARES, Code XI3, NASA/JSC, Houston, TX 77058 (Lindsay.P.Keller@nasa.gov). [2]Jacobs, NASA/JSC, Code XI, Houston, TX, 77058. [3]Laboratory for Atomic and Surface Physics, University of Virginia, Charlottesville, VA 22904.

Introduction: Space weathering effects are widely recognized to have altered the optical, chemical, and physical properties of regolith materials exposed on airless bodies. Their effects on primitive carbonaceous asteroids however, are poorly understood and will be critical for interpreting the nature of regolith materials returned by future missions (Hayabusa 2 and OSIRIS-REx) that are targeting primitive, dark, organic-rich near-Earth asteroids.

We performed an irradiation experiment on the Murchison CM2 carbonaceous chondrite to simulate space weathering by solar wind exposure and characterized the irradiated material with infrared spectroscopy and transmission electron microscopy techniques [1,2]. Helium ion irradiation of Murchison matrix resulted in amorphization of the matrix phyllosilicates, loss of OH, surface vesiculation, and a significant reduction of the Fe^{3+}/Fe^{2+} ratio in fine-grained phyllosilicates.

Materials and Methods: A polished thin section of Murchison was irradiated with 4 kV He^+ (normal incidence) to a total dose of $1x10^{18}$ He^+/cm^2. We obtained *ex situ* Fourier-transform infrared (FTIR) reflectance spectra from multiple areas of matrix, ~150 μm^2 in size, using a Hyperion microscope on a Vertex Bruker FTIR bench. A JEOL 7600F field emission scanning electron microscope (SEM) was used to study the morphological effects of the irradiation. We extracted thin sections from both irradiated and unirradiated regions in matrix using focused ion beam (FIB) techniques with electron beam deposition for the protective carbon strap to minimize surface damage artifacts from the FIB milling. The FIB sections were analyzed using a JEOL 2500SE scanning and transmission electron microscope (STEM) equipped with a Gatan Tridiem imaging filter. Electron energy-loss spectroscopy (EELS) data were collected from 50 nm diameter regions at low electron doses to minimize possible artifacts from electron-beam irradiation damage [2, 3].

Results and Discussion: The irradiated matrix showed lower reflectance in the near-IR and a red-sloped continuum compared to the un-irradiated matrix spectra. The depth of the 3 μm OH/H_2O feature (relative to the 10 μm silicate feature) is decreased in the irradiated regions. SEM imaging shows that the irradiated matrix regions have a "bubbly" or "frothy" texture, with numerous sub-μm rounded holes and voids relative to the un-irradiated material. TEM analysis of the FIB sections show that the frothy texture in the irradiated matrix results from the formation of irregulary-shaped 50-100 nm voids at the sample surface. High-resolution TEM imaging shows that the phyllosilicates (mainly serpentine group minerals) have been rendered amorphous from the irradiation to a depth of ~150-200 nm. There is excellent agreement between the total thickness of the amorphized layer and the He^+ ion damage depth obtained from SRIM calculations [5].

Fe $L_{2,3}$ EELS spectra from fine-grained matrix phyllosilicates in CM chondrites show mixed Fe^{2+}/Fe^{3+} oxidation states with abundant $Fe^{3+}/\Sigma Fe$ ~0.7 [4]. Fe $L_{2,3}$ spectra from the irradiated/amorphized matrix phyllosilicates show higher Fe^{2+}/Fe^{3+} ratios (Fe^{2+}/Fe^{3+} ~0.52) compared to spectra obtained from pristine material at depths beyond the implantation/amorphization layer (Fe^{2+}/Fe^{3+} ~0.28). Fe metal was not detected in the EELS spectra from the irradiated material.

We also obtained O *K* spectra from phyllosilicates in both regions of the sample. The O *K* spectra show a pre-edge feature at ~530.5 eV that is related to O 2*p* states hybridized with Fe 3*d* states. The intensity ratio of the O *K* pre-edge peak relative to the main part of the O *K* edge (that results from transitions of O 1*s* to 2*p* states) is lower in the irradiated layer compared to the pristine material and may reflect the loss of O (as OH) as was observed by IR spectroscopy.

Conclusions: Irradiation of Murchison matrix with 4 keV He^+ produced several changes including: the amorphization of the phyllosilicates to a depth of ~200 nm, blistering and void/vesicle development at the surface, a loss of OH from the hydrated silicates, and partial reduction of Fe^{3+} to Fe^{2+} in fine-grained phyllosilicates. The lack of nanophase Fe metal in the irradiated materials suggests that the darkening and reddening observed in the near-IR is likely due to the surface roughness changes or possibly to Fe^{2+}-Fe^{3+} charge transfer effects.

References: [1] Keller, L. P. *et al.* (2015) *LPS* 46, #1913. [2] Keller, L. P. *et al.* (2015) *MAPS* 50, #5354. [3] Garvie, L. A. (2010) *Am. Min.* 95, 92. [4] Zega, T. J. *et al.* (2004) *EPSL* 223, 141. [5] Ziegler, J.F. *et al.* (2006) Stopping and Range of Ions in Matter http://srim.org.

MULTI-BAND POLARIMETRY OF LUNAR REGOLITH MATERIALS IN LABORATORY. Il-Hoon Kim, Minsup Jeong, Chae Kyung Sim, Kilho Baek, and Sungsoo S. Kim, Dept. of Astronomy & Space Science, Kyung Hee University, Yongin, Gyeonggi 17104, Korea.

Introduction: To understand the polarization characteristics of the lunar regolith, we have carried out multi-band (U, B, V, and R passbands) polarimetric measurements. Powders of the four materials that are found in the lunar regolith (SiO2, Fe2O3, Al2O3, CaO) and JSC-1A, the lunar soil simulant, were considered. Although numerous laboratory measurements have dealt with powdered volcanogenic products and chemicals (*e.g.*, [1-3]), their laboratory environments such as the preparation methods of the materials, observing wavelengths, the light source simulating the sunlight are quite different from each other. In this work, we carried out multi-band polarimetric measurements of five materials in a consistent way.

Laboratory Measurements: We prepared powders of four materials (SiO_2, Fe_2O_3, Al_2O_3, CaO), which compose a large percentage of the lunar regolith, size-sieved silicon carbide (SiC) in three different sizes ranging from 12.7 μm to 127 μm, and the lunar soil simulant JSC-1. Powdered sample was placed on a black tray between the lighting unit and the imaging unit. The phase angle (*i.e.* the angle lamp–sample–camera) is acquired by adjusting the positions of the lighting unit and the imaging unit keeping a fixed 110 cm distance to both directions.

A 3800K white lamp and a depolarizer compose the lighting unit. The imaging unit, CCD camera, color filter set and polarization filter are identical to those used in the ground-based observations on the moon by [4].

For each material, we have measured the degree of polarization as a function of phase angle at U, B, V, and R passbands. We also obtained albedo of each material at phase angle of 90°.

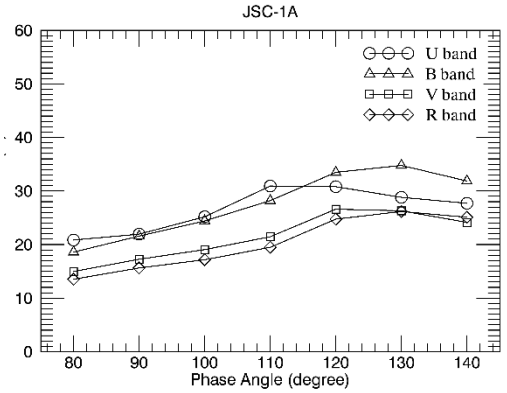

The degree of polarization increases when the phase angle (α) is small, reaches its polarization maximum P_{max} at α_{max} ~ 110°-130°, and then decreases. We note that α_{max} is smaller in U band. The polarization phase curves show plateau-like features around α_{max}.

We also carried out the same measurements for different porosities. We achieved higher porosity by pouring the material very slowly through three separate sieves placed vertically with some gaps. We find that higher porosity results in smaller degree of polarization and that such a change is larger when α is larger..

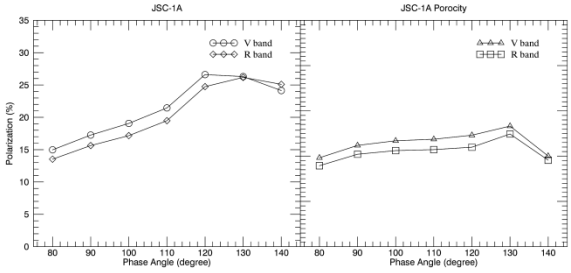

References: [1] Clarke, D. (1965) *MNRAS, 130*, 83C. [2] Coffeen, D. L. (1965) *AJ. 70*, 403-413. [3] Pellicori, S. F. (1969) *AJ, 74*, 1077-1072. [4] Jeong, M. (2015) *this workshop*.

SPACE WEATHERING INDUCED SLOPE CHANGES IN PYROXENE AND HOWARDITE SPECTRA.
T. Kohout[1, 2], O. Malina[3], A. Penttilä[1], A. Kröger[1], D. Britt[4], J. Filip[3], K. Muinonen[1,5], R. Zbořil[3], [1] Department of Physics, University of Helsinki, Finland (tomas.kohout@helsinki.fi), [2] Institute of Geology, The Czech Academy of Sciences, Prague, Czech Republic, [3] Regional Centre of Advanced Technologies and Materials, Departments of Physical Chemistry and Experimental Physics, Palacky University Olomouc, Czech Republic, [4] Department of Physics, University of Central Florida, USA, [5] Finnish Geospatial Research Institute, Masala, Finland.

Introduction: The major reason for spectral changes in lunar-type space weathering is production of nanophase iron ($npFe^0$) in the lunar regolith. The spectral changes include attenuation of silicate absorption bands, darkening, and slope change (reddening). Observations of the asteroid Vesta recently visited by DAWN mission revealed a different pattern of spectral changes (e.g. [1]). The darkening and the absorption band attenuation occur in similar way as on the Moon. The reddening, however, is not apparent. Thus, is space weathering on Vesta distinct from that we see on the Moon? Or is another mechanism, such as the addition of carbonaceous darkening material responsible for spectral darkening of Vesta?

Space weathering experiments with pyroxene and howardite: In order to study effects of $npFe^0$ on reflectance spectra a pyroxene (En 90) and howardite (NWA 1929) powder samples were subjected to the space weathering experiments using the double-heating method described in [2]. The aim of the experiments is to produce the $npFe^0$ on the silicate mineral grains with control of their concentration and size and to quantify related spectral changes.

Reflectance spectra: Both enstatite and howardite show progressive changes in their spectra as a function of the increasing $npFe^0$ amount (Fig. 1). In general, pyroxene is more resistant to space weathering than olivine (e.g. [3]) what is also seen in our simulations. Higher heating temperatures are needed to produce the same amount of $npFe^0$ than in the olivine [2] case.

This quantitative comparison confirmed a trend observed earlier in olivine where spectral parameters change with logarithm of the [2]. An interesting feature was observed in the comparison of the slope over the 1 and 2 μm bands in both pyroxene and howardite. While the slope over 2 μm band show progressive reddening with increasing $npFe^0$ amount (similarly to olivine), the situation is reversed in 1 μm band region (Fig. 1). The relative reduction in red slope is observed in this region.

This is due to the fact that the decrease in reflectance when adding $npFe^0$ is a nonlinear process where higher reflectance values will decrease more than lower values. If the original slope is positive, as the slope over the 1 μm band in pyroxene and howardite, the slope will decrease with increasing $npFe^0$, and vice versa. In addition, the $npFe^0$ has a small positive slope itself in the VIS-NIR range, and that will turn originally zero slopes in the host mineral into positive slopes when adding $npFe^0$.

This finding can potentially explain some of the space weathering observations for Vesta. The majority of DAWN observations were done in the 1 μm region where lack of reddening is observed, similar to our pyroxene and howardite results.

Conclusions: Based on our space weathering laboratory results the lack of reddening over 1 μm region as observed on Vesta does not contradict the space weathering mechanism driven by the presence of $npFe^0$. In order to confirm this more NIR data from Vesta are needed over the 2 μm region where our experiments predict progressive reddening.

References:

[1] Reddy V. et al. (2012) *Science* 336, 700-704 [2] Kohout T. et al. (2014) *Icarus, 237,* 75-83. [3] Quadery A. et al (2015) *JGR-Planets* 120, 1-19.

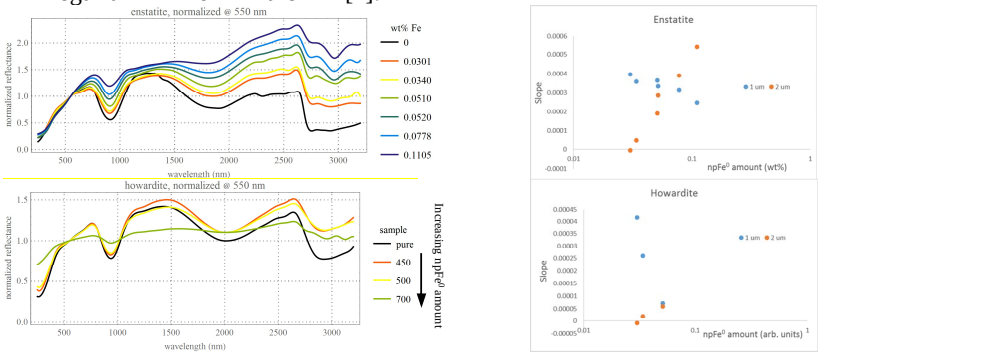

Fig. 1. Normalized reflectance spectra and slope change of pyroxene and howardite as a funnction of $npFe^0$.

SPACE WEATHERING EFFECTS IN THE VISIBLE-IR DOMINATED BY SOLAR WIND AT EARTH-MOON DISTANCE. G. Y. Kramer, Lunar and Planetary Institute Houston, TX 77058, kramer@lpi.usra.edu.

Introduction: Although it is generally agreed that the micrometeorites and solar wind ions are the agents largely responsible for weathering the surfaces of airless bodies, it is still a matter of debate as to which of these plays a more important role [e.g., 1-5]. However, the lunar swirls demonstrate the dominance of the solar wind on space weathering, at least at the Earth-Moon distance. This is based on mounting evidence that the lunar swirls and their characteristic properties are manifestations of the solar wind's interaction with the complex patterns and variable field intensities of the lunar magnetic anomalies [e.g., 6-15]. As such, the swirls are ideal for distinguishing between solar wind ions and micrometeorites, as well as their effects because one is influenced by the magnetic anomalies, while the other is not.

Discussion: Evidence that the swirls mature at a much slower rate, and that adjacent, off-swirl regions mature at an accelerated rate (compared with maturation rates at non-swirls regions) derived from a comparison of the density of immature craters on- vs. off-swirl, and plots of the spectra from these immature craters and soils at on- or off-swirl regions [10,11]. These plots showed differential spectral maturation trends. Immature craters on-swirl exhibited a wide range in albedos, and only slight spectral reddening compared to the mature (off-swirl) soil. This is evidence of retarded weathering on the swirls. In contrast, spectra sampled from fresh craters and the mature regolith in off-swirl regions were all very dark, had a very limited range in albedos, and exhibited little to no spectral reddening. This is evidence of accelerated weathering at off-swirl regions.

Nanophase iron ($npFe^0$) is the space weathering product that has the strongest influence on reflectance spectra, and its abundance in a soil is correlated with that soil's exposure age [16]. $NpFe^0$ is created in three ways: (1) sputtering, (2) impact vaporization and deposition, and (3) agglutination [e.g., 17-21]. The first two ways create $npFe^0$ by breaking the Fe-O bond, liberating O, and depositing native iron. These two processes typically work on very small scales (i.e., grain surfaces up to a few molecule layers deep), and create npFe0 particle sizes usually <10 nm in diameter. The third way involves micrometeoroid impacts of sufficient size to provide the energy for melting to occur, and generates a much broader size distribution of $npFe^0$ particle sizes. Here, smaller $npFe^0$ particles are created through chemical reduction by implanted solar wind hydrogen, while larger sizes are created via coalescence of smaller particles. Sputtering is largely caused by solar wind particles, 95% of which are protons. Micrometeorites are responsible $npFe^0$ created by impact vaporization and agglutination. A solar wind proton is the only space weathering agent that can be influenced by the lunar magnetic anomalies. Magnetic shielding deflects solar wind ions away from the on-swirl surfaces and diverts them onto off-swirl surfaces. On-swirl maturation is retarded because (1) the flux of space weathering agents that create $npFe^0$ is reduced and (2) the creation of larger $npFe^0$ by agglutination is restricted by the decreased availability of small $npFe^0$. Spectrally, this retarded space weathering process begins with a slow spectral reddening in the UV-VIS as the abundance of smaller $npFe^0$ created by sputtering and vaporization deposited on grain surfaces increases. Eventually, the spectral effects of larger $npFe^0$ particle sizes are observable once the abundance of $npFe^0$ is sufficient to create these particle sizes by agglutination. Sampled off−swirl craters exhibit only spectral darkening (and accompanying reduction in absorption band depth) with little to no reddening. Off-swirl regions do not simply experience an increased flux in solar wind ions, the deflected protons create a greater proportion of larger $npFe^0$ particles off-swirl relative to both on-swirl and lunar surfaces not influenced by a magnetic field.

Conclusions: These results underscore the importance of the solar wind as an agent of space weathering. Studying the swirls and magnetic anomalies on the Moon is ideal for distinguishing the optical, chemical, and physical effects of space weathering by solar wind ions vs. micrometeorites. The dominance of one of these agents over the other may be very different at locations other than the Earth-Moon distance, but the knowledge gained from studying space weathering at lunar swirls will improve interpretation of remote sensing observations of other airless bodies. Indeed, it has been suggested that anomalous color on asteroids could be indicative of the presence of a magnetic field [22].

References: [1] Jedicke, R. et al. (2004) *Nature 429,* 275-277. [2] Willman, M. et al. (2008) *Icarus 195*, 663-673. [3] Mothe-Diniz, T. and Nesvorny, D. (2008) *Astron. Astrophys. 486*, L9-L12. [4] Strazzulla, G. et al. (2005) *Icarus 174,* 31-35. [5] Marchi, S. et al. (2005) *Astron. Astrophys. 443*, 769-775. [5] Hood, L. and Schubert, G. (1980) *208,* 49-51. [6] Hood, L. and Williams, C. (1989) *PLPSC 19,* 99-113. [7] Richmond, N. et al. (2005) *J. Geophys. Res. 110,* E05011. [8] Wieser M. et al. (2010) *Geophys. Res. Lett., 37,* 5103-5107. [9] Blewett, D. et al. (2011) *J. Geophys. Res. 116,* E02002. [10] Kramer, G. et al. (2011) *J. Geophys. Res. 116,* E04008. [11] Kramer, G. et al. (2011) *J. Geophys. Res. 116,* E00G18. [12] Neish, C. et al. (2011) *Icarus 215,* 186-196. [13] Hemingway, D. and Garrick-Bethell, I. (2012) *J. Geophys. Res. 117*, E10012. [14] Poppe, A. et al. (2014) *Geophys. Res. Lett. 41,* 4865-4872. [15] Glotch, T. et al. (2015) *Nat. Comm. 6,* 6189. [16] Morris, R. (1976) *PLPSC 7,* 315-335. [17] Hapke, B. et al. (1975) *The Moon 13,* 339-353. [18] Keller, L. and McKay, D. (1993) *Science 261,* 1305-1307. [19] Keller, L. and McKay, D. (1997) *GCA 61,* 2331-2340. [20] Hapke, B. (2001) *J. Geophys. Res. 106,* 10039-10074. [21] Noble, S. et al. (2007) *Icarus 192,* 629-642. [22] Vernazza et al. (2006) *Aston. Astophys. 41, L*43-L46

CORRELATIVE MICROSCOPY AND VISIBLE/NEAR-INFRARED SPECTRAL ANALYSIS OF SIMULATED SOLAR WIND IMPLANTED OLIVINE. K. R. Kuhlman[1], A. Kvit[2], K. Baba[3], J. D. Poplawsky[4], T. Hiroi[5], and D. Isheim[6], [1]Planetary Science Institute. E-mail: kim@psi.edu; [2]University of Wisconsin-Madison, [3]Industrial Technology Center of Nagasaki, [4]Center for Nanophase Materials Sciences, Oak Ridge National Laboratory; [5]Department of Earth, Environmental and Planetary Sciences, Brown University; [6]Department of Materials Science & Engineering, Northwestern University.

Introduction: In an extensive review of the literature on "space weathering", Hapke defines the term as an "aggregate of the physical and chemical changes that occur to material exposed on the surface of an airless body" [1]. The processes that can affect these changes include the solar wind, ultraviolet radiation, meteorite and micrometeorite impacts, and solar and galactic cosmic rays. It has been demonstrated that small particles (<50 nm) of $npFe^0$ darken and redden spectral properties while large particles (>50 nm) of $npFe^0$ only darken spectra [2,3]. Recently it has also been shown using scanning transmission electron microscopy (STEM) that hydrogen implanted into silicates generates H_20 and -OH [4]. The mechanism(s) of $npFe^0$ formation within low-iron materials and their kinetics are not well understood and remain contentious [5,6]. In fact, some investigators have found that hydrogen implantation causes depletion in the water content of irradiated samples [7].

Methodology: Here we present the results of the first correlative microscopy study of a sample of San Carlos olivine (Fo90.1 [8]) exposed to simulated solar wind-based space weathering due to hydrogen (~1keV/amu). This work was accomplished using plasma source ion implantation (PSII) similar to work performed previously on orthopyroxene [9], except that here we used a fluence of 10^{17} H ions/cm^2. A pressed pellet consisting of ground SCO sieved to less than 75 micrometers and previously analyzed at RELAB (Brown University) using VNIR was implanted alongside the polished sample for further VNIR analysis. The samples were removed from the PSII chamber and returned to the U.S. where the polished sample was coated with 100 nm nickel and prepared for atom probe tomography (APT) and scanning transmission electron microscopy (STEM) using standard focused ion beam (FIB) liftout methods [10]. The pressed pellet was returned to RELAB for VNIR analysis. STEM was performed using the TITAN microscope (FEI, Inc.) at the University of Wisconsin and APT was performed using the local electrode atom probe (LEAP; Cameca, Inc.) at Oak Ridge National Laboratory.

Results: The VNIR analysis of the pressed olivine pellet demonstrated no change in darkening or reddening, contrary to previous results from a polished specimen implanted with 10^{18} H ions/cm^2. STEM imaging indicates that dislocation loops *may* be forming in the implantation damaged olivine. The highly defective and very unstable hydrogen implanted olivine was found to be very easily damaged in the electron beam, with damage occurring within 2-10 seconds using a 20 pA probe (probe size 8, resolution ~0.8 A) to amorphise this area completely. The APT analysis revealed a very complex structure within the outer 20 nm of the specimen's surface, corresponding to the STEM images. A proximity histogram concentration profile ("proxigram") generated using a 50 at.% nickel isosurface to approximate the original surface of the implanted SCO before nickel capping yields a nominal concentration profile of the sample. The profiles of hydrogen ions as part of hydroxyl ions at 17 amu as seen by APT roughly matches the profile calculated by a basic SRIM Monte Carlo simulation [11]. The implanted layer hosts clusters enriched in iron approximaly 4-7 nm below the surface.

Acknowledgements: This research was partially conducted at the Center for Nanophase Materials Sciences, which is a DOE Office of Science User Facility. The authors also gratefully acknowledge use of facilities and instrumentation supported by NSF through the University of Wisconsin Materials Research Science and Engineering Center (DMR-1121288).

References: [1] Hapke, B. (2001) *Journal of Geophysical Research-Planets* 106:10039-10073. [2] Lucey, P. G. and M. A. Riner (2011) Icarus 212:451-462. [3] Noble, S. K., et al. (2007) Icarus 192:629-642. [4] Bradley, J. P. et al., *Proceedings of the National Academy of Science U.S.A.*, 111:1732-1735. [5] Marchi S., et al. (2010) *Astrophysical Journal Letters* 721:L172-L176. [6] Pieters, C. M. (2000) *Meteoritics & Planetary Science* 35:1101-1107. [7] Burke, D. J., et al. (2011) Icarus 211:1082-1088. [8] Fournelle, J. (2009) AGU Fall Meeting, Abstract #V31E-2009. [9] Kuhlman, K. R., et al. (2015) *Planetary and Space Science*, 115:110-114. [10] Miller, M. K., et al. (2007) *Microscopy and Microanalysis* 13:428-436. [11] Ziegler, J.F., M.D. Ziegler and J.P. Biersack (2010) *Nuclear Instruments and Methods in Physics Research, Section B*, 268:1818-1823.

SPACE WEATHERING ON PRIMITIVE ASTEROIDS: ION IRRADIATION OF CARBONACEOUS CHONDRITES. C. Lantz[1], R. Brunetto[2], and M.A. Barucci[1], [1]LESIA – Observatoire de Paris, CNRS/Univ. Pierre et Marie Curie/Univ. Paris Diderot, Meudon, France (cateline.lantz@obspm.fr), [2]IAS, CNRS/Univ. Paris Sud, Orsay, France.

Introduction: The exposition of airless bodies to the harsh environment in which they evolve (solar ion irradiations, micrometeorite bombardments, etc.) leads to surface alterations affecting spectra. This phenomenon is known as space weathering (SpWe). Lot of studies have been made on S-type asteroids and silicate materials, including laboratory experiments [1] and direct confirmation on Itokawa grains [2] of the well know darkening and reddening trends. On the contrary, few results have been obtained on C-type asteroids and no general trend has been found [3-5]. In order to understand the influence of SpWe on primitive asteroids, we conduct laboratory simulations on carbonaceous chondrites. The goal is to develop a model of SpWe which will also support sample return missions (OSIRIS-REx/NASA and Hayabusa-2/JAXA).

Study: We are investigating the effects of space weathering on primitive asteroids using ion irradiation on their meteoritic analogs.

To do so, we exposed several carbonaceous chondrites (CV Allende, COs Lancé and Frontier Mountain 95002, CM Mighei, CI Alais, and ungrouped Tagish Lake) to 40 keV He^+ ions as a simulation of solar wind irradiation using fluences up to 6.10^{16} ions/cm^2 (implantation platform IRMA at CSNSM Orsay). As a test for our new experimental setup, we also studied samples of olivine and diopside. We confirm the reddening and darkening trends on S-type objects in the visible to near infrared range {Fig. 1}, but carbonaceous chondrites present a continuum of behaviors after ion irradiation as a function of the initial albedo and carbon content: from red to blue and from dark to bright {Fig. 2}.

This trend confirms what we began to observe on specific studies of Allende [6] and Murchison [7] meteorites.

It appears clearly on all samples that in the 10 µm region, bands of silicates and/or phyllosilicates move toward longer wavelength. The aqueous altered meteorites also present a band shift in the 3 µm region. These modifications toward the Fe-rich spectral region suggesting a loss of the element Mg are probably due to a preferential sputtering of Mg and/or amorphization of Mg-rich materials. These results can not confirm the presence of npFe^0, but do not disagree with the forming mechanism [8].

References: [1] Brunetto, R. et al. (2006), Icarus, 184, 327-337. [2] Hiroi, T. et al. (2006), Nature, 443, 56-58. [3] Moroz, L. et al. (2004), Icarus, 170, 214-228. [4] Lazzarin, M. et al. (2006), ApJ, 647, 179-18. [5] Lantz, C. et al. (2013), A&A, 554, A138. [6] Brunetto, R. et al. (2014), Icarus, 237, 278-292. [7] Lantz, C. et al. (2015), A&A, A41. [8] Hapke, B. (2001), JGR, 106, 10039-10073.

Acknowledgements: This research is part of a joint IAS-CSNSM project (INGMAR) and it has been funded by the French national program "Programme National de Planétologie" (PNP), by the Faculté des Sciences d'Orsay, Université Paris-Sud ("Attractivité 2012"), by the French National Research Agency "Agence Nationale de la Recherche" (contract ANR-11-BS56-0026, OGRESSE), and by the P2IO LabEx (ANR-10-LABX-0038) in the framework "Investissements d'Avenir" (ANR-11-IDEX-0003-01) managed by the French National Research Agency (ANR).

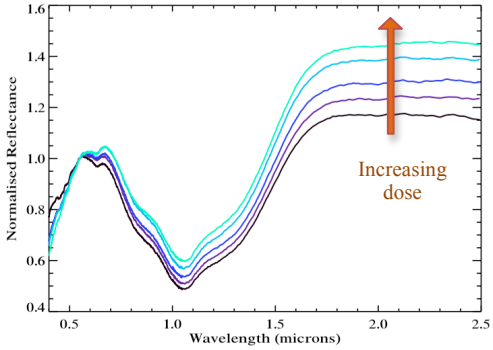

Figure 1: Spectra before and after irradiations (the brighter color, the stronger dose) for olivine.

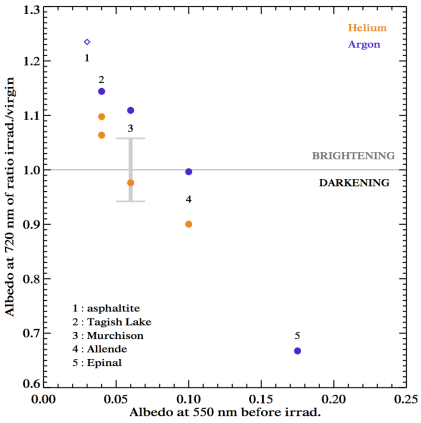

Figure 2: Reflectance of ratioed spectra (irradiated/unirradiated) as a function of the initial albedo. The grey error bar indicates the variations due to our Murchison sample heterogeneity.
Figure from [7].

VNIR EFFECTS OF SPACE WEATHERING: MODELING STRONG ABSORBERS IN A SCATTERING MATRIX. C. Legett IV[1], T. D. Glotch[1] and P. G. Lucey[2], [1]Geosciences Department, Stony Brook University 255 ESS Building, Stony Brook, NY 11794-2100 carey.legett@stonybrook.edu, [2]Planetary Geosciences/SOEST, University of Hawaii.

Introduction.

Previous Work. Nanophase iron ($npFe^0$) bearing rims on lunar regolith particles have been identified as the product of space weathering processes, including solar wind sputtering/implantation and micrometeoroid bombardment [1]. The spectral effects due to $npFe^0$ appear to be dependent on the abundance and size of the $npFe^0$ particles [2,3]. Laboratory work with lunar soils and analog materials has shown that if the $npFe^0$ is less than approximately 50 nm in size, the overall effect will be to both redden and darken the spectra whereas larger $npFe^0$ particles lead to only darkening without reddening [4].

Recent modeling efforts based on Mie theory and Hapke's radiative transfer model [5] have been successful at reproducing laboratory spectra using Maxwell-Garnett effective medium theory with empirical corrections [2]. These modeling efforts have not yet fully reproduced the transition from darkening and reddening to only darkening with the $npFe^0$ grain sizes indicated by laboratory work. In the models, the transition occurs at approximately 300 nm instead of 50 nm [3].

Multiple Sphere T-Matrix Model. We are investigating the use of the Multiple Sphere T-Matrix (MSTM) model to improve upon the success of the previous Mie-Hapke models and to resolve the $npFe^0$ grain size discrepancy. The MSTM model is a first-principles, direct simulation method for calculating an exact analytical solution to the time-harmonic Maxwell's equations for multiple sphere systems [6]. Our previous work shows that the MSTM/Hapke approach improves the modeled spectra of fine particles over Mie/Hapke methods [7].

Methods.

Model and Theory. We model the space weathered, iron bearing rims as silica gels containing spherical nanophase iron particles. These gels are collections of nanoscale silica spheres with a packing density roughly equivalent to the porosities indicated in laboratory work. A second approach is to generate a single large sphere to represent the silica gel, apply effective bulk optical constants given the porosity, and populate it with $npFe^0$ particles to reach the desired iron content.

In the first approach, we generate a spherical volume containing several thousand spheres using Pack-LSD molecular dynamics software [8,9] and assign an index of refraction (n) and extinction coefficient (k) to each sphere depending on the phase it is intended to represent and the wavelength we are modeling. Wavelength-dependent optical constants for Fe^0 are taken from [10] while those for silica are from [11]. Where necessary, we apply either a sixth order polynomial or piecewise linear fit to interpolate between provided n and k values from the literature over our model spectrum range (700-1700 nm, 100 nm steps).

We take the output of the MSTM model at each wavelength analyzed and extract the scattering and extinction efficiencies and calculate single scattering albedo and use it to calculate the bidirectional reflectance via a simplified Hapke bidirectional reflectance model [5].

Results. We ran 23 model runs with between 0.0057 and 19.65 wt% iron with iron particle sizes between 20 and 300 nm. A broad parameter space with iron particles smaller than 100 nm and iron contents from ~0.5 to 8 wt% Fe show relatively steep red slopes in the 700-1700 nm region. Runs outside of this region show flatter spectra, and by 300 nm, spectra are effectively flat.

Discussion: These results are consistent with previous modeling efforts but do not yet constrain the size at which the transition from reddening and darkening to darkening only.

Future work and Conclusions: More runs will be conducted to constrain the transition region. Additionally, more runs will be conducted with very small (<10 nm) particle sizes and very low iron contents to further examine the behavior of the system at these conditions. Companion laboratory work using an aerogel matrix with carbon black and iron nanopowder absorbers is also currently ongoing and will contribute to the interpretation of the modeling results.

References:

[1] Keller, L.P. & McKay, D.S. *Geochim. Cosmochim. Acta* (1997), **61**, 2331. [2] Lucey, P. & Noble, S. *Icarus* (2008), **197**, 348. [3] Lucey, P.G. & Riner, M.A. *Icarus* (2011), **212**, 451. [4] Noble, S.K. *et al. Icarus* (2007), **192**, 629. [5] Hapke, B. *J. Geophys. Res.* (2001), **106**, 10039. [6] Mackowski, D.W. & Mishchenko, M.I. *J. Quant. Spectrosc. Radiat. Transf.* (2011), **112**, 2182. [7] Ito, G. & Glotch, T.D. *LPSC XLVI* (2015). [8] Donev, A. *et al. J. Comput. Phys.* (2005), **202**, 737. [9] Donev, A. *et al. J. Comput. Phys.* (2005), **202**, 765. [10] Khashan, M.A. & Nassif, A.Y. *Opt. Commun.* (2001), **188**, 129. [11] Cahill, J.T.S. *et al. Geophys. Res. Lett.* (2012), **39.**

EFFECTS OF SOLAR HEATING ON ASTEROIDS. G. Libourel[1], M. Delbo[1], J. Wilkerson[2], C. Ganino[3], P. Michel[1], [1]Laboratoire Lagrange, Université Côte d'Azur, Observatoire de la Côte d'Azur, CNRS, Blvd de l'Observatoire, 06304 Nice, France, libou@oca.eu; [2]Department of Mechanical Engineering Engineering Building OneUTSA, Circle, San Antonio, TX 78249-0670, USA; [3]Laboratoire Géoazur, Université Côte d'Azur, Observatoire de la Côte d'Azur, 250 rue Albert Einstein, Les Lucioles 1, Sophia-Antipolis, 06560 Valbonne, France.

Introduction: The surfaces of atmosphere-less solar system bodies are weathered in space by the action of several processes, such as the implantation of ions of the solar wind and the bombardment of micrometeorites. It is well known that these phenomena alter the spectroscopic properties of asteroids [1,2]. Here we describe the great effects of another process, whose importance has been considered only recently, that can alter the original surface nature of asteroids: the radiative heating by the light from the Sun.

In particular the surfaces of Near-Earth objects (NEOs) can easily reach temperatures >400 K, and the heat penetration depth is of the heat is in the order of some centimetres [3]. At perihelion distances (q), smaller than 0.5 AU temperatures can be >550 K leading to the breakup of organic components (e.g. 300–670 K [4,5]). The knowledge of the temperature range of materials at different depth over the orbital evolution of space mission target asteroids is important for defining sampling strategies that ensure the likelihood that unaltered and pristine material will be brought back to Earth [6].

There are for instance NEOs with extremely close Sun approaches, such as the asteroids 3200 Phaethon and 1566 Icarus. Temperature on these asteroids can reach 1000 K, inducing mineralogical changes, thermal fracture and/or desiccation cracking and the production of dust particles. In particular, 3200 Phaethon is the parent body of the Geminids meteors and activity near perihelion has been detected for this asteroid [7].

Moreover, the surfaces of NEOs are also subject to large temperature variations (e.g. 150 K): these are due to the change of the insolation intensity caused by the diurnal cycle between day and night, by seasonal effects, by the orbital eccentricity or simply by a shadowing effect. Are the surface make up and mineralogy of these asteroids altered by these strong temperature variations ?

Experimental and theoretical analysis: It is known that temperature cycles can lead to mechanical load cycles inducing stresses in surface rocks. Cracks can thus form and propagate due to temperature variations and the resulting temperature gradients set up by the thermal cycles. Several works have suggested that such thermal fatigue may play an important role in the evolution of airless landscapes on bodies such as the Moon, Mercury, and on the asteroid Eros [8,9,10].

Here we will describe laboratory experiments and numerical modeling devoted to investigating whether thermal fatigue is active on asteroid surfaces. Laboratory experiments of thermal cycling (Fig. 1) were performed on meteorites - taken as analogues of asteroid surface material - to study under which conditions rock cracking on NEAs occurs and how this process may alter asteroid surfaces.

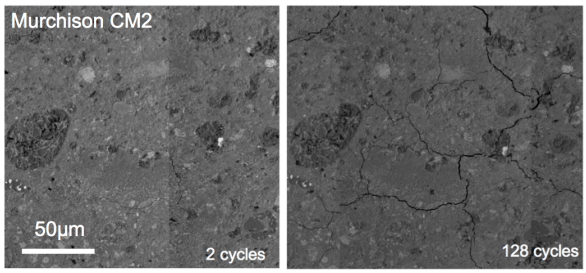

Fig. 1. CO_2 pulsed laser thermal fatigue experiments on the same Murchison CM2 carbonaceous chondrite sample after 2 and 128 thermal cycles ($\Delta T \approx 180K$).

Discussion: Our results [11] demonstrate that thermal fatigue is a dominant process governing regolith generation on small asteroids. We find that thermal fragmentation induced by the diurnal temperature variations breaks up rocks larger than a few centimetres more quickly than do micrometeoroid impacts. Because thermal fragmentation is independent of asteroid size, this process can also contribute to regolith production on larger asteroids. Production of fresh regolith originating from thermal fatigue fragmentation may be an important process for the rejuvenation of the surfaces of near-Earth asteroids. The efficiency of thermal fragmentation is controlled by the amplitude of the temperature cycles and by the temperature change rate, which in turn depend on heliocentric distance, rotation period, and the surface thermal inertia.

References: [1] Hapke B. (2001) *JGR*, 106, 10039. [2] Sasaki S. et al. (2001) *Nature*, 410, 555. [3] Spencer J. R. et al. (1989) *Icarus*, 78, 337. [4] Frost, R. et al. (2000) *Thermochim. Acta*, 346, 63. [5] Kebukawa Y. et al. (2010) *Meteoritis and Planetary Science*, 45, 99. [6] Michel P. and Delbo M. (2010) *Icarus*, 209, 520. [7] Jewitt et al. (2013) *AJL* 771:L36. [8] Duennebier, F. and Sutton, G.H. (1974) *Journal of Geophysical Research* 79, 4351. [9] Molaro, J. L. and Byrne, S. (2011) *42nd LPSC*, 1494. [10] Dombard, A.J. et al. (2010) *Icarus* 210, 713. [11] Delbo, M. et al. (2014) *Nature*, doi:10.1038/ nature13153.

SPACE WEATHERING OF SILICATES SIMULATED BY LASER IRRADIATION. M. J. Loeffler[1], C. A. Dukes[2], R. Christoffersen[3], and R.A. Baragiola[2,†], [1]NASA Goddard Space Flight Center, Greenbelt, MD 20771, [2]University of Virginia, Laboratory for Atomic and Surface Physics (LASP) Charlottesville, VA 22904, [3]Jacobs, NASA Johnson Space Center, Mail Code XI2, Houston, TX 77058.

Introduction: The surfaces of airless bodies are constantly being altered by energetic particles and micrometeorite impacts, and the resulting optical, chemical and structural changes that result from this processing are commonly referred to as space weathering. Previously, we have studied the role that the solar wind may play in altering iron-bearing minerals, such as San Carlos olivine, using a combination of near-infrared reflectance spectroscopy and x-ray photoelectron spectroscopy [1]. In this study, we present some of our more recent work where we have simulated the role that micrometeorite impacts may play in space weathering of silicate samples using a ns-pulsed laser. Specifically, we laser irradiated pressed pellets of SiO_2 and two different olivine compositions (Fo_{90} and Fo_{99+}), while monitoring our sample with *in situ* analysis using near-infrared reflectance spectroscopy and x-ray photoelectron spectroscopy. Follow-up *ex situ* analysis with ultraviolet-visible spectroscopy and electron microscopy were also performed on select samples. Results from the *in situ* measurements, as well as the ultraviolet-visible measurements, will be presented and discussed.

References: [1] Loeffler, M.J. et al. (2009), *JGR*, 114, E03003, 13 pp.

† deceased

QUANTITATIVE MODELING OF THE OPTICAL EFFECTS OF SPACE WEATHERING. P. G.. Lucey,[1] D. Trang,[1] H. Kaluna,[1] M. Lemelin,[1] J. Gillis_Davis, [1] T. Glotch,[2] D.T. BLewett,[3]. [1]Hawaii Institute of Geophysics and Planetology, University of Hawaii at Manoa, 1680 East West Road, Honolulu, Hawaii 96822, U.S.A, lucey@higp.hawaii.edu. [2]Department of Geosciences, Stony Brook University, Stony Brook, NY 11794-2100. [2]The Johns Hopkins Applied Physics Laboratory, Laurel MD, 20723

Introduction: Hapke [1] first modeled the optical effects of space weathering with a simple algorithm that captures the spectral properties of nanophase iron on, and in, mineral grains. Quantitative modeling of the optical effects of space weathering has a number of potential and realized benefits, including improved estimates of the modal abundance of the minerals in planetary regoliths of airless silicate surfaces [e.g. 2] and estimating the intensity of space weathering through derivation of the amount of altered material [e.g. 3].

Hapke used a simple representation of lunar space weathering components: nanophase iron coating mineral grains, and dark glass representing agglutinates, which Hapke found was required to match the slope and albedo of the Apollo soil he modeled. The presence of $npFe^0$ causes the red slope observed in lunar soil spectra. Dark and relatively neutral agglutinate glass tempers the aggressive reddening effect of the nanophase iron; together these components enable arbitrarily good matches between the slopes and albedos of soils and their models.

We slightly extended Hapke's work by developing a method to represent the spectral properties of agglutinate glass, which contains nanophase iron with somewhat larger grain size than that in rims on mineral grains, and not accurately modeled by the Hapke 2001 treatment. Lucey and Riner [3] used Mie theory to model the effects of submicroscopic iron over a range of sizes finding that above a model particle size of about 300 nm, submicroscopic iron darkens, but does not redden.

Applications: We tested this model against the empirical measurement of the effect of nanophase particle size on spectra by Noble et al. [4], and reasonably reproduced the slope and albedo of Lunar Soils Characterization Consortium soils given the known abundances and particle sizes of nanophase iron [5]. The model, applied to MESSENGER MASCS data for Mercury suggested Mercury contains more submicroscopic iron than the Moon, in turn suggesting that space weathering is more intense on Mercury[3].

A strength of this model is that any nanophase material can be modeled, not just iron. Applied more recently to MASCS data, the model shows that inclusion of substantial carbon produces a better match to the spectrum of Mercury than iron alone, demonstrating added value of the modeling.

We also applied the model to the Moon using data from the Multiband Imager. Unsurprisingly more space weathering derived iron is found in the maria than the highlands. Interestingly, the abundance of nanophase iron differs in detail from that of submicroscopic iron larger than the wavelength. Finally, we are in the process of applying this model to Dawn data for Vesta, in case where space weathering effects are weak.

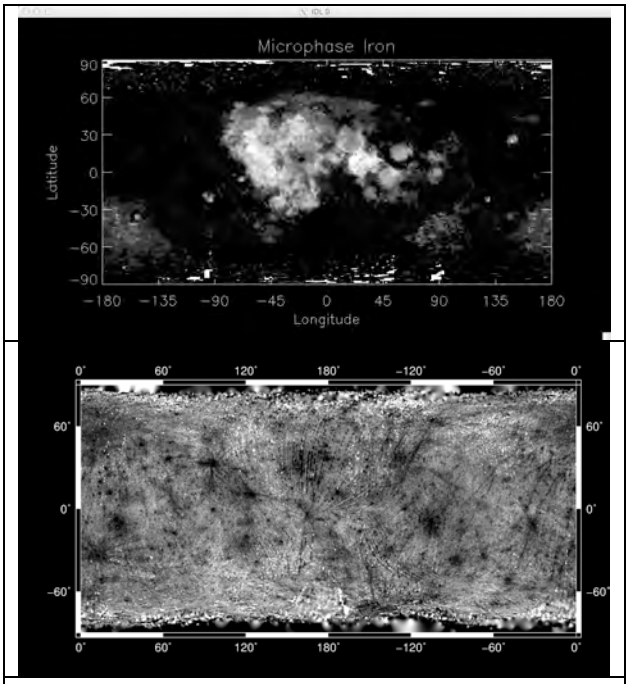

Figure 1. Top: distribution of lunar nanophase iron (smaller than the wavelength). As is well known from lunar samples, this material is more abundant in the lunar maria. Bottom: nanophase iron on Mercury. Fresh craters are evident in nanophase iron lows.

References: [1] Hapke B., 2001, J. Geophys. Res. 106, 10039–10073. [2] Denevi, B. W., et a. 2008, J. Geophys. Res. 113, E02003, doi:10.1029/2007JE002929. [3] Lucey, P.G. and M.A. Riner, Icarus, 212, p. 451-462, doi:10.1016/j.icarus.2011.01.022 2011. [4] Noble, S. K.. et al.,, 2007. Icarus 192, 629–642, doi: 10.1016/j.icarus.2007.07.021. [5] Taylor, L. A., et al., 2001. Meteor. Planet. Sci. 36, 285–299.

ASSESSMENT AND CHARACTERIZATION OF SPACE WEATHERING STYLES ON ASTEROID SURFACES. E. M. MacLennan[1], J. P. Emery[1], M. P. Lucas[1], N. Pinilla-Alonso[1,2], [1]Earth & Planetary Sciences Department, University of Tennessee, Knoxville, TN 37996 (emaclenn@utk.edu); [2]Florida Space Institute, University of Central Florida, Orlando, FL 32816.

Introduction: Solar wind exposure and micrometeoroid bombardment are known to cause mineralogical changes in the upper few microns of silicate grains (by forming amorphous rims with embedded nano-phase Fe^0), which affect the light-scattering properties [1]. Changes in the albedo, spectral slope, and absorption band depths observed on silicate surfaces are used as proxies for the amount of alteration due to increased nano-phase Fe^0 [2].

Observations of the Moon have allowed for the characterization of a "lunar-style" of space weathering, characterized by a decrease in albedo, increase in spectral slope, and suppresion of absorption bands [2]. However, images (from spacecraft missions) of (243) Ida and (433) Eros suggest that different space weathering "styles" exist among the silicate-bearing S-complex asteroids (e.g., [3]). While Eros generally shows only an albedo difference [4], Ida's surface only shows changes in spectral slope and band depth [5]. In many space weathering studies, it is often assumed that the lunar style is relevant, and there has been no comprehensive investigation involving all three observable changes relevant to space weathering.

In addition to searching for different space weathering styles, we aim to quantify the factors (solar wind exposure, regolith grain size, mineralogy, and surface age) affecting the degree of space weathering. It has already been shown that asteroids with higher olivine abundance and older surface ages show increased evidence of space weathering [6]. [7] suggests that smaller regolith particles, which have more surface area per volume, should enhance the spectral effects associated with space weathering, but this has not yet been observationally tested for asteroid regoliths.

We present the preliminary results of a new project aimed at searching for and characterizing differing styles of space weathering among S-complex asteroids and quantifying the dependence on solar wind exposure, regolith grain size, mineralogy, and surface age using a large set of near-infrared (NIR) reflectance spectra.

Hypothesis: We hypothesize that increased solar wind exposure, smaller regolith particles, higher olivine abundance, and older asteroid surfaces will exhibit enhanced evidence of space weathering.

Methods: The first task of this project is to derive spectral parameters from Visible-NIR (0.4 to 2.5 μm) spectra for ~500 S-complex asteroids. Most of the data will be taken from existing databases (e.g., MIT-UH-IRTF Joint Campaign for NEO Reconnaissance [8]). In addition, we will target 52 S-complex asteroids using IRTF-SpeX of which we will have grain size estimates (from a separate project). Spectral slopes and absorption band depths will be calculated using the SARA band analysis code developed by [9]. Geometric albedos will be calculated using thermal emission data from the WISE [10] survey.

Search for Space Weathering Styles: We will compile a set of asteroid albedos, band depths, and spectral slopes for approximately 500 asteroids. This will allow us to identify objects that undergo different space weathering "pathways" (e.g., surfaces that experience albedo changes but no spectral reddening).

Space Weathering Factors: The goal of the project is to quantify how solar wind exposure, regolith grain size, mineralogy, and surface age influence the degree of space weathering. At the workshop, we will focus on asteroids in which we will have grain size estimates from thermal infrared data. The approach here is to approximate an un-weathered spectrum for each object, by using a bootstrap method involving a combination of laboratory spectra from the NASA RELAB facility and Hapke's radiative transfer model [7]. Using estimated mineralogy from the set of corrected band parameters [11][12][13] the expected un-weathered albedo, spectral slope, and band depth will be compared to the observed quantities to determine the degree of space weathering and its dependence on regolith grain size.

Preliminary results presented at the workshop include our search for different space weathering styles and newly acquired asteroid spectra from the IRTF, with the corresponding estimated regolith grain size.

References: [1] Clark B. E. et al. (2002) In *Asteroids III*, pp. 585-599. [2] Pieters C. M. et al. (2000) *Meteor. Planet. Sci.* 35, 1101-1107. [3] Gaffey M. J. et al. (2010) *Icarus*, 209, 564. [4] Bell J. F. III et al. (2002) *Icarus*, 155, 119. [5] Helfenstein P. et al. (1996) *Icarus*, 120, 48. [6] Vernazza P. et al. (2009) *Nature*, 458, 993. [7] Hapke B. (2001) *J. Geophys. Research: Planets*, 106, E5. [8] Binzel R. P. et al. (2006) *LPSC XXXVII*, Abstract #1491. [9] Lindsay, S. S. et al. (2015) *Icarus*, 247, 53. [10] Mainzer A. et al. (2011) *AJ,* 731, 53. [11] Cloutis E. A. et al. (1986) *J. Geophys. Research*, 91, 11641. [12] Dunn T. L. et al. (2010) *Icarus*, 208, 789. [13] Sanchez J. A. et al. (2013) *Icarus*, 220, 36.

METHODOLOGY OF SPACE WEATHERING SIMULATION AND ITS APPLICATION ON OLIVINE AND PYROXENE SAMPLES. O. Malina[1], T. Kohout[2, 3], J. Tuček[1], J. Filip[1], D. Britt[4], R. Zbořil[1], [1] Regional Centre of Advanced Technologies and Materials, Departments of Physical Chemistry and Experimental Physics, Palacky University Olomouc, Czech Republic (ondrej.malina@upol.cz), [2] Department of Physics, University of Helsinki, Finland, [3] Institute of Geology, The Czech Academy of Sciences, Prague, Czech Republic, [4] Department of Physics, University of Central Florida, USA.

Introduction: Formation of metalic iron nanoparticles ($npFe^0$) during the space weathering process causes changes in reflectance spectra of airless planetary bodies. The main spectral effects of space weathering are attenuation of the silicate absorption bands, darkening, and slope change (reddening) [1].

There are a number of laboratory methods for the production of $npFe^0$ including short duration laser irradiation, ion bombardment, or microwave irradiation. In present work, a two-step thermal treatment method [2] for the controlled production of $npFe^0$ on the surface of two different materials is introduced.

Characterization of the methodology: In the first step, a pyroxene or olivine powder sample was heated under ambient oxygen atmosphere in a muffle furnace. The oxidizing conditions have been used to induce a partial breakdown of the crystal structure and oxidation of iron ions situated close to the crystal surface. Various temperatures and heating durations were selected to study the effects on mineral spectroscopy and $npFe^0$ generation.

In the second step, induced iron oxide nanoparticles were reduced into $npFe^0$ in the pure hydrogen atmosphere. For the passivation of of $npFe^0$, the gas mixture flow of N_2, with 2 % O_2 was used.

Comparison of real samples: The two-step synthesis method has been used on two different samples – olivine and pyroxene. In general, the main goal is in controled size of $npFe^0$ formed on the surface of olivine and pyroxene and in quantification of the related spectral changes. The transmission electron microscopy (TEM) images (Fig. 1) after double-heating method revealed two significant features. First, different sizes and concentration of $npFe^0$ are observed, and secondly, due to more resistance of pyroxene (e.g. [3]), higher temperatures are needed to produce the same amount of $npFe^0$ as in the olivine case.[2]

Results from TEM are fully consistent with reflectance spectra (Fig. 2), which show a progressive changes as a function of the increasing $npFe^0$ amount.

Conclusion: The two-step synthesis method was introduced to simulate the space weathering conditions in a laboratory. TEM results of both samples confirm the necessity of using higher temperatures in pyroxene to producing the similar amount of $npFe^0$ as in the olivine sample. Furthermore, the control over $npFe^0$ size and concentration allows for quantitative evaluation of spectral changes.

References: [1] Hapke, B., 2001. *J. Geophys. Res. 106*, 10039-10073. [2] Kohout T. et al. (2014) *Icarus, 237*, 75-83. [3] Quadery A. et al (2015) *JGR-Planets 120*, 1-19.

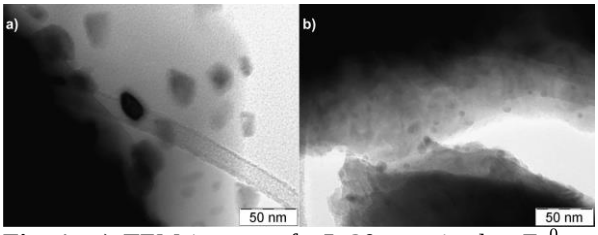

Fig. 1 a) TEM images of ~5–20 nm sized $npFe^0$ on olivine powder grains after heating at 750 ˚C, b) TEM images of ~5 nm sized $npFe^0$ on pyroxene powder grains after heating at 1000 ˚C.

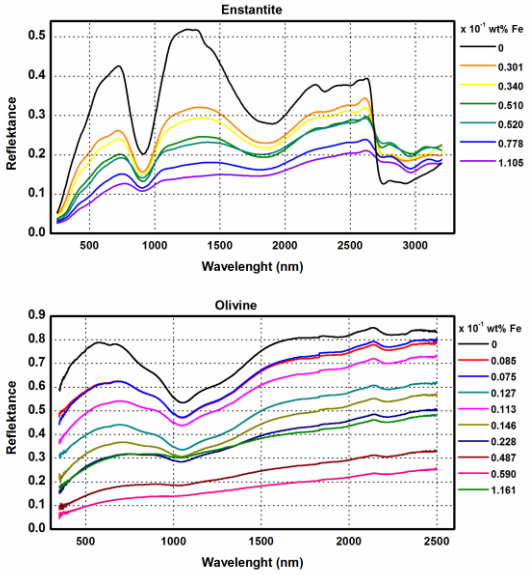

Fig. 2 Raw reflectance spectra of pyroxene and olivine with increasing amount of $npFe^0$.

Systematic ion irradiation experiments to olivine: Comparison with space weathered rims of Itokawa regolith particles. T. Matsumoto[1], A. Tsuchiyama[2], N. Watanabe[3], K. Yasuda[4], A. Miyake[2] Y. Nakauchi[1], T. Okada[1], M. Abe[1], T. Yada[1], M. Uesugi[1], Y. Karouji[1], A. Nakato[1], M. Hashiguchi[1], K. Kumagai[1]. (tmatsumoto@planeta.sci.isas.jaxa.jp) [1]Japan Aerospace Exploration Agency, [2]Kyoto University. [3]Hokkaido University, [4]Kyoto Prefectural University

Introduction: Space weathering feature of the spectrum of airless bodies is considered to be the cumulative result of alterations of the optical properties of surface material of the body [1]. Space weathered rims, one of such alterations, were identified in the regolith grains recovered from S-type asteroid 25143 Itokawa.

The space weathered rims of Itokawa grains consist of thin rims of vapor and/or sputtered deposition and thick amorphous rims [2]. The time-scale of rim formation is unclear, which is calculated indirectly by solar flare track (SFT) density [2]. The rims contain Fe-rich nanoparticles and often contain vesicles and blisters. The blisters might have been formed by mainly solar wind 4 keV $^4He^+$ implantation, because the depth of the rims is almost consistent with $^4He^+$ implantation depth [2]. On the other hand, [3] proposed different formation processes of the blisters in lunar samples, by solar wind implantation with heating by impact, because micrometeorite bombardment is dominant for rim formation of lunar soils [3]. It is not fully understood whether the blisters can be formed by only solar wind implantation. In this study, we conducted ion irradiation experiments in order to reveal formation time-scales of space weathered rims and formation processes of blisters by solar wind irradiation.

Experiments: An olivine fragments of Sri Lanka $(Mg_{1.4}Fe_{0.6}SiO_4)Fa_{30}$, which is almost the same as the composition of olivine ($Fa_{28.6\pm1.1}$) in Itokawa grains [4], were placed on Au plates. The irradiation experiments were performed at the Wakasa Wan Energy Research Center, Tsuruga, Japan. Olivine samples were irradiated with $^1H_2^+$, and $^4He^+$ ions accelerated at 10 to 50 keV with dose from 1×10^{16} to 1×10^{18} ions/cm^2. The irradiation experiments with $^4He^+$ ions accelerated at 4 keV $^4He^+$ with dose of 3×10^{17} ions/cm^2 were performed using the irradiation system at Institute of Low Temperature Science Hokkaido University. The surfaces of the fragments were observed using FE-SEM (JSM-7001F). After FE-SEM observation, FIB sections of olivine fragments irradiated by 4 keV $^4He^+$, and 10 keV $^4He^+$ were prepared and observed by TEM and STEM (JEM-2100F). In order to evaluate heating by ion irradiation, the temperature of an irradiated polished olivine plate was examined during 4 keV $^4He^+$ irradiation by thermography.

Results and Discussion: SEM observation of olivine surfaces irradiated by 4 keV – 50 keV $^4He^+$ revealed that the dose between 1×10^{17} ions/cm^2 and 1×10^{18} ions/cm^2 is a threshold of dose for blister formation. The doses of 1×10^{18} ions/cm^2 correspond to the solar wind $^4He^+$ irradiation duration of ~5000 years [5], which is almost consistent with SFT ages of Itokawa particles with blisters [2]. A threshold of dose for blister formation by H_2^+ takes a value between 1×10^{16} ions/cm^2 and 1×10^{17} ions/cm^2. Using TEM, we observed development of internal structures of olivine irradiated with 10 keV $^4He^+$ at different dose at the same flux (2.7×10^{13} ions/cm^2/sec). In the case of olivine irradiated at dose of 1×10^{16} ions/cm^2, fully amorphous rim developed beneath the surface with $npFe^0$ and precursors of vesicles. Rim of olivine irradiated at the dose of 1×10^{17} ions/cm^2 contain numerous vesicles filling the amorphous rim. In the case of olivine irradiated at dose of 5×10^{17} ions/cm^2, some of larger vesicles lift up the surface and form blisters.

In the case of olivine irradiated at different flux of 1×10^{13} ions/cm^2/sec with 4 keV $^4He^+$ at the same dose (3×10^{17} ions/cm^2), numerous vesicles and blisters formed in totally amorphous rims. When the flux is low (1×10^{12} ions/cm^2/sec), only precursors of vesicles appear in totally amorphous rims. It suggests that damages by ion irradiation could depend on incidental ion flux. Space weathered rims with blisters of Itokawa particles consist of partly amorphous structures [2]. On the other hand, damage rims with blisters formed by 4keV $^4He^+$ ion irradiation are completely amorphous. The difference may come from difference of flux between the ion irradiation experiment and solar wind, which is calculated to be 1×10^7 ions/cm^2/sec/AU^2 for $^4He^+$ [6]. Temperature of surface of an olivine plate rose approximately four degrees during 4 keV $^4He^+$ irradiation, suggesting that heating is not necessary for blister formation.

References: [1] Pieters et al. (2000) *Meteoritics & Planet. Sci., 35*,1101-1107. [2] Noguchi et al. (2014) *Meteoritics & Planet. Sci., 49*,188-214. [3] Keller and McKay. (1997) Science, *Geochimica et Cosmochimica Acta 61*, 2331–2341. [4] Nakamura et al. (2011) *Science 333,*1113-1116. [5] Reisenfeld et al. (2007) *Space Science Review, 13*,79-86. [6] Goldstein et al. (1996) *Astron. Astrophys, 316,* 296-303.

Thermal Desorption Kinetics of Volatiles on Silicate "Smokes": Analog to Micrometeoric Impact Vapor Condensates. J. M. McLain[1,2], M. Sarantos[1,3], N. M. Johnson[1], J. W. Keller[1], J. A. Nuth[1], W. M. Farrell[1]. 1. NASA GSFC, Greenbelt, MD. 2. University of Maryland, College Park. 3. University of Maryland, Baltimore College.

Motivation: The regolith of rocky airless bodies like the Moon, Mercury, asteroids and extinct comets is constantly weathered by radiation and impacts. These space weathering processes are very important due to the constant alteration in the physical and chemical properties of the regolith. As the regolith matures, the porosity, comminution, and number of chemical defects of the material increases. The mature regolith can act as a natural absorbent for volatile species as well as a catalyst for surface reactions. Many of the altered physical parameters during the volatile/regolith interaction such as the desorption energies, sticking lifetimes, and reaction rates are not known for some of the most common volatiles for ISRU, In Situ Resource Utilization, such as water, oxygen, methane, carbon dioxide and nitrogen. Currently, improved Monte Carlo volatile transport models used to interpret exospheric observations from LADEE, LRO and MESSENGER are relying on data in the literature from inappropriate substrate materials. The primary goal of this study is to obtain desorption kinetic data at applicable temperatures (20-700 K) that can be used directly in our transport models to track and identify the sources and sinks for volatile exospheric species. In order to advance our theoretical models, the effects of space weathering to alter the physical and chemical properties such as desorption activation energies, dissociation, and oxidation/reduction reactions must be assessed.

Thermal Desorption: Lab measurements of the thermal desorption kinetics of Ar, H2O and other common lunar volatiles on silicate smokes will be presented. Silicate smokes are vapor condensates of refractory material that are grown in a flow chamber by condensing gaseous silane with metallic elements such as Na, K , and Fe. These smokes are filamentous in structure, highly porous and rich in chemical defects, i.e., unsatisfied chemical bonds, and are used as analogs of the vapor condensates formed after micrometeoric impacts. The focus of the presentation will be on comparing the desorption energies and surface chemistry with other regolith analogs. A sample holder transfer system is used to transport the smokes simulates into a thermal desorption test chamber to prevent atmospheric contamination. The smokes samples are then cooled with a cryostat and dosed with a pulsed-beam source. After deposition, thermal treatment is controlled via an external CO2 infrared laser. Desorption products are continuously monitored with a differentially-pumped mass spectrometer.

Exospheric Abundances: The total abundance of a species in the exosphere and the resulting local time dependence is a function of the binding or desorption energy, desorption order, and the pre-exponent factor, aka, prefactor which represents the empirical temperature dependence of the rate coefficient. To improve our exospheric estimates, complimentary surface science data can be used in conjunction with current observations to understand the origin of exospheric species which are solely derived from the relationship between the regolith and its local environment. Space-based observations suggest a continuous presence of volatiles in Mercury's and the Moon's exosphere, sourced by micrometeoritic impacts and solar wind induced surface chemistry. Currently, our simulations have demonstrated that assumed binding energies for volatiles sequestered on the nightside dictates the distance from the dawn terminator these volatiles are reintroduced into the gas phase as well as maximum abundances.

THE MICROSTRUCTURE OF A MICROMETEORITE IMPACT INTO LUNAR OLIVINE. S. K. Noble[1] L. P. Keller[2], R. Christoffersen[2,3] and Z. Rahman[2,3], [1]NASA Headquarters, 300 E St SW Mail Code 3D75, Washington DC 20546, sarah.k.noble@nasa.gov, [2]NASA JSC, Houston TX 77058, [3]Jacobs Technology Inc, Houston TX.

Introduction:

The peak of the mass flux of impactors striking the lunar surface are particles ~200 μm that erode rocks, comminute regolith grains, and produce agglutinates. The mechanisms by which these micro-scale impacts form nanophase Fe metal (npFe^0) in the lunar regolith are still not fully understood. Current efforts are focused on simulating the physical and optical effects of micrometeorite impacts on lunar and meteoritic material using hypervelocity impacts and pulsed lasers [e.g. 1, 2]. Here we provide some ground-truth for those studies from a natural lunar sample. Through TEM analysis of the cross-section of a ~20 μm diameter crater into an olivine single crystal we can see first-hand the effects of a single impact, including the creation of npFe^0 in the melt.

Sample: Lunar rock 12075 is an olivine basalt with large olivine phenocrysts (1-2 mm). The surface contains numerous micrometeorite impact craters ranging from 100 μm down to 1 μm. The solar flare track density in olivine (~10^{11}/cm^2) indicates a minimum surface exposure of ~10^6-10^7 years.

Methods: A small chip of 12075 was examined by SEM to locate an impact crater into olivine of appropriate size for FIB sectioning and analytical TEM characterization. A FIB cross-section was prepared using the FEI Quanta 3D600 FIB at JSC (Fig. 1). TEM work was done using a JEOL 2500SE 200 keV field-emission scanning-transmission electron microscope.

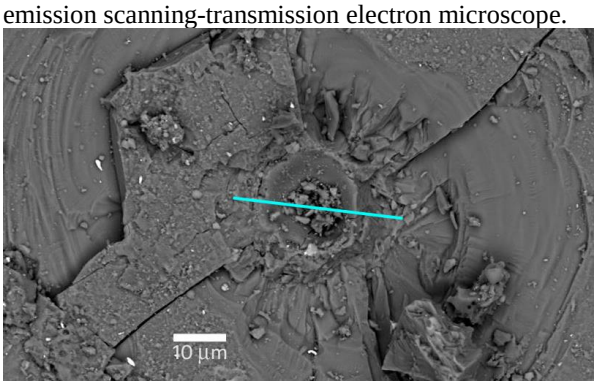

Fig 1. Micrometeorite impact into olivine crystal. The line represents the approximate location of the FIB sample.

Results: Extending from the crater cavity outward into the host olivine grain, the crater walls are composed of a shock-melted lining ~0.5 – 2 um thick of glassy olivine that sharply transitions to an underlying layer of polycrystalline olivine with recrystallization textures. The recrystallized olivine becomes progressively finer-grained as it transitions to the underlying olivine single-crystal.

An extensive zone of shocked and deformed olivine containing radial fractures and numerous defects and dislocations extends outward 15-20 um from the melt recrystallized zone. Unshocked areas of the host olivine contain a high density of solar flare particle tracks (~10^{11}/cm^2), but closer to the crater, the tracks are erased.

NpFe^0 is present throughout the melt and recrystallized layer; it is remarkably consistent in size, ~3-7 nm. The upper ~70 nm is vesiculated, likely the result of implanted solar wind gases, and the top surface is highly enriched in npFe^0. A small amount of Ca and Al is present at the uppermost surface, indicating a very thin layer of post-event vapor-deposited material.

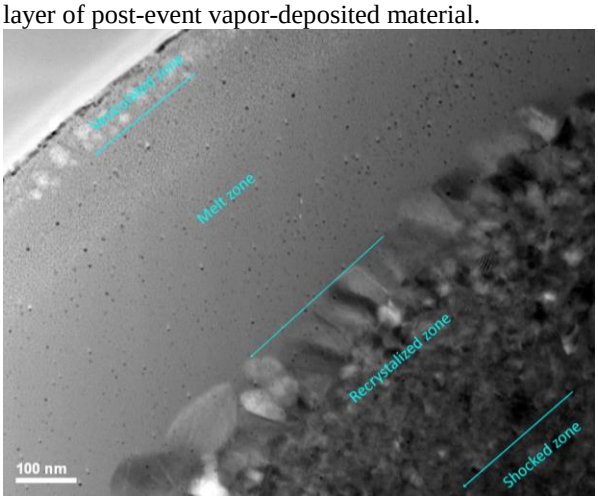

Fig 2. TEM bright field image of the impact melt lining.

Discussion: This sample clearly demonstrates that a natural micrometeorite impact into an Fe-bearing olivine single-crystal can produce glassy olivine with abundant npFe^0 inclusions. It does not, unfortunately, inform us whether solar wind H^+ is required in the impacted surface for npFe^0 formation, since most exposed lunar surfaces are saturated with solar wind ions. The size distribution and narrow range of the npFe^0 is most similar to that in grain rims rather than the much larger sizes and wider size range observed in agglutinitic glasses. This suggests that sequential impact processing is required for npFe^0 to coarsen to the sizes seen in lunar agglutinitic glass.

Future work: Future work will focus on analyzing additional craters in olivine as well as other phenocrysts in the 12075 (e,g, pyx and ilm) and comparing the results to laboratory impact experiments.

References: [1] Sasaki et al. (2001) *Nature, 410,* 555-557. [2] Brunetto R. et al. (2006) *Icarus, 180,* 546-554.

SPACE WEATHERING OF ASTEROIDS, MERCURY AND THE MOON. T.M.Orlando[1], K. Fiege[1], C.J. Bennett[1], M.Trieloff[2] and R.Srama[3]. [1]Georgia Institute of Technology, School of Chemistry and Biochemistry, 901 Atlantic Drive, Atlanta, GA 30332, USA (thomas.orlando@chemistry.gatech.edu), [2]University of Heidelberg, Institute for Geosciences, Heidelberg, Germany, [3]University of Stuttgart, Institute for Space Systems, Stuttgart, Germany.

Introduction: Solar wind, meteorites, micrometeorites and cosmic rays continuously bombard the surfaces of airless bodies in the solar system. These processes summarized under the term "Space Weathering" cause strong alterations of the surfaces of these bodies. Astronomical observations aim to reconstruct the surface properties of asteroids, moons and planets primarily by infrared spectra, but space weathering severely modifies the optical, compositional and physical properties of thin surface layers and thus precludes proper identification of chemistry and mineralogy. The effects of space weathering have been experimentally studied mainly with respect to ion bombardment, sputtering and photodesorption [1]. Other studies aimed to simulate the influence of micrometeoroid bombardment by using laser ablation techniques. We summarize some recent laboratory studies on photon, ion and micrometeorite "weathering" of Mercury and asteroid surface analogs as well as actual lunar regolith samples [2-6]. Specifically, we have measured the absolute cross sections for VUV photon-stimulated desorption and dissociation of water from lunar surfaces (both maria and highland) samples as well as solar wind proton induced hydroxylation of lunar samples. For Mercury samples, we have examined photon-stimulated desorption of Ca from CaS and address whether the photon stimulated desorption (PSD) of CaS in the hollows can be a source term for the observed Ca in the exosphere. Finally, meteorite bombardment studies have been carried out on several asteroid samples and surrogates and compared directly to samples irradiated with electrons and ions.

Method: The photodesorption from the lunar samples utilized pulsed laser (157 nm) excitation of water-covered regoliths followed by resonance enhanced multiphoton ionization of the neutral molecular water and the atomic fragments that desorb from the surface. We utilized a similar experimental approach for the Ca PSD studies. In addition, we are extending our space weathering studies to include meteoroid impact events. This is accomplished using a 2MV dust accelerator at the Institute for Space Systems at University of Stuttgart, Germany in combination with energetic irradiation experiments at the Electron and Photon Induced Chemistry on Surfaces (EPICS) - laboratory at Georgia Institute of Technology, USA. By systematically simulating highly realistic irradiation conditions, we are able to investigate both particle and solar wind irradiation on solid planetary surfaces. This allows us to study processes such as i) the formation of nanophase iron in amorphous rims and ii) OH-formation in nominally anhydrous minerals. Using a variety of mineralic materials, this work aims to contribute to a better understanding of the general alteration mechanisms of different space weathering agents in a variety of space environments.

References:[1]C.J. Bennett, C. Pirim, T.M. Orlando, (2013) *Chem. Rev*, 113(12), 9086-9150, [2]M. J. Poston, G. A. Grieves, A. B. Alexandrov, C. A. Hibbitts, M. Darby Dyar and T. M. Orlando, *Icarus* (2014). [3]A. DeSimone and T. M. Orlando, *Icarus* (2014). [4]A. DeSimone and T. M. Orlando, *J. Geophys. Res*. (2014) 119, 894-904, *J. Geophys. Res.* (2014) 119, 884-893. [5] M. Poston, G. A. Greives, A. Alexandrov, C. A. Hibbitts, M. Darby Dyar, T. M. Orlando, *J. Geophys. Res.* (2013) 118 (1), 1-160. [6]J. Mclain, G. A. Grieves, A. Sprague, P. Tavenshik, D. Schriver, and T. M Orlando, *J. Geophys. Res.* (2011) 116, E03007.

ONLINE SPECTRAL FIT TOOL FOR ANALYZING REFLECTANCE SPECTRA. A. Penttilä[1] and T. Kohout[1], [1]Department of Physics, P.O. Box 64, 00014 University of Helsinki, Finland (Antti.I.Penttila@helsinki.fi).

Introduction: The Online Spectral Fit Tool (OSFT)[1] was developed to our own needs in analyzing Vis-NIR spectral behavior of asteroids and meteorites. Our approach is similar to the Modified Gaussian Model (MGM) -software[2,3], but with certain differences in the model and in the implementation. We extended the applicability of our software by implementing it in JavaScript/HTML so that it can be used through a web browser. The OSFT runs in the client-side, and is self-consistent needing no plug-ins to be installed.

We use no pre-determined spectral data, but fit the spectra using mathematical continuum model and analytical functions for absorption bands. The OSFT does not relate the fit directly to known spectral elements, but gives statistics describing the behavior of the continuum and the absorption bands.

OSFT Model Formulation: Our model for UV-Vis-NIR spectra is based on continuum with superimposed absorption bands. The model parameters are fitted using constrained non-linear optimization.

Absorption bands. We use the shape of the Gamma distribution for the absorption bands. The Gamma shape seems to fit the data better than the Gaussian, Lorentzian or modified Gaussian shape. The Gamma distribution is more peaked than the Gaussian, and is favored by our data. The distribution is defined for positive values, supporting its use with wavelengths. If the expected value μ of the Gamma distribution is large, i.e., $\mu/\sigma>>0$, the distribution is almost symmetric. We use an alternative parameterization of the distribution where μ and the standard deviation σ are the parameters of the distribution. The actual absorption peak in the model is the normalized Gamma distribution with maximum value of 1, multiplied by the peak strength parameter.

The area of the band can be derived analytically, while the full-width-at-half-max of the peak needs to be solved numerically.

Continuum. We wanted the continuum model to be more flexible than the first-order polynomials. For this reason, we chose cubic splines as the basis of the continuum. The continuum is modeled as the linear combination of five *B*-spline basis functions of third degree with knots in the range from the smallest wavelength to the largest wavelength in the data. The coefficients of the linear combination are to be fitted.

Optimization. The function containing the absorption bands and the continuum is fitted to the data using constrained non-linear optimization. The sum-of-squared-errors (SSE) between the data and the model is minimized. Constraints need to be set for the band parameters. In addition to minimizing SSE, we also introduce two other penalizations with small weights. These penalizations are related to the continuum being smooth and the bands to extend only to the area of absorption and not to continuum.

Usage: The beta version of the OSFT is publicly available [1]. The user can upload a text-file of wavelength-reflectance pairs. The data is shown graphically, and the user can select the number of absorption bands. Initial parameter guesses need to be given for band centers, deviations, and depths. With initial values for bands, the continuum is fitted using the linear least-squares fit, and the initial fit is displayed with the data. Once the initial fit is in the right neighborhood, the algorithm will do the actual non-linear fit for the band and continuum parameters together. When completed, the software can compute fit statistics, i.e., band locations, deviations, depths, FWHM-values, and band areas, together with the slope and albedo parameters. Spectra is normalized only after the fitting, since we rather normalize with the value from the fitted continuum than with a single measured reflectance value.

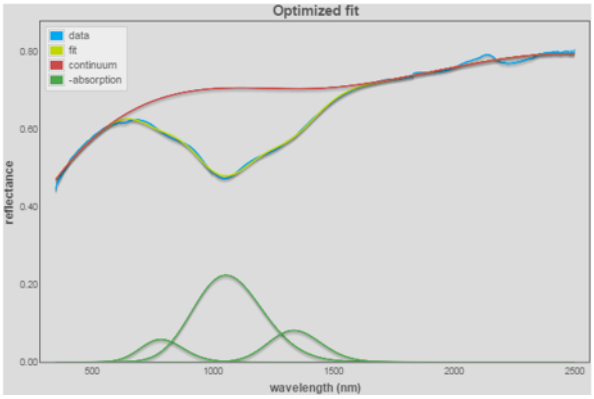

Figure: OSFT fit with three overlapping absorption bands for olivine including nanophase Fe^0.

References: [1] Penttilä A. and Kohout T. (2015), *http://www.helsinki.fi/project/psr/OSFT/*. [2] Sunshine J.M., Pieters C.M., and Pratt S.F. (1990), *JGR*, 95, 6955–6966. [3] Sunshine J.M., Pieters C.M., Pratt S.F., and McNaron-Brown K.S. (1999), *LPSC 30*, Abstract.

Acknowledgements: European Research Council Advanced Grant project No. 320773 (SAEMPL).

EXPLAINING SPACE-WEATHERING EFFECTS ON SPECTRA WITH LIGHT-SCATTERING SIMULATIONS. A. Penttilä[1] , T. Väisänen[1], T. Kohout[1], and K. Muinonen[1,2], [1]Department of Physics, P.O. Box 64, 00014 University of Helsinki, Finland (Antti.I.Penttila@helsinki.fi), [2]Finnish Geospatial Research Institute, Geodeetinrinne 2, 02430 Masala, Finland.

Introduction: Space-weathering (SW) introduces changes to the reflectance spectra of asteroid surfaces. In silicate minerals, SW is known to darken the spectra and reduce the silicate absorption band depths. In olivine, the spectral positive slope in Vis and NIR wavelengths is increasing (see, e.g., [1] and references therein). In pyroxene, however, the positive slope over the 1 µm absorption band is decreasing, while the negative slope over the 2 µm absorption band is increasing towards positive values with increasing SW [2].

The SW process is believed to influence the spectra by generating small nanophase iron ($npFe^0$) inclusions in the surface layers of mineral grains. The $npFe^0$ inclusions are believed to be some tens of nanometers in size. This mechanism has been linked to the Moon and to a certain extent also to the silicate-rich S-complex asteroids and to the ordinary chondrite meteorites.

Laboratory measurements: We have UV-Vis-NIR spectral measurements of both olivine and pyroxene (EN 90 enstatite) that have been prepared to mimic various levels of SW using methodology described in [1]. The minerals have been ground into powder, and the sizes and weight fractions of $npFe^0$ inclusions have been measured. These well-described, controlled samples, together with high-quality laboratory-measured spectra, offer us an excellent case to explain the observed spectral effects using light-scattering methods.

Methodology: The spectral effects from increasing amount of $npFe^0$ can be explained with light-scattering theory and simulations. To fully understand the mechanisms, we need to combine exact methods, derived directly from Maxwell equations, with approximate methods from radiative transfer theory.

Exact methods. Exact light-scattering simulations are very computer-intensive, and can be applied only on wavelength-scale targets. Fortunately, the $npFe^0$ inclusions in the host mineral have sizes around 10–20 nm [1]. With UV-Vis-NIR wavelengths, these are small enough so that their scattering properties, namely their extinction cross-section and single-scattering phase function, can be computed. Because the inclusions are quite spherical and small compared to the wavelength, the Mie theory is sufficient.

Radiative transfer. While we can compute the scattering properties of single $npFe^0$ exactly, to simulate the light-scattering response of macroscopic collection of mineral powder grains with inclusions, we need to apply approximate methods. We have successfully applied the Monte Carlo geometric optics and diffuse scattering SIRIS code [3] to SW olivine. With SIRIS, we first compute the exact scattering properties of $npFe^0$, and then insert them as diffuse scatterers in the host mineral grain. Both Fresnel-type surface scattering and radiative transfer inside the mineral grain with diffuse scatterers ($npFe^0$) are modeled. While using only the laboratory-measured inputs (sizes, refractive indices and weight fractions of $npFe^0$), we are able to reproduce the spectra of pure and SW olivine (Fig. 1).

Some of the slope changes observed can be explained with even more fundamental light-scattering theory. Due to the high absorption coefficient of Fe, the $npFe^0$ will mostly affect spectra via absorption. The effective absorption coefficient k of host mineral-$npFe^0$ mixture can be approximated using, e.g., the Maxwell-Garnet mixing theory. The relation of increasing $npFe^0$ and k is linear. However, the absorption in the material can be approximated with ~exp(-k l / λ) –type factor, where l is the distance traveled in the medium, and λ is the wavelength. Due to this nonlinear relation, the same Δk from $npFe^0$ inclusions will decrease more for the higher reflectance values than for the lower ones. This can explain why, in enstatite, the first and second slope are behaving differently — the first slope is originally positive (from lower to higher reflectance), and the second is originally negative.

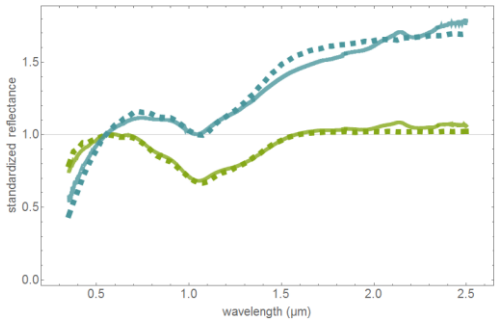

Figure 1: Measured olivine spectra (solid lines; green for pure, blue for space-weathered) with modeled spectra (dashed lines).

References: [1] Kohout T. et al. (2014) *Icarus*, 237(15), 75–83. [2] Kohout T. et al. (2015) *Workshop on Space Weathering of Airless Bodies*, Abstract. [3] Muinonen K. et al. (2009) *JQSRT*, 110, 1628–1639.

Acknowledgements: European Research Council Advanced Grant project No. 320773 (SAEMPL).

THE MANY FORMS OF SPACE WEATHERING. C. M. Pieters, [1]SSERVI-SEEED, Dep. Earth, Environment, and Planetary Sciences, Brown Univ., Providence, RI 02912 USA; email: Carle_Pieters@brown.edu.

Introduction: Understanding the causes and effects of space weathering on planetary surfaces across the solar system is complex. Materials exposed to the harsh space environment are altered over time in both physical and compositional properties. The generic definition of *space weathering* simply refers to this alteration. There are multiple processes, however, that can and do alter materials on the surface of an airless body: comminution, melting, vaporization by energetic impacts; gardening of a particulate soil and mixing with local and foreign materials by repeated impacts; sputtering at the atomic/molecular scale by solar wind; crystal damaging by UV radiation and energetic particles; structural fatigue from diurnal thermal cycling; mobility or loss of volatile species by radiant heating and sublimation; etc. Thus, *space weathering* takes many forms and its alteration products are a direct function of a) location in the solar system, b) composition and texture of the surface, c) mass and magmatic evolution of the body, and d) length of time exposed.

The regolith of only two extraterrestrial bodies has been directly sampled (The Moon and Itokawa). These samples and the ongoing detailed analyses in Earth-based laboratories provide a cornerstone for recognizing and understanding some aspects of space weathering effects. A handful of additional bodies have been visited by spacecraft and studied in detail for extended periods with remote sensors (Mercury, Eros, Vesta, and most recently dwarf planet Ceres and comet Churyumov-Gerasimenko). Seven additional asteroids have been observed with instruments during a spacecraft flyby, while the satellites of Mars, Jupiter, and Saturn, have been studied to different degrees through multiple flybys, and the Pluto system has now revealed some of its secrets through the immaculately planned detailed flyby sequence. The amount and type of data now available to study the surfaces of airless bodies is exceptional - but it is also extremely uneven in character and quality. Summarized below are a few of the various forms of space weathering that are now recognized (or hypothesized) based on the clues currently available in the data.

Lunar-like space weathering. After decades of searching for an explanation of why the optical properties of lunar soils are so very different from particulate lunar rocks, a breakthrough came identifying nanophase metallic iron ($npFe^0$) on the surface of lunar soil grains [1]. This provided the physical basis for an integrated perspective [2] that explained all the observed properties of well developed 'mature' lunar soils (low albedo, weak absorptions, relative steep nearIR continuum). [Note: lunar swirls do not meet the requirements of 'immature' lunar soils, howevef [3]].

Itokawa-like space weathering. Return of soil grains from the S-Type near-Earth asteroid Itokawa identified a LL chondrite composition with similar nano-phase opaque rims on several grains [4]. Important distinctions are a lower abundance of the space weathered rims and the presence of both Fe and S nanophase components, consistent with derivation from the bulk composition of the asteroid.

Mercury-like space weathering. Although no samples are available, the detailed data from MESSENGER portray a highly processed regolith resulting from severe conditions [5]. Mercury soil appears to represent the opposite extreme of Itokawa's.

Vesta-like space weathering. For the large main-belt asteroid Vesta, we have both meteorite (rock) samples and detailed orbital data from Dawn. Although the surface of Vesta is basaltic and old, it does not exhibit optical properties indicating accumulation of $npFe^0$ on soil grains [6]. Instead, observed space weathering processes are dominated by regolith gardening and mixing with opaque-rich foreign material [7]. A foreign contribution to the regolith is also supported by the distribution of notable hydrous materials delivered to the anhydrous surface [8].

Ceres-like space weathering. The largest asteroid, Ceres (now being studied by Dawn), presents a completely different environment and bulk composition (density suggest ~35% water). Globally, Ceres is exceedingly dark and exhibits ammonia hydrates with no detectible water ice [9], but small exceptionally bright areas are also identified [10]. Space weathering on Ceres is undoubtedly complex and dominated by processes less common on previously studied bodies.

References:

[1] L.P. Keller, D.S. McKay, *GCA* **61**, 2331 (1997); S.K. Noble, et al, *Meteorit. Planet. Sci*. **36**, 31 (2001); S.K. Noble, et al, *Icarus* **192**, 629 (2007) [2] C.M. Pieters, et al. *Meteorit. Planet. Sci.* **35**, 1101 (2000); B. Hapke, *J. Geophys. Res.* **106**, 10039 (2001) [3] C.M. Pieters et al., LPSC45-1408 (2014);--- LPSC46-2120 (2015). [4] T. Noguchi, et al, *Science* **333**, 1121 (2011) [5] D. Domingue et al., (2014) *Space Sci Rev.* 181:121-214. [6] D.T. Blewett et al., *these volumes*; [7] C.M. Pieters et al., *Nature*, 491 (2012); [8] C.M. De Sanctis et al., *Astro Phys J.* 758, L36 (2012); T. Prettyman et al, *Science*, (2012); [9] C.M. De Sanctis et al., *Nature*, submitted; [10] A. Nathues et al., *Nature*, submitted.

Visible and Infrared Spectra of Weathered Solar System Ices

Michael J Poston[1], Jordana Blacksberg[2], Mike Brown[1], Elizabeth Carey[2], Robert Carlson[2], Bethany Ehlmann[1,2],John Eiler[1], Kevin Hand[2], Robert Hodyss[2], Ahmed Mahjoub[2], and Ian Wong[1].
([1]California Institute of Technology, Pasadena, CA. [2]Jet Propulsion Laboratory, California Institute of Technology, Pasadena, CA. *mjposton@caltech.edu.*)

Introduction: The Jupiter Trojan asteroids lack atmospheres, and thus are subject to space-weathering processes. Given their location at ~5 AU, and possible origin in the Kuiper Belt [eg. 1,2], the Trojan asteroids would be expected to be ice and organic rich, but telescopic observations have yet to identify bands for such compounds [3]. The only bands possibly detected to date are interpreted as belonging to silicates [4]. The relatively featureless spectra observed in the mid-infrared are likely to be related in some way to space weathering. However, the composition of these objects and therefore the likely weathering products remain an open question.

An additional observable is the slope of the spectra of reflected sunlight in the visible and near infrared ranges of the spectrum. Emery et al. [3] observed the spectral slopes of the Trojans and found a bimodal distribution consistent with two, dynamically well-mixed populations. Brown et al. [5] reviewed what data exist for Centaur and Kuiper Belt Objects (KBOs) and found both populations to have a bimodal distribution of spectral slopes. All of the objects studied had 'red' spectral slopes, a phenomenon also observed for weathered silicates [eg. 6]. Emery et al. [3] suggested the slopes are due to a compositional difference. Brown et al. [5] took this further and hypothesized, based on limited laboratory studies of the visible spectra of weathered organic ices [7], that the bimodality may reflect differing compositions of refractory residues formed at locations spaning the stability line for a critical elemental or chemical species. The bodies would then migrate to the present, warmer location (where exposed ices may sublime) and retain the refractory residue as a record of the location where they were weathered. (The residue may dominate the surface, or be mixed with silicates.) Wong et al. [8] have found that the frequency-magnitude distribution of the Trojan asteroids is consistent with this hypothesis. We are currently simulating the irradiation and thermal histories predicted by this hypothesis with laboratory simulations of irradiation weathering of mixed ices.

Methods and Materials: Laboratory simulations are being carried out in the Minos chamber at the Icy Worlds Simulation Laboratory at NASA's Jet Propulsion Laboratory. Reflectance is collected in the visible and near infrared range (~0.5 to 1.7 um) and by an FTIR in the mid IR. Mixed ices of water (H_2O), methanol (CH_3OH), ammonia (NH_3), and hydrogen sulfide (H_2S) are deposited at 50 K on a gold mirror. After deposition, the ices are irradiated at 50 K with a beam of 10 keV electrons (measured current about 0.5 µAmps). The ices are then warmed (while continuing irradiation) to 120 K and held there for several days before ending the irradiation. This process is intended to simulate a likely history for an object that forms beyond the present orbit of Neptune and eventually migrated inward to the orbit of Jupiter.

Results: Several pure and mixed ice irradiation experiments have been conducted, including: a 3:3:3:1 mixture of H_2S: NH_3: CH_3OH: H_2O; and a 3:3:1 mixture of NH_3: CH_3OH: H_2O. The spectral slope increased dramatically after irradiation of the mixture containing H_2S. This is consistent with sulfur being the critical component determining which of the spectral populations an object belongs to in the present inventory of outer solar system objects.

References: [1] Morbidelli et al. (2005) *Nature*, 435, 462. [2] Nesvorny et al. (2013) ApJ, 768, 45. [3] Emery et al. (2011) *AJ*, 141, 25. [4] Emery et al. (2006) *Icarus*, 182, 496. [8] Brown et al. (2011) *ApJL*, 739, L60. [6] Bennett et al. (2013) Chem. Rev. 113, 9086. [7] Brunetto et al. (2006) *ApJ*, 644, 646. [8] Wong et al. (2014) AJ, 148, 112.

This work has been supported by the Keck Institute for Space Studies (KISS). The research described here was carried out at the Jet Propulsion Laboratory, Caltech, under a contract with the National Aeronautics and Space Administration (NASA) and at the Caltech Division of Geological and Planetary Sciences.

Lunar Reconnaissance Orbiter LAMP Investigations of Space Weathering. K. D. Retherford[1], Y. Liu[1], A. R. Hendrix[2], T. K. Greathouse[1], G. R. Gladstone[1], K. E. Mandt[1], E. L. Patrick[1], A. F. Egan[3], D. E. Kaufmann[3], D. M. Hurley[4], J. T. S. Cahill[4], W. R. Pryor[5],; [1]Southwest Research Institute, San Antonio, TX (kretherford@swri.edu), [2]Planetary Science Institute, Tucson, AZ, [3]Southwest Research Institute, Boulder, CO, [4]Johns Hopkins University Applied Physics Laboratory, Laurel, MD, [5]Central Arizona University, Coolidge, AZ.

Abstract. Far ultraviolet (far-UV) albedo maps are obtained using the Lunar Reconnaissance Orbiter (LRO) Lyman Alpha Mapping Project (LAMP)'s innovative nightside observing technique [1]. Similar dayside FUV maps obtained using the more traditional photometry technique with the Sun as the illumination source are very complementary. LRO-LAMP measurements provide a unique perspective on space weathering topics, as described more fully in Hendrix et al., *this meeting* [2] and [3].

Introduction. LAMP data products include global nightside and dayside brightness maps over specific wavelength ranges within LAMP's 57-196 nm bandpass [4], and similarly constructed albedo maps (i.e., brightness maps normalized by the varying surface illumination). Lyman-α, on-band and off-band maps (i.e., on and off the water frost absorption band at ~165 nm) and more detailed spectral image cubes are useful for identifying UV-brightenings associated with enhanced space weathering effects [1,2,5,6,7,8].

Results. The far-UV spectral inversion property of the lunar albedo discovered by the Apollo 17 UVS Lyman-α reflectance measurements [9] is confirmed with the LAMP observations [5].

Hendrix et al., *submitted to Icarus*, 2015 [3] report that swirl regions, i.e., previously characterized higher albedos in the visible and near-infrared, also exhibit far-UV spectral characteristics different from the surrounding regions. Specifically, the swirls are found to be less UV-blue than non-swirl terrains, likely in response to changes in space weathering processes within these regions.

Numerous craters are observed with Lyman-α albedos distinctly enhanced along their crater rims [5], which is consistent with the enhanced space weathering there as first identified using Apollo 17 UVS measurements [9]. For craters observed at high latitudes these Lyman-α albedos are distinctly enhanced along their equator facing rims, in agreement with relatively higher rates of surface proccessing by the higher fluxes of solar UV and solar wind incident on these regions.

A lab study of the FUV reflectance properties of Apollo samples, lunar simulants, and water ice is underway to further develop UV reflectance techniques for constraining composition and space weathering. Future LAMP and lab efforts to measure the far-UV spectral effects of iron and sub-microscopic iron (SMFe) understood to exist in/on the weathered rims of grain materials will be discussed.

References [1] Gladstone, G. R. et al., Far-Ultraviolet Reflectance Properites of the Moon's Permanently Shadowed Regions, *J. Geophys. Res.*, *117*, E00H04, 2012. [2] Hendrix, A. R. et al., Lunar Space Weathering Effects in the Ultraviolet, *this meeting*, 2015. [3] Hendrix, A. R. et al., Far UV Characteristics of Lunar Swirls, *submitted to Icarus*, 2015. [4] Gladstone, G. R. et al., LAMP: The Lyman Alpha Mapping Project on NASA's Lunar Reconnaissance Orbiter Mission, *Space Sci. Rev.*, *150*, 161-181, 2010. [5] Retherford, K. D. et al., LRO/LAMP Far-UV Albedo Maps, *in preparation*, 2015. [6] Hayne, P. O. et al., Evidence for Exposed Water Ice in the Moon's South Polar Regions from Lunar Reconnaissance Orbiter Ultraviolet Albedo and Temperature Measurements, *Icarus*, *255*, 58-69, 2015. [7] Hendrix, A. R. et al., Lunar Albedo in the Far-UV: Indicator of Hydrated Materials and Space Weathering, *J. Geophys. Res.*, 117, E12001, 2012. [8] Mandt, K. E. et al, LRO-LAMP Detection of Geologically Young Craters within Lunar Permanently Shaded Regions, *Icarus in press*, doi:10.1016/j.icarus.2015.07.031, 2015. [9] Lucke, R. L. et al., Far-Ultraviolet Albedo of the Moon, Astron. J., 81, 12, 1976.

SPACE WEATHERING: FROM ITOKAWA TO MERCURY VIA THE MOON. S. Sasaki[1], M. Okazaki[1], T. Hiroi[2], A. Tsuchiyama[3], A. Miyake[3], and T. Matsumoto[4], [1]Department of Earth and Space Science, Osaka University (1-1 Machikaneyama, Toyonaka, Osaka 560-0043, Japan), [2]Department of Earth, Environmental and Planetary Sciences, Brown University (Providence, RI 02912, U.S.A.), [3]Department of Geology and Mineralogy, Kyoto University (Kitashirakawaoiwake-cho, Sakyo, Kyoto, 606-8502, Japan), [4],ISAS/JAXA. (Sagmihara, Kanagawa, Japan)

Itokawa Observed by Remote Sensing:

In November 2005, Japanese Asteroid Sample Return Mission HAYABUSA spacecraft rendezvoused and observed S-type asteroid (25143) Itokawa. The surface of Itokawa is divided into brighter (and bluer) areas and darker (and redder) areas [1. 2]. In rough zones, dark boulder-rich surfaces usually superpose on bright materials. The near-infrared spectrometer (NIRS) confirmed previous disk-integrated results that suggested Itokawa's spectrum closely matched a weakly weathered LL5/6 chondrite [3]. Although the surface is covered with rocks and is apparently deficient of fine regolith, Itokawa's surface show darkening and reddening by space weathering. Experimental results suggest rocky meteorite fragments can be weathered [4]. The presence of opposition effect in rocky terrain of Itokawa suggested that the surface would be covered by particulate materials or porous enough to scatter light. Spectral variations were observed, that can be explained by Hapke's space weathering model, where the amount of npFe0 controls spectral reddening. As for color variation of Itokawa, we can interpret that seismic shaking caused by impacts or planetary encounters should lead to exposure of underlying relatively fresh bright area by removing weathered darker boulder-rich layer.

Itokawa – Evidence from Returned Samples

In 2011, HAYABUSA returned more than 1000 particulate samples of Itokawa back to the Earth. Analysis of mineral assemblies and composition of Itokawa particles supports that Itokawa has LL-chondrite composition. The most notable discoveries in Itokawa particles is amorphous space-weathering rims containing npFe0 [5-6]. Sometimes ion-implanted type-II layers contains vesicles, probably due mainly to trapping solar wind energetic helium with penetration depth up to a few tens μm (composite vesicular rim).

Large vesicles are observed as blisters on the surface of Itokawa particles. Matsumoto et al. [7] identified space weathered rims with blisters on eleven out of twenty regolith particles of Itokawa. It was confirmed that a blister corresponds to a vesicle in npFe0-bearing amorphous layer. These rims with blisters are heterogeneously distributed even in one particle. Sometimes blistered rims are observed in opposite surfaces of the same particle. This is a strong evidence of regolith mixing. So far, there is no correlation between the blister distribution and surface morphologies such as roundness of particles. A few 10 nm amorphous rim can be developed in timescale 1000 yr, based on solar flare trackdensity. Regolith mixing processes may prolong timescale of optical maturation on smooth regions of Itokawa.

Possible Role of Sulfur
Returned Sample from Itokawa

Another type of rim found is a thin (a few to 5 nm) amorphous layer (tyoe-I) on the outermost surface. The outermost irradiated rim contains npFe0 with size around 2-3 nm; they are usually observed typically as a monolayer of iron particles. Sulfur and magnesium abundances suggest the presence of nanophase FeS (and MgS)[6]. The presence of npFeS in asteroidal regolith is compatible with observation of regolith breccia meteorites [7,8].

Laboratory Simulation: Space weathering simulation using a pulsed laser on the Ehole H5 chondrite produced a vapor-deposited coating, which consists of amorphous Mg-rich silicate glass and abundant nanophase (2-5 nm) FeS (npFeS) particles [9]. Spectral changes (space weathering reddening and darkening) of olivine samples using pulse laser were facilitated when 5% FeS is added [10]. npFeS and npMgS may play an important role on the surface of Mercury. On Mercury, MESSENGER revealed a high sulfur abundance (2wt% on average up to 4wt%), which can account for all of Fe by FeS. Spectral feature showed significant darkening/reddening (compared with fresher interior materials), which could not be solely responsible. Addition of FeS promoted melting and nFe0 would reside in the thick amorphous layer where nFe0 concentrate both at top and bottom layer.

References: [1] Saito J., et al. (2006) Science 312, 1341. [2] Ishiguro M. et al. (2006) Meteorit. Planet. Sci., 42, 1791. [3] Hiroi T., et al. (2006) Nature, 443, 56. [4] Sasaki et al. (2006) Lunar and Planetary Science Conference 37, #1705. [5] Noguchi, T., et al.: Science 333 (2011), 1121-1125. [6] Noguchi, T., et al.: Meteorit. Planet. Sci., 49 (2014), 188-214. [7] Matsumoto, T. et al. Icarus (2015) 257, 230. [8] Noble S. K. et al. (2011) Meteorit. Planet. Sci., 45, 2007. [9] Keller, L.P. et al.(2013) Lunar and Planetary Science Conference 43, #2404. [10] Okazaki, M. et al. (2015) Lunar and Planetary Science Conference 46 #1890.

A PROPOSED APPARATUS TO STUDY THE IMPACT OF SOLAR WIND IONS ON THE SURFACES OF MERCURY, THE MOON, AND ASTEROIDS. D. W. Savin[1], D. L. Domingue[2], and K. A. Miller[1], [1]Columbia University, (Astrophysics Laboratory, 550 West 120th Street, MC 5247, New York, NY 10027; savin@astro.columbia.edu), [2]Planetary Science Institute (1700 East Fort Lowell Road Suite 106, Tucson, AZ 85719-2395; domingue@psi.edu).

Introduction: On both Mercury and the Moon there is a complex interplay between the space environment, weathering processes, regolith modification and evolution, and exosphere generation. Some of the most important weathering processes are solar wind ion irradiation, micrometeroid impact vaporization and gardening, photon-stimulated desorption, and thermal desorption. Understanding how these processes work together to create a whole first requires teasing apart the underlying microphysics for each [1].

Understanding the formation of the rocky planets in the inner Solar System builds upon data from the asteroid remnants of that epoch; but sample return missions are few and far between, given their cost and complexity. For that reason, spectroscopic observations are the primary means for studying asteroids. If definitive links could be made between various meteorite classes and asteroid types, then meteorites would provide a low cost asteroid sample set for study. The primary means to make these connections relies on spectroscopy. However, space weathering alters asteroid reflectance spectra and hinders making clear connections [2].

We propose to study the role of solar wind ion irradiation in the physical and chemical alteration of planetary surfaces and the generation of exospheres for planetary bodies neither protected by an atmosphere nor significantly shielded by a magnetic field. We will apply our experimental findings to studies of Mercury, the Moon, and asteroids. The solar wind sputters particles from the surfaces of these bodies, contributing to the formation of their exospheres. It alters the surface and internal structure of the regolith grains, altering both the chemical structure, mineralogical make-up, and spectral properties of the regolith. Spectra are expected to vary as a function of the time-integrated solar wind flux, known as the solar wind fluence.

Proposed Apparatus: We propose to construct a unique instrument that will enable developing a quantitative understanding of the effects of solar wind ion irradiation on the regolith surfaces of Mercury, the Moon, and asteroids. Regolith-like loose power samples will be generated in an inert environment and next baked in vacuo to drive off any remaining atmospheric impurities. The samples will then be irradiated using ion beams of H and He, which respectively make up 95% and 5% of the solar wind. Beam energies that are typical of the solar wind, ~1 keV/amu, will be used. A novel beam line configuration will be constructed to irradiate regolith-like loose powders from above and to perform in situ analyses in vacuo, thereby avoiding atmospheric contamination of the sample after it has been chemically activated by the ion irradiation. Changes in the reflectance spectra of the irradiated samples will be studied using spectral analysis tools frequently applied to Mercury, the Moon, asteroids, and meteorites. The role of solar wind ions in exosphere formation will be studied using catcher foils to collect the atoms sputtered from the regolith analogs. These samples will be studied ex situ using both conventional and synchrotron-based X-ray sources. We know of no groups currently working in the field with all of these capabilities in a single laboratory set-up.

Limitiations of Past Work: Published state-of-the-art ion irradiation studies have used slabs or powders which have either been highly compressed or epoxied, as opposed to more realistic loose powers. Most previous irradiation studies using H and He ion beams have been performed at energies ~10-1000 times higher than the typical solar wind. Other studies have used ions of C, N, O, Ne, and Ar at energies much higher than the typical solar wind. These elements comprise less than 0.1% of the solar wind and it is unclear whether the results can be reliably scaled to H and He at the relevant energies.

Questions to be Studied: Some of the questions that we will investigate include: 1. Does the sputter yield of the regolith change with solar wind fluence? 2. What is the angular distribution of sputtered atoms from the regolith? 3. How does the spectral reflectance of the regolith change with solar wind fluence? We will examine how these questions depend on regolith properties such as grain size and porosity (i.e., the fraction of the powder volume not occupied by grains). From our lab results, we will generate critically needed data for models of the formation of exospheres, which are use to interpret direct measurements of exospheric species, their spatial distribution, and their temporal variability. Our data will also be important for analyzing surface spectra, which are used to determine surface mineral and elemental composition, and to connect meteorites to their parent asteroid taxonomy.

References: [1] Domingue, D. L. et al. (2014) *Space Sci. Rev., 181,* 121-214. [2] Gaffey, M. J., 2010, *Icarus, 209,* 564-574.

ATOMIC-SCALE MODELING AND THEORY OF SPACE WEATHERING PROCESSES: MECHANISMS AND SURFACE PROPERTIES. P.K. Schelling[1], D. T. Britt[1], A. H. Quadery[1], W. C. Tucker[1], and R. Blair[1], [1]Department of Physics, 4000 Central Florida Blvd., University of Central Florida, Orlando Florida 32816. Email: patrick.schelling@ucf.edu.

Introduction: Space-weathering in airless bodies includes a number of complex processes that act to modify surface chemistry and morphology. High-energy particles including solar-wind protons generate point defects, which may tend to cause amorphization of surfaces. In addition, high-energy impacts lead to sputtering, vaporization, and sputter redeposition. These processes tend to reduce surfaces. Thermodynamically, it is favorable to reduce iron before other elements, and hence evolution of minerals in the airless environment of space generate nanophase Fe ($npFe^0$) [1,2].

Much of the efforts in this field have been directed towards understanding how weathering processes affect optical reflectivity. While this field has reached some level of maturity, it is less understood about how different minerals evolve in the space environment. This includes the "rate" at which they weather, and more specifically how defects and stoichiometry changes occur at the surface. In addition, very little is known currently about how other surface properties evolve, including chemical reactivity and adhesive properties. The latter includes both the tendency of molecules to adhere to surfaces, and also the adhesive forces between mineral grains.

Atomic-Scale Modeling Approach: One approach that can be used to understand differences between weathering mechansisms in different minerals, and their resultant surface properties. The basic idea is to integrate the equations of motion for a system with interactions based on a simple empirical potential, or possibly a more sophisticated electronic-structure based approach.

We have developed empirical potentials capable of predicting basic mechanisms of radiation damage and surface reduction in olivine, orthopyroxene, and silica [2]. Point defects are generated by simple algorithms, and their structure is evolved in time to elucidate how overall morphological changes occur. Finally, surface properties, including chemical reactivity and adhesive mechanisms can be elucidated.

Results and Summary: In the case of olivine and orthopyroxene, we have obtained extensive data that details differences in weathering mechanisms. Specifically, we have shown that differences in migration pathways might partially explain weathering rates and tendencies to amorphize[3]. In orthopyroxene, point defects, and specifically oxygen interstitials, tend to migrate rapidly in comparison to olivine. In addition, oxygen migration tends to be one-dimensional and hence can persist over very long range without recombination. This should render surfaces in orthopryoxene less susceptible to surface reduction. However, the diffusion mechanism in orthopyroxene tends to amorphize the silica network. In olivine, by contrast, cations defects migrate rapidly and either heal defects or become trapped in clusters.

In the description of surface properties beyond optical reflectivity, space weathering has profound implications. Specifically, we find that the absorption energy of small molecules, including organic species and other volatiles, depends significantly on surface reduction and space weathering. This likely also has a significant impact on chemical reactions occurring at surfaces. In addition, we find that rather minor differences in surface chemistry can have major effects on the adhesive forces between mineral grains. In contrast to the most widely accepted view, we find that interactions between mineral grains in close proximity are not consistent with weak dipolar van der Waals interactions. Instead, we find a very broad range of interaction energies which depends on whether or not surfaces are passivated. For example, we find more than an order of magnitude difference in the adhesive energies between reduced surfaces and surfaces fully passivated by oxygen or hydroxyls. Because surface passivation and space weathering are closely linked, these results suggest that potentially much larger adhesive forces exist in surface regoliths exposed to the space environment.

References: [1] Elsila, J.E. *et al* (2012) *MAPS, 47,* 1517-1536. [2] Quadery, A. H. *et al* (2015) *JGR-Planets., 120,* 643-661. [3] Yamada, M. *et al* (1999) *EPS 51,* 1255-1265.

PRECIPITAITON OF ELECTRONS AT MERCURY'S SURFACE FROM THE MAGNETOSPHERE. D. Schriver[1], P.M. Trávníček[2], D.L. Domingue[3], Jörn Helbert[4], [1]Department of Physics and Astronomy (University of California Los Angeles, 3860 Slichter Hall, Los Angeles, CA 90095-1567; dave@igpp.ucla.edu), [2]Space Sciences Laboratory, (University of California, Berkeley, CA, pavel@ssl.berkeley.edu), [3]Planetary Science Institute (1700 East Fort Lowell Road Suite 106, Tucson, AZ 85719-2395; domingue@psi.edu), [4]Institute for Planetary Research (DLR, Rutherfordstrasse 2, 12489 Berlin, Germany; joern.helbert@dlr.edu)

.

Introduction: Observations by the MESSENGER spacecraft in orbit around Mercury from 2011 to 2015 have established that Mercury's magnetosphere hosts a quasi-trapped population of electrons with bulk energies of 1–10 keV centered about the magnetic equator. Although there are occasional observations of higher-energy (≥ 35 keV) electrons within the magnetosphere, there is no high-energy radiation belt present at Mercury similar to those at the other planets in our solar system with global magnetic fields, including Earth, Saturn, Jupiter, Uranus and Neptune. Observations from MESSENGER's X-Ray Spectrometer and simulations have also established that the 1–10 keV electron population around Mercury precipitates to the surface in an auroral-oval-type pattern with fluxes of ~10^9–10^{10} $cm^{-2}s^{-1}$.

Magnetospheric Modeling: Global kinetic simulations of Mercury's magnetosphere has been carried out using three dimensional hybrid simulations and particle trajectory tracing methods. These simulations have determined that the quasi-trapped electrons within Mercurys' magnetosphere are energized in Mercury's magnetotail via a combination non-adiabatic particle acceleration near magnetic reconnection regions and betatron/Fermi acceleration. The precipitation profile of electrons from the simulations is shown in Figure 1.

Consequences of Electron Precipitation: The precipitating 1–10 keV electrons can cause X-rays to be generated and emitted from the surface [1], and also can result in the ejection of sodium ions into the magnetosphere through the process of electron-stimulated desorption [2]. Long-term electron precipitation may result in space weathering of the surface regolith [3]. The results from the simulations and consequences will be discussed in detail.

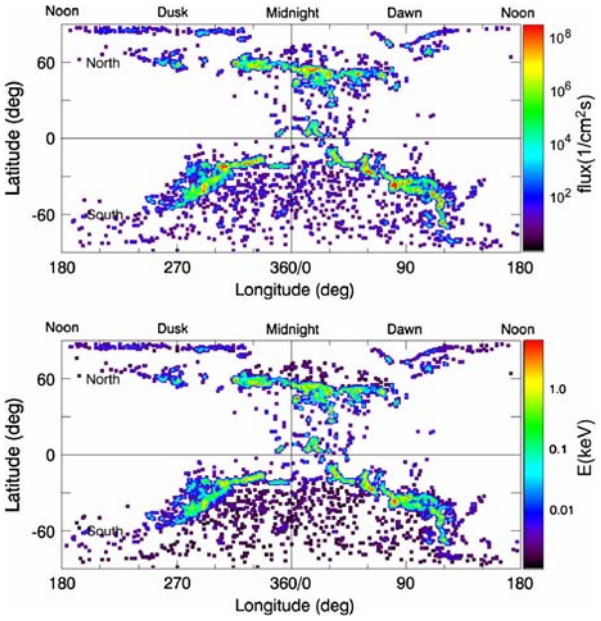

Fig. 1. Taken from Schriver et al. (2011) [2] and Domingue et al. (2014) [3], these graphs show the electron precipitation flux (top) and the electron precipitation energy (bottom) simulation correlating to MESSENGER's first flyby of Mercury. Longitude is a function of local time and not geographic longitude.

References: [1] Starr, R.D. et al. (2012), *J. Geophys. Res.*, 117, E00L02, doi:10.1029/2012JE004118 [2] Schriver et al. (2011) Planet. Space Sci. 59, 2026 [3] Domingue, D. L. et al. (2014) *Space Sci. Rev., 181,* 121-214

SPACE WEATHER IN THE SATURN SYSTEM. F. SCIPIONI[1], P. Schenk[1], and F. Tosi[2], [1]Lunar and Planetary Institute, 3600 Bay Area Boulevard, 77058 Houston, TX – Scipioni@lpi.usra.edu; [2]IAPS/INAF, Via del fosso del cavaliere 100, 00133 Rome, Italy.

Introduction: Water ice is the most abundant component of Saturn's mid-sized moons. However, these moons show an albedo asymmetry – their leading sides are bright while their trailing side exhibits dark terrains. Such differences arise from two surface alteration processes.

The first is due to bombardment of charged particles from the interplanetary medium and driven by Saturn's magnetosphere (e.g. [1]). These particles fracture the surface, forming sub-micron ice particles, and get contaminants implanted in the upper ice layer (e.g. [2]). The second process results from the impact of E-ring particles on the satellites' leading side. The E-ring is composed primarily of pure water ice grains, which originate from Enceladus' southern polar plumes. Tethys, Dione, and Rhea orbit outside the E-ring, while Mimas orbits inside. E-ring ice particles are continuously refreshing the leading hemisphere surfaces of Tethys, Dione, and Rhea, thereby making them bright (e.g. [3] [4] [5] [6] [7] [8]).

Data analysis: Space weather effect translates in a variation of the main water ice absorption bands on the surface of Saturn' satellites. In general, absorption bands will be shallower if the water ice's abundance is reduced, or the ice grains are smaller, or if the ice layer is covered or mixed by some contaminants.

We present here the analysis of data retuned by the Visual and Infrared Mapping Spectrometer (VIMS) onboard the Cassini mission. We focuse on the infrared portion of the spectrum, between 0.8 and 5.1 μm. In this spectral range the main water ice absorption bands are located, at 1.04, 1.25, 1.52, and 2.02 μm.

To understand the degree of surface alteration in the Saturn' system, we will map the variation of the water ice absorption bands at 1.25 and 2.02 μm for five Saturn' satellites, Mimas, Enceladus, Tethys, Dione, and Rhea. In Figure 1 we show the variation of the band at 2.02 μm for Enceladus.

For Dione and Rhea, we will also show the results published by [7] and [8] respectively, about the identification of homogeneous terrain units on their surface. The different terrain types had been identified by applying a classification technique to the spectra of the two satellites. The differences in composition between terrains are all due to the space weather mechanisms acting on the surface of Dione (Figure 2, TOP) and Rhea (Figure 2, BOTTOM).

Results: The variation of the depth of the water ice absorption bands across the surface reflects the different space weather mechanisms acting on them. Terrains where E-ring's ice particles deposit have in general deeper water ice absorption bands, meaning that this mechanisms refreshes that portion of surface. On the other hand, terrains subject just to bombardment of charged particles and micrometeorite gardening have shallower absorption bands. This can be due to and increase in contaminats abundance, and/or to a finer grain size.

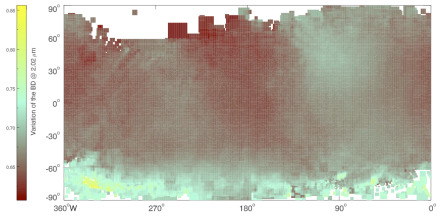

Figure 1: Variation of the 2.02 μm water ice absorption band across Enceladus' surface

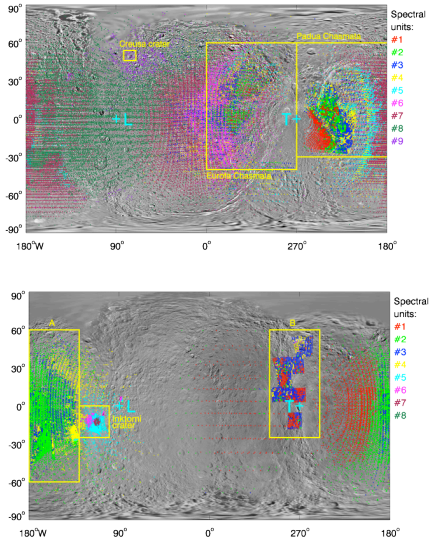

Figure 2: Homogeneous terrain units identified on Dione' (TOP) and Rhea' (BOTTOM) surface by applying the Spectral Angle Mapper classification technique to their VIMS spectra

References: [1] Schenk, P., et al., 2011. Icarus 211, 740– 757. [2] Baragiola, R. A., et al., 2013. In: Gudipati, M. S., Castillo-Rogez, J. (Eds.), Vol. 356, p. 527. [3] McCord, et al., 1971. Astrophys. J. 165, 413–424. [4] Blair, G., Owen, F., 1974. Icarus 22, 224–229. [5] Buratti, et al., 1990. Icarus 87, 339-357. [6] Verbiscer, A.J. and Veverka, J., 1992. Icarus 99, 63-69. [7] Scipioni, F., et al., 2013. Icarus 226, 1331-1349. [8] Scipioni, et al., 2014. Icarus 243, 1-16.

MATURITY OF THE CRATER RIM WALLS AS A FUNCTION OF THE CRATER SIZE. Chae Kyung Sim, Sungsoo S. Kim, and Minsup Jeong, Dept. of Astronomy & Space Science, Kyung Hee University, Yongin, Gyeonggi 17104, Korea, cksim@khu.ac.kr.

Introduction: Space weathering agents such as micrometeoroids and solar wind particles continuously age the uppermost regolith of the lunar surface by comminuting as well as darkening and reddening the grins. Among several maturity indices, optical maturity (OMAT) and the median grain size <d> suggested by [1] and [2-3], respectively, have been widely used. <d> quantifies the external modification and its estimation comes from the relationship between the maximum degree of linear polarization and albedo in visible wavelength range [2-3]. OMAT illustrates spectral alteration and darkening and is deduced from the near-infrared ratio-reflectance plot [1].

The vertical and horizontal regolith-mixing processes such as excavation and ejecta blanket formation by impact cratering and mass-movement by seismic and thermal activities stop and (re)start the maturation clock of each regoligh grain that ticks only when exposed to the space. Studying maturity indices of impact crater features that show a diversity of maturation rate as functions of its size and/or formation age gives us a hint to understand the maturation and mixing process of the covering regoith.

Methods: We investigate median grain size <d> and optical maturity (OMAT) of the regolith covering ~140 near-side craters. The crater diameter ranges from 2.5 km to 110 km and their formation periods from Copernican to pre-Nectarian. Here we focus on the crater rim walls where the vertical mixing process by mass-movement can enhance the gardening of regolith and the supply of immature materials in the deeper layer to the surface.

We obtained <d> values from our multi-band polarimetric observations of the Moon using a 15-cm reflecting telescope [4]. We obtained OMAT values from the Clementine data using the formula suggested by [1]. We subtract the median value of the 'outside' (background) of the crater from that of the interior rim wall. For both <d> and OMAT, the larger the value, the less mature the regolith.

Analyses: Both <d> and OMAT values of the interior rim wall initially increase as the crater size increases until ~10-20 km, then decrease. This transition crater size happens to correspond to the transition diameter from simple to complex craters.

For larger craters, *i.e.*, complex craters, it is clear that the interior rim wall of the craters formed in recent eras tend to remain fresh and become mature along with time. For the simple crater case, smaller craters are more mature, which is opposite to the case of complex craters. This is thought to be because smaller craters become flattened more quickly [5], thus have smaller vertical mixing in the regolith due to mass movement.

We will also discuss on the maturity indices of the crater rim walls at high latitudes as a function of the position angle to see the latitude dependence of the space weathering process [6].

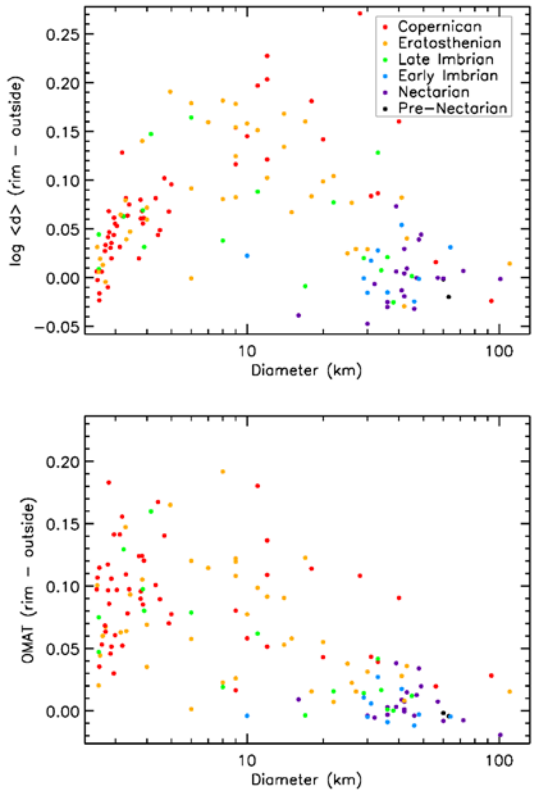

References: [1] Lucey P. G. et al. (2000) *JGR, 105*, E8, 20377-20386. [2] Shkuratov Yu. G. & Opanasenko N., V. (1992) *Icarus*, 99, 468. [3] Dollfus A. (1998) *Icarus, 136*, 69. [4] Jeong et al. (2015) *This workshop*. [5] Fassett C. I. & Thomson B. J. (2014) *JGR Planet., 119*, 2255-2271. [6] Hemingway D. J. et al. (2015) *Icarus, in-press*.

PARTICLE RADIATION ENVIRONMENTS AND THEIR EFFECTS AT PLANETARY SURFACES OF AIRLESS BODIES: REMOTE SENSING LESSONS LEARNED AT THE MOON BY LRO/CRATER AND EXTENSION TO OTHER PLANETARY OBJECTS. H. E. Spence[1], N. A. Schwadron[1], J. K. Wilson[1], A. P. Jordan[1], R. Winslow[1], C. Joyce[1], M. D. Looper[2], A. W. Case[3,8], T. J. Stubbs[4], C. Zeitlin[5], J. B. Blake[3], J. Kasper[3,6,8], J.E. Mazur[3], S. S. Smith[1], and L. W. Townsend[7], [1]Space Science Center, University of New Hampshire, Durham, NH (harlan.spence@unh.edu), [2]The Aerospace Corporation, Los Angeles, CA, [3]High Energy Astrophysics Division, Harvard CFA, Cambridge, MA, [4]Goddard Space Flight Center, Greenbelt, MD, [5]Southwest Research Institute, Boulder, CO, [6]AOSS, College of Engineering, Univeristy of Michigan, Ann Arbor, MI, [7]Dept. of Nuclear Engineering, Univ. of Tennessee, Knoxville, TN, [8]NASA Lunar Science Institute.

Energetic Particle - Planetary Surface Interactions: We focus on the interaction of energetic particles with the surfaces of planets that are surounded by extremely tenuous atmospheres and weak intrinsic planetary-scale magnetic fields. For this study, we define energetic charged particles as those with sufficient energy to penetrate significantly (at least 100 millimeters and up to several meters) into the planet's regolith. For practical purposes, the energetic particles of interest herein are those with energies greater than ~1 MeV. At sufficiently high energies (>500 MeV protons, for instance), this population not only penetrates substantially into a planet's regolith in an energy-dependent manner, but they also lose energy through nuclear interactions, in turn producing secondary nuclear by-products, including those that can be sensed remotely by orbiting spacecraft.

Energetic Particle Sources – GCR and SEP: Such highly energetic charged particles have two primary sources near planetary bodies – galactic cosmic rays (GCR) and solar energetic particles (SEP). GCR provide an incessant source of extremely energetic particles, emanating from outside our solar system and produced in association with processes occurring at supernova explosions throughout our galaxy. This source of energetic charged particles waxes and wanes slowly (over the ~11 year solar cycle) and comparatively weakly (well less than a factor of 10) both in space and time throughout the solar system.

Energetic charged particles are also produced episodically in association with explosive events on the Sun. These impulsive bursts of energetic charged particles, called solar energetic particles (SEP), stream outward from the Sun, producing many order of magnitude increases in high energy particle fluxes, lasting hours to days. SEPs race away from the Sun through interplanetary space, with the chance of encountering and interacting with planetary objects in their path.

Science Goal and Approach: Our focused goal is to provide a comparison of how GCR and SEP intensities vary throughout the solar system, and how they interact directly with the surfaces of similar atmospherless planetary objects. In this study, we use Earth's Moon as the most well-studied object, enabled by the extensive radiation mesurements obtained by NASA's Lunar Reconnaissance Orbiter (LRO).

Lessons Learned from LRO/CRaTER: The Cosmic Ray Telescope for the Effects of Radiation (CRaTER) [1] has been immersed in the radiation environment of the Moon since its launch on LRO [2] in June 2009. CRaTER measures the linear energy transfer (LET) of extremely energetic particles traversing the instrument, a quantity that describes the rate at which particles lose kinetic energy as they pass through matter.

Though designed to measure principally GCR and SEPs coming from zenith and deep space, CRaTER observations can and have been used also to remotely sense the energetic particle albedo coming from the lunar surface [3,4,5]. CRaTER observations have been used to quanify the collective radiation environment, including all sources, as well as the effects of the particles on the Moon's surface. These include various physical mechanisms, such as chemical weathering [6,7] of regolith lunar volatiles, as well as the effects of deep dielectric breakdown [8], just to name two.

Summary: We summarize the physics of GCR and SEP interactions with the Moon and how these processes depend also on the physical properties of the lunar surface (e.g., bulk composition, meteoritic gardening rates, temperature, etc.). Based on this core knowledge, we then quantify how these same processes operate at similar airless objects throughout the solar system, including at Mercury, in the Mars system, at Ceres as a core asteroid belt representative, and at the Pluto system.

References: [1] Spence H. E.. et al. (2010) Space Sci. Rev., 150(1-4), 243-284. [2] Chin G. S. et al. (2007) Space Sci. Rev., 129(4), 391-419. [3] Wilson, J. K. et al. (2012) JGR, 117, E00H23. [4] Spence, H. E. et al., (2013) Space Weather, 11, 643-650. [5] Looper, M. D., et al., (2013) Space Weather, 11, 142-152. [6] Schwadron et al. (2012) JGR, 117, E00H13. [7] Jordan et al. (2013) JGR, 118, 1257. [8]] Jordan et al. (2014) JGR, 119, 1806.

RADIATIVE TRANSFER MODELING OF NEAR-INFRARED REFLECTANCE DATA OF AIRLESS PLANETARY BODIES. K. R. Stockstill-Cahill[1] , D. L. Domingue[1], and J. T. S. Cahill[2], [1]Planetary Science Institute (1700 East Fort Lowell, Suite 106, Tucson, AZ 85719-2395; cahill@psi.edu), [2]The Johns Hopkins University Applied Physics Laboratory (11100 Johns Hopkins Road, Laurel, MD 20723).

Introduction: In this study we applied the radiative transfer model of Hapke [1-3] to predict the bidirectional reflectance spectra in a forward modeling approach [4,5]. In Hapke's model, the reflectance spectrum of a regolith or powder is computed from the single-scattering albedos of the mineral end-members included [2,3]. The single-scattering albedo (*w*) is the probability that a photon incident on a regolith particle will be scattered rather than absorbed. This property is independent of illumination or viewing geometry and is a function of a grain's scattering behavior and absorption coefficient. The absorption coefficient is in turn governed by the material's complex index of refraction, which is a function of the optical constants. The optical constants (*n*, *k*) are wavelength-dependent quantities that are unique to each particle type in a regolith and represent the inherent physical and chemical properties of each material [6].

To accurately interpret reflectance spectra for airless bodies, the effects of opaque phases (e.g., Fe, Ni, sulfides) must be considered properly. Opaque metals are present as native igneous minerals in meteorites and on planetary surfaces in the form of grains significantly larger than the wavelength of the incident light. However, nanophase metal grains are also a key byproduct of space weathering [3,7-9] and introduce confounding effects on ultraviolet (UV), visible (VIS), and near-infrared (NIR) spectra as seen in laboratory and spacecraft data for airless bodies.

To address this issue, our model also included optical constants for opaque metal and mineral phases. Metals are present in planetary regolith in three possible physical forms categorized by grain size: macroscopic, microphase, and nanophase [3, 10-15]. Macroscopic metal particles are large relative to the wavelength of light and grains of this size are often found as native igneous species in meteorites and lunar samples [16]. Microphase particles have diameters from ~50 nm to ~3000 nm and produce an overall decrease in reflectance with few effects on the continuum slope of a spectrum [9, 14, 15] and have been dubbed "Britt-Pieters (BP) particles". Finer-grained metal, <50 nm in diameter, is referred to as "nanophase metal" (e.g., npFe0) and decreases the overall reflectance and introduce a strong positive spectral slope across the visible to near-infrared (i.e., spectral "reddening") [8, 9].

Methods: The model used for this study was adapted from the work of [17], which uses optical constants for metals (Fe, Ni) to introduce the darkening and/or reddening effects macroscopic, microscopic, and nanophase metal on reflectance spectra. Required inputs are the abundance and composition of phases (including plagioclase, ilmenite, olivine, orthopyroxene, clinopyroxene, glass, agglutinates, macrometal, nanophase metal, microphase metal) as well as the grain sizes of the (macrophase) host particles and the BP particles. Use of a look up table allows the user to vary the amounts of macroscopic host phases to produce spectra that can then be compared to a spectrum of interest (SOI). BP particle sizes are modeled for a range of sizes (50-3000 nm) and compared to the SOI.

We seek to adapt the algorithm for applications to other airless planetary bodies, including (but not limited to) Mercury and asteroids. In order to do so, there are three main goals of the current study. First, since we do not have known samples in the meteorite collection from all airless bodies (e.g., Mercury) in order to constrain the mineralogy and chemistry, one desired application is to mix spectra of surface types in place of, or in addition to, end-member minerals in order to model the spectrum of another surface type. Second, we seek to extend the opaque phases available for spectral mixing and space weathering, which were previously centered on the Fe-rich nature of the Moon (e.g., metallic Fe). Third, we aim to dissociate the microphase and the nanophase opaque phases within the model. Results of these models relative to laboratory and planetary spectra will be presented.

References: [1] Hapke, B. (1981), *JGR, 86(B4)*, 3039–3054. [2] Hapke, B. (1993), *Theory of Reflectance and Emittance Spectroscopy*, Cambridge Univ. Press, U.K. [3] Hapke, B. (2001), *JGR, 106*, 10,039–10,073. [4] Lucey (1998) *JGR*, *103*, 3679–3699. [5] Wilcox et al. (2006), *JGR*, *111*. [6] Palik (1991), *Handbook of Optical Constants v.2*, Academic Press, Boston. [7] Keller and McKay (1997), *GCA, 61*, 2331–2341. [8] Pieters et al. (2000), *Meteorit. & Planet. Sci., 35*, 1101–1107. [9] Noble, et al. (2007) *Icarus*, 192, 629–642. [10] Britt and Pieters (1994), *GCA, 58*, 3905–3919. [11] Pieters et al. (2000) *Meteorit. Planet. Sci*., *35*, 1101–1107. [12] Noble and Pieters (2003), *JGR, 111*. [13] Nobel et al. (2006) *JGR*, *111*. [14] Lucey and Noble (2008) *Icarus*, *197(1)*, 348–353. [15] Lucey and Riner (2011) *Icarus*, *212*, 451–462. [16] Lawrence and Lucey (2007) *JGR, 112*. [17] Cahill et al. (2015) *JGR, 115*.

Experimental Space Weathering: A coordinated LIBS, TEM, VIS and NIR/MIR study. A. N. Stojic[1], S.G. Pavlov[2], A. K. Markus[1,2], Weber, I.[1], A. Morlok[1], H. Hiesinger[1], [1]WWU Muenster Wilhelm-Klemm-Str.10, D-48149, Muenster, [2]Deutsches Zentrum fuer Luft-und Raumfahrt (DLR), Institute for Optical Sensor Systems, Rutherfordstraße 2, 12489 Berlin

Introduction: Space weathering effects can be observed on many planetary bodies that do not have a protective atmosphere surrounding them. This includes asteroids, comets and satellites, but also planets, like Mercury, which has only a tenuous exosphere surrounding it. An overview over many influencing factors is given by [1].

In our current study, a project that is embedded in the framework of the BepiColombo – MERTIS Mercury mission, we pursue the approach of [2,3] to simulate thermal effects of impacting (micro)meteorites on surface regolith material. We therefore irradiate pellets, made of comminuted typical mantle minerals, with a Nd:YAG laser. A part of the altered areas is cut out as a lamellae by using the focused ion beam technique to investigate the inflicted damage by TEM. The remaining part of the pellet surface is measured spectrally in the VIS, NIR and MIR range. Our goal is to correlate the damage documented by means of TEM with the corresponding VIS/NIR and MIR spectra.

Experimental: Single crystals of pyroxene (En87) and olivine (Fo93) were ground in an agate mortar for 1h. The resulting powder was not sieved and loosely pressed at 4 bar for 10 min. The pellet diameter is 10 mm and the surface was subsequently irradiated with a pulsed (8 ns) laser operating at 1064 nm. We performed 20 shots per single spot at 15 mJ and irradiated the entire pellet surface manually moving at 0.4 mm increments. Both mineral pellets were treated identically. The experiments were carried out under a vacuum of 2×10^{-6} mbar and the pellet remained in the chamber until one portion of the pellet was cut off to extract a TEM lamella and the remaining pellet was investigated applying infrared spectroscopy. Diffuse reflectance spectra were acquired in the VIS, NIR and MIR range under vacuum using a Bruker Vertex 70v and 80v. HAADF-STEM, SAED patterns, EDX measurements and BF micrographs were obtained using a FEI Tecnai G2 F20 X-Twin transmission electron microscope at the Geoforschungszentrum in Potsdam.

Results: TEM observations show very distinct patterns for olivine and pyroxene, respectively. Olivine is more susceptible to the thermal damage induced by the laser than pyroxene. This shows in the thickness of the developed weathered rim (at times twice as large as that of pyroxene) and in the inherent structure of the rim. Also, the affected area is distributed evenly over the entire length of the TEM specimen. Nanoparticles were distributed in different layer and display sizes from 3 nm – 40 nm. The outermost layer on the weathered single crystal shows no visible metal particles. The structure could successfully be determined by SAED and FFT of HRTEM images as alpha Fe. Pyroxene displays a range of different features within the rim and shows only a little section in which nanoparticles developed. Also, the nanoparticles in case of pyroxene remained very small and are distributed differently than in olivine. A common feature were vesiculated rims with bubble sizes ranging from 50 – 150 nm. The vesiculated rims showing in pyroxene can be attributed to the water content in the crystal. The natural pyroxene shows a typical water absorption band at 3 µm that is ascribed to hydration. Olivine lacks this type of rim and contains no volatiles except for traces of adsorbed water. For both minerals the spectral changes in the VIS/NIR range were significant in terms of darkening and reddening of the slopes. The MIR range slight modifications that could be attributed to further particle comminution.

Results: Examining pyroxenes (a nominally anhydrous mineral, NAM) from enstatite chondrites [4] suggests that pyroxene can be hydrated by water bearing impacting material, inferring that this could be the source of the 3 µm feature in the NIR. If this assumption is correct this could be an additional source of volatiles apart from solar wind implanted material. Also, the different zones within our rims show striking similarities to Itokawa material returned by Hayabusa [5]. Material, which is considered to show incipient space weathering. Although pyroxene contains only very few metal nanoparticles the spectral reddening is as pronounced as in the olivine sample. This can be explained by experiments conducted by [6] who state that the major reddening agent in the VIS/NIR is the size fraction of particles < 10 nm.

References:

[1] Domingue D. et al. (2014) *Space Science Reviews, 181,* 121–214. [2] Yamada M. et al. (1999) Earth Planets Space, 51, 1255–1265. [3] Sasaki S. et al. (2002) Advances in Spacce Research, 29, 783–788. [4] Izawa M.R.M. et al. (2010) Planetary Space Science, 58, 1347–1364. [5] Noguchi T. et al. (2014) Meteoritics&Planetary Sci, 49, 188-214. [6] Noble S.K. et al. (2007) Icarus, 192, 629-642.

Additional Information: This work is funded by the DLR grant 50 QW 1302.

Lunar Soil Simulants Cannot Reproduce Apollo Lunar Soils With Many Space Weathering Products.

Lawrence A. Taylor[1] and Carle M. Pieters[2] [1] Planetary Geosciences Institute, Earth and Planetary Sciences Dept., The University of Tennessee, Knoxville, TN 37996; lataylor@utk.edu [2] **SSERVI - SEEED**, Department of Geological Sciences, Brown University, Providence, Rhode Island.

Introduction – Since the Apollo Missions first brought back lunar rocks and soils to Earth, scientists and engineers have needed these lunar materials for their experiments. Yet, because they are a "National Treasure", it has been particularly difficult for the engineering community to obtain samples of suitable size for their studies [1] The various NASA-sponsored lunar sample committees [LSAPT, LAPST, CAPTEM] over the years have become more accommodating, yet they remain cautious in allocation of the size of samples that the engineers typically need (e.g., kg) This has naturally led to the development of many materials that reportedly simulant one or more of the physical and chemical properties, starting with Minnesota Lunar Simulant (MLS-1), followed some 20 years later by NASA's versions of lunar soil - JSC-1 and more recently, JSC-1A. Impatient to get their studies accomplished and not always capable or knowledgeable enough to get some of these simulants, the world community, especially since 2004, has produced well over 50 additional simulants, many without the proper duplication of the correct properties. Much of these ineffective efforts have centered round a general lack of sufficient knowledge of the details of lunar soil engineering properties.

NASA has attempted to remedy the problem of lunar soil simulants, both in quality and quantity, with major endeavors since 2004, the magic year the junior President Bush declared that human exploration would extend to the Moon, then Mars, and Beyond. Marshall Space Flight Center established an effective lunar simulant "Clearing House" at MSFC, and began to supervise the production and distribution of lunar simulants, spending $Ms in their development of simulants through SBIR contracts. However, due in part to a deficiency of knowledge of the true lunar soil properties, many of these endeavors have only contributed more inefficiency in the generation of lunar simulants manufactured with the exact properties that duplicate the actual Apollo lunar soils. The properties that have been imposed upon the lunar regolith to produce the soils are all part of the complicated topic of "Space Weathering", and we have not been able to duplicate several of these unique features.

Space Weathering – The collective processes that form and alter the soils on all airless bodies is called space weathering. Having originally gone to the Moon with our "terrestrial hats on", it soon became apparent that the airless space on the Moon permitted an entirely different and foreign type of weathering processes to occur – e.g., it took us almost three (3) years to begin to understand the origin of the ferromagnetic properties of the soil – the effects of single-domain (later, nanophase) metallic Fe. Yet, the general scientific understanding of its origin took another 25 years, and we still investigate the details of nanophase Fe formation. It is just these space weathering properties that will be addressed in this talk.

References: [1] Taylor, L.A., and Liu, Y., 2010, Important considerations for lunar soil simulants. *Earth & Space Sci. 2010: Engr., Sci., Constr., & Oper.*, ASCE, 106-118.

SIMULATION OF MICROMETEORITE IMPACTS THROUGH IN SITU DYNAMIC HEATING OF LUNAR SOIL. M. S. Thompson[1] and T. J. Zega[1]. [1]Lunar and Planetary Laboratory, Department of Planetary Sciences, University of Arizona, 1629 E. University Blvd, Tucson, AZ 85721. E-mail: mst@lpl.arizona.edu.

Introduction: Space weathering is driven by the interaction of surface materials on airless bodies with energetic particles from the solar wind and by micrometeorite impacts [1]. Such interactions result in changes to the microchemical and microstructural characteristics of soil grains and thus, optical properties. Recently, new space-weathering features in the form of vesiculated textures have been reported in returned samples from Itokawa, e.g., [2]. To understand the formation of these and other space-weathering features, experiments that simulate solar wind irradiation, micrometeorite impact, or heating events have been performed on a variety of target materials, e.g., [3-7]. While such static investigations provided insight into space-weathering characteristics, in situ experiments enable direct observation of chemical and structural changes that result from simulated space-weathering conditions in real-time. Here we present results on a dynamic heating experiment, performed inside a transmission electron microscope (TEM), to simulate a micrometeorite impact of lunar soils.

Samples and Methods: Grains of mature mare lunar soil 79221 were crushed, suspended in methanol, and drop cast onto carbon-coated grids and thermal e-chips for analysis in the TEM. We employed two different methodologies for simulating micrometeorite impacts. In the first, we heated the samples incrementally using a Gatan slow-heating stage inside a Philips CM200-FEG TEM and the FEI Titan ETEM at Arizona State University from room temperature to nearly 1000 ºC over the course of 15 minutes. We collected bright-field TEM (BF-TEM) images of the material at a variety of magnifications at roughly 150 ºC increments over the course of the experiment. We also performed energy-dispersive x-ray spectroscopy (EDS) mapping of the samples before and after heating. In the second method, we flash-heated samples inside the CM200 and the Titan from room temperature to 1000 ºC and back to room temperature in 1s. We collected BF-TEM images before and after heating, and recorded a video of the experiment.

Results and Discussion: Select grains of interest, which included nanophase Fe (npFe), were chosen for continuous monitoring throughout the experiments.

Slow-heating Experiments: Between room temperature and 500 ºC we did not observe noticeable microstructural changes in the target grain. Beginning at 500 ºC, where solar wind embedded H and He may become mobile [8], we observed changes in the size and distribution of Fe nanoparticles in the sample, with new nanoparticles forming at ~575 ºC. The npFe concentration and grain size size increased significantly between 500 to 1000 ºC, with individual nanoparticles growing from 5 nm to as large at 40 nm. Some of the new nanoparticles are euhedral in shape. EDS mapping indicates the nanoparticles are composed of Fe. We did not observe the development of vesiculated textures during this experiment. Figure 1 shows the target grain before and after heating.

Rapid-Heating Experiments: After rapid heating we observed the formation of high concentrations of new, spherical, and mostly amorphous, Fe nanoparticles. Agglutinitic grains and glass spherules also formed during the heating event. We observed collisional features where molten glassy particles impact other grains after moving across the grid during heating. We also identified microstructural features in the rims of soil grains which may be vesicles.

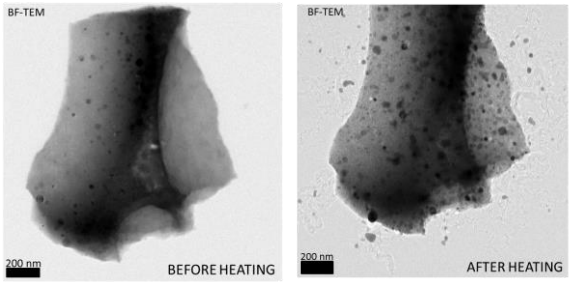

Fig. 1: *BF TEM images of the grain before heating (left) and after heating to 1000 ºC. Note the increased concentration of npFe particles in the grain after heating.*

These experiments produced features in lunar soil that are consistent with space-weathering processes occurring on the lunar surface, indicating that in situ heating experiments are a worthwhile approximation for micrometeorite impacts. Observing development of npFe at 575 ºC provides a temperature constraint for nanoparticle formation. These experiments also provide a possible mechanism for the development of vesiculated textures that have been reported in returned samples from Itokawa. Additional experiments will determine whether these results are unique to this soil or are broadly characteristic of in situ heating.

References: [1] Hapke B. (2001) *J. Geophys. Res-Planet.*, *106*, 10,039-10. [2] Matsumoto T. et al. (2015) *Icarus 257*, 230-238. [3] Keller L. P. et al. 2015. *LPSC XXXXVI*, Abstract #1913. [4] Brownlee D. E. et al. (2005) *LPSC XXXVI*, Abstract #2391. [5] Noble S. K. et al. (2011). *LPSC XXXXII*, Abstract #1382 [6] Sasaki S. et al. (2001) *Nature, 410*, 555-557. [7] Loeffler, M. et al. (2009) *J. Geophys. Res – Planet.*, 114:E03003. [8] Gibson E. K. Jr. and Johnson S. M. (1971) Lunar Science Conference 2:1351-1366.

THE OXIDATION STATE OF NANOPHASE FE PARTICLES IN LUNAR SOIL: IMPLICATIONS FOR SPACE WEATHERING. M. S. Thompson[1], T. J. Zega[1], J. T. Keane[1], P. Becerra[1], and S. Byrne[1]. [1]Lunar and Planetary Laboratory, Department of Planetary Sciences, University of Arizona, 1629 E. University Blvd, Tucson, AZ 85721, mst@lpl.arizona.edu.

Introduction: Grains on the surfaces of airless bodies such as the Moon are continually modified by micrometeorite impacts and interactions with solar-wind ions, a process that is collectively known as space weathering. This phenomenon alters the optical properties of surface soils, which has been attributed to the production of Fe nanoparticles (npFe) through space-weathering processes [1,2]. The nanoparticles in lunar soil samples are typically reported as containing Fe in the reduced metallic state, i.e., Fe^0, and are widely referred to as $npFe^0$ in the literature, e.g., [3-6]. However, previous work has shown a mixture of Fe oxidation states in agglutinitic glasses that contain Fe nanoparticles [4]. Here we expand on previous efforts and measure directly the oxidation state of individual nanoparticles. Understanding the oxidation state of these nanoparticles provides insight into the conditions of their formation, and the nature of space weathering mechanisms across the inner solar system.

Samples and Methods: We embedded <1 mm grains of three Apollo lunar soils in epoxy and prepared them through ultramicrotomy for analysis in a transmission electron microscope (TEM). The samples include: 12033, an immature mare soil, 15071, a submature mare soil, and 79221, a mature mare soil. We measured over 100 individual nanoparticles from the three lunar soil samples, with at least 30 nanoparticles in each sample.

The oxidation state(s) of the npFe was measured with electron energy-loss spectroscopy (EELS) coupled to the TEM. All measurements were performed using the 100 keV monochromated and aberration-corrected Nion UltraSTEM at Arizona State University, equipped with a Gatan Enfinium Spectrometer. Line profiles for individual nanoparticles were collected with a dispersion of 0.1 eV/channel and energy resolution between 200 to 300 meV. Measurements had variable dwell times, ranging from 0.01 s/px to 0.5 s/px.

EELS spectra were collected at the Fe $L_{2,3}$ core-loss edge. All spectra were compared to measurements of Fe metal, FeO (wüstite), and Fe_2O_3 (hematite) standards for reference to Fe^0, Fe^{2+}, and Fe^{3+}, respectively, using the same experimental conditions. We also acquired spectra from the glass surrounding each nanoparticle and subtracted this 'matrix' spectrum from that of the nanoparticle in order to isolate the contribution solely from the nanoparticle. For each sample spectrum, we determined the relative contribution of Fe^0, Fe^{2+}, and Fe^{3+} by performing a linear, least-squares regression between the observed sample and the three respective standards. From this procedure we obtained the $Fe^0/\Sigma Fe$, $Fe^{2+}/\Sigma Fe$, and $Fe^{3+}/\Sigma Fe$ ratios for each nanoparticle.

Results and Discussion: We collected and successfully quantified EELS spectra for over 100 nanoparticles with a coefficient of determination (R^2) >0.90.

The data suggest that there is an increase in Fe oxidation state with an increase in soil maturity. The Fe in nanoparticles in the immature soil are composed primarily of Fe^0, whereas those in the submature soil contain a mixture of Fe^0 and Fe^{2+}, and nanoparticles in the mature soil contain oxidized Fe, as Fe^{2+} and small components of Fe^{3+}. We also made structural measurements using high resolution TEM (HRTEM) imaging of individual nanoparticles in each of the samples. These measurements give *d*-spacings consistent with either Fe metal, or Fe oxide minerals such as wüstite or magnetite, further supporting the Fe EELS measurements.

Implications for Space Weathering Processes: Mature soils, which contain oxidized Fe nanoparticles, have significant exposure times on the lunar surface and are therefore subjected to prolonged weathering processes. We hypothesize that O in the silicate glass matrix could be a source of npFe oxidation. Supporting evidence for this pathway includes observations of oxidized shells and reduced cores in nanoparticles from submature soil 15071. These results suggest that space weathering products such as Fe nanoparticles are dynamic and their microchemical characteristics are evolving with time.

To understand the effects that oxidized npFe have on the optical properties of lunar soil, we modeled the reflectance spectra of lunar soils to include nanoparticles of variable oxidation states. Our data show differences in optical properties among nanoparticles with varied oxidation states, and the implications of these results will be discussed at the meeting.

References: [1] Hapke B. (2001) *J. Geophys. Res-Planet., 106*, 10,039-10,073. [2] Pieters C. M. et al. (2000) *Meteorit. Planet. Sci., 35*, 1101-1107. [3] Keller L. P. and McKay D. S. (1997) *Geochim. Cosmochim. Ac., 61*, 2331-2341. [4] Keller L. P and Clemett S. J. (2001) *LPS XXXII*. [5] Keller et al. (1998) *LPS XXIX*. [6] Noble et al. (2007). *Icarus 192*, 629-642.

RADIATIVE TRANSFER MODELING OF MESSENGER VIRS SPECTRA OF MERCURY: DETECTION AND MAPPING OF SUBMICROSCOPIC IRON AND CARBON. D. Trang[1], P. G. Lucey[1], and N. R. Izenberg[2], [1]Hawai'i Institute of Geophysics and Planetology, University of Hawai'i at Mānoa, Honolulu, HI (dtrang@higp.hawaii.edu), [2]Applied Physics Laboratory, The Johns Hopkins University, Laurel, MD.

Introduction: Mercury exhibits a low albedo and a red-sloped featureless visible-to-near-infrared reflectance spectrum. Studies suggest that these characteristics are due to the presence of opaque minerals and space weathering products in a silicate matrix [1–3]. Radiaitve transfer modeling proved effective in reproducing the major properties of Mercury's spectra obtained by MESSENGER VIRS (Visible and Infrared Spectrograph) instrument (specral range is from 0.3–1.45 μm) with the inclusion of the optical effects of submicroscopic iron. However, small scale structures in the spectral fits are imperfect, suggesting the presence of other components.

The recent possible detection of carbon on Mercury [4] and the discovery that carbon-bearing compounds can produce Mercury-like products in impact experiments [5] promped us to investigate the ability of nanophase and mircrophase carbon to provide a better fit to the spectra of Mercury.

Methods: We used the radiative transfer equations from [3,6,7] to make spectral models of transparent host minerals containing various combinations and abundances of submicroscopic particles. The host mineral had an assumed grain size of 20 μm [8]. The submicroscopic particles consisted of nanophase and microphase particles composed of iron, amorphous carbon, and/or graphite.

Results: We found that the best spectral matches relied on model spectra derived from iron and amorphous carbon in nanophase and iron in microphase particles in combination. Maps of the distribution of nanophase iron and carbon and microphase iron are shown in Fig. 1.

Discussion: The spatial distribution of microphase iron abundance is consistent with Ostwald ripening [9]. Because Mercury is in a 3:2 resonance, at perihelion, the regions at 0° and 180° longitude, called hot poles, always face the Sun. As a result, these regions experience maximum temperatures of ~700 K, whereas the surfaces at 90°W and 90°E are <600 K [10]. Similarly the geographic poles are consistently 100s of degrees colder than the equatorial regions. The surface temperatures at the equatorial and hot poles are great enough that metallic iron particles will enlarge by diffusion.

The modeling abundances are consistent with the results from other interpretations, which used instruments such as, the Gamma-Ray Spectrometer (GRS), the X-Ray Spectrometer (XRS), and MASCS (Mercury Atmospheric and Surface Composition Spectrometer). The XRS result shows that the Fe abundance in the southern hemisphere is ~1.5 wt.% [11] The GRS results for Fe and C abundances north of 20°S is 1.9 and 1.4 wt.%, respectively [12,4]. Within the same region as the GRS data, our Fe abundance (i.e., total nanophase and microphase wt.% Fe) is 1.7±0.5 wt.% and C abundance is 1.4±0.3 wt.%. The predicted nanophase iron abundance based upon the strength of the OMCT (oxygen-metal charge transfer) is 0.2–0.3 wt.% [13]. Our global nanophase iron abundance is 0.3±0.1 wt.%.

References: [1] Denevi et al. (2009), *Science*, 324, 613–618. [2] Blewett et al. (2009), *EPSL*, 285, 272–282. [3] Lucey and Riner (2011), *Icarus*, 212, 451–462. [4] Peplowski et al. (2015), *PSS*, 98–107. [5] Bruck Syal et al. (2015), *Nature Geosci.*, 8, 352–356. [6] Hapke (2001), *JGR*, 106, 10039–10073. [7] Lucey (1998), *JGR*, 103, 1703–1713. [8] Warell et al. (2010), *Icarus*, 138–163. [9] Noble and Pieters (2003), *Solar Sys. Res.* 37, 31–35. [10] Vasavada et al. (1999), *Icarus*, 141, 179–193. [11] Weider et al. (2014), *Icarus*, 235, 170–186. [12] Evans et al. (2012), *JGR*, 117, E00L07, [13] McClintock et al. (2008), *Science*, 321, 62–65.

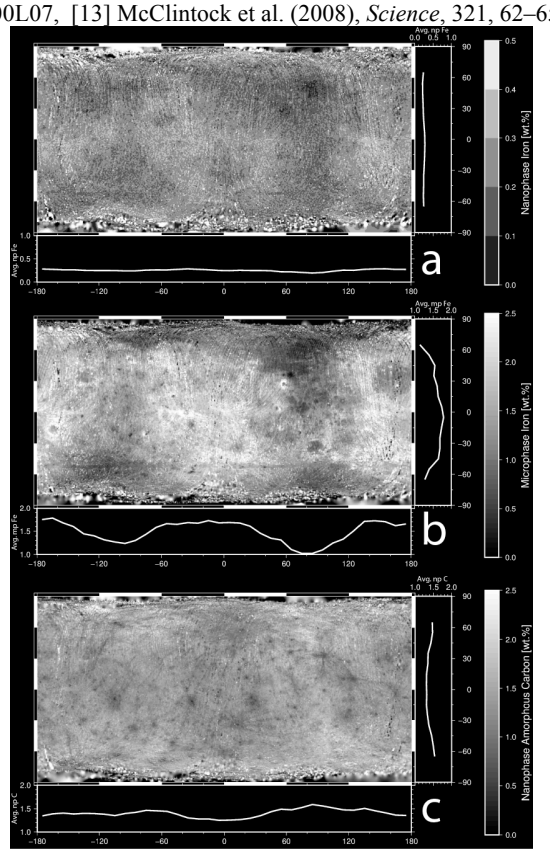

Fig 1: Space weathering maps a) nanophase iron, b) microphase iron, c) nanophase amorphous carbon map. The graphs are longitudinal and latitudinal averages.

SPACE WEATHERING ON ITOKAWA SURFACE DEDUCED FROM SHAPE AND SURFACE FEATURES OF HAYABUSA REGOLITH PARTICLES. A. Tsuchiyama[1], T. Matsumoto[2], M. Uesugi[2], T. Yada[2], A. Shimada[1], T. Sakurama, T. Kadokawa. [1]Kyoto University, Japan (atsuchi@kueps.kyoto-u.ac.jp), [2]ISAS/JAXA, Japan.

Introduction: Regolith particles on the surface of S-type Asteroid 25143 Itokawa were recovered by the Hayabusa mission of JAXA (e.g., [1]). Analysis of tiny sample particles (20-200 μm) shows that the Itokawa surface material is consistent with LL chondrites suffered by space weathering (e.g., [1-3]). Such regolith particles on this small airless body can be regarded as an interface with the space environment, where the impacts of small objects and irradiation by cosmic rays should have been recorded. In order to understand the space weathering processes, our research group has been examined external 3D shapes and surface features of Itokawa regolith particles (e.g., [2,4-6]).

Analytical procedures and samples: We have systematically examined particle surface features with spatial resolutions from a few μm to ~1 nm. The 3D structures of eighty-one Itokawa particles were obtained by micro-tomography with the voxel size of about 100 nm at BL47XU of SPring-8. The external 3D shapes gives surface features with the effective spatial resolution of ~a few μm. The axial ratios of the particles were also obtained to compare those of lunar regolith particles and fragments of impact experiments. The surfaces of twenty-six particles were observed using FE-SEM for nano-morphology with the spatial resolution of >~10 nm. After the SEM observation, cross sections of one particle were prepared by FIB and examined with TEM/STEM-EDX [6].

Results and Discussion:

Origin of Itokawa regolith particles. The shape (three-axial ratios) distribution of Itokawa particles compared with an impact experiment suggest that the Itokawa regolith particles formed as a result of mechanical disaggregation, primarily as a response to impacts although the numbers of Itokawa particles and impact experiment were limited [2,4]. Analysis of larger number of Itokawa particles together with new impact experiments show that the shape distribution of the Itokawa particles is consistent with that of impact experiments of limited conditions.

Space-weathered rim formation. It has been proposed that space-weathered rims, which are responsible for the spectral change of Itokawa, were mainly formed by solar wind irradiation [3,5]. Blister structures originally observed in cross sections by TEM [5] were recognized on the particles surfaces by SEM [6]. About half of the Itokawa particles have space-weathered rims with blisters. These rims are heterogeneously distributed and often present in opposite particle surfaces, suggesting particle migration on Itokawa.

Particle surface abrasion. The particle 3D shapes showed that ~2/3 particles have only sharp edges, consisting with mechanical disaggregation, while ~1/3 have some rounded edges. SEM observation showed two types of surface morphologies having sharp and rounded edges, which are consistent with the 3D shapes. The above results showed that the rounded surfaces formed from fresh surfaces by abrasion processes on Itokawa. As the rounded surface features are not correlated with the blister distribution, the abrasion process can be regarded as a different type of space weathering with a longer timescale than the space-weathered rim formation. The abrasion is probably the result of grain migration caused by seismic waves due to impacts [2] although different mechanisms (e.g., tidal disruption and YORP effect) are possible.

Impact on Itokawa. Molten objects (drops and splashes) were observed on eight particles. Nano-craters [7] were observed only on one particle and heterogeneously distributed with molten objects. This strongly suggests that they were formed by impacts of nano-particles secondarily produced by local impact processes on Itokawa. Particles with partially abraded and fresh surfaces, which were probably formed by impact disaggregation, were also observed.

Space weathering on Itokawa. In summary, space-weathered rims developed on the surfaces of individual regolith particles mainly by solar wind implantation promoted the spectral change of Itokawa, while refreshment of particle surfaces by mechanical abrasion due to grain motion and fragmentation due to impact suppressed the spectral change. This can explain the moderate spectral evolution of Itokawa in contrast to fast space-weathered rim formation in 10^3-10^4 yr. [5].

Shape distribution of many types of lunar regolith particles show that they are more spherical than Itokawa and impact experiment particles. We do not know whether this is due to gain abrasion for a long time or disaggregation of regolith particles by repeated impact.

References: [1] Nakamura T. et al. (2011) *Science*, *333*, 1113. [2] Tsuchiyama A. et al. (2011) *Science*, *333*, 1125. [3] Noguchi T. et al. (2011) *Science*, *333*, 1121. [4] Tsuchiyama A. et al. (2014) *Meteoritics & Planet. Sci. 49*, 172. [5] Noguchi T. et al. (2014) *Meteoritics & Planet. Sci. 49*, 188. [6] Matsumoto T. et al. (2015) *Icarus*, in press. [7] Nakamura E. et al. (2012) *Proc. Nat. Acad. Sci.*, *109*, E624.

EVOLUTION OF SHOCK MELT COMPOSITIONS IN LUNAR AGGLUTINATES. A.M. Vance[1], R. Christoffersen[2], L.P. Keller[3], [1]Department of Geology, Beloit College, 700 College St, Beloit, WI 53511 (vancea@beloit.edu), [2]Jacobs, NASA Johnson Space Center, Mail Code XI, Houston, TX 77058, USA, (roy.christoffersen-1@nasa.gov), [3]Code XI, NASA Johnson Space Center, 2101 NASA Parkway, Houston, TX 77058.

Introduction: Lunar *agglutinates* are aggregates of regolith grains fused together in a glassy matrix of shock melt produced during smaller-scale (mostly micrometeorite) impacts [1]. Agglutinate formation is a key space weathering process under which the optically-active component of nanophase metallic Fe ($npFe^0$) is added to the lunar regolith [1,2,3,4]. Here we have used energy-dispersive X-ray (EDX) compositional spectrum imaging in the SEM to quantify the chemical homogeneity of agglutinitic glass, correlate its homogeneity to its parent soil maturity, and identify the principle chemical components contributing to the shock melt compositional variations.

Samples and Method: A JEOL JSM-7600F field-emission SEM (FE-SEM) was used to collect quantitative EDX element maps on agglutinates in lunar soils 10084, 73241, 78501, 76281, and 78421, with approximately 16-21% Al_2O_3 and varying maturity (respective Is/FeO ratios: 78, 18, 36, 45, 92) [4]. Numerical methods were devised to plot ternary oxide compositions of only the glassy matrix, minimizing contributions from entrained grains, to create large, highly spatially resolved datasets showing mixing trends and relationships. Soil samples 73241 and 78501 were also characterized using the JSA-8530 field-emission electron probe microanalyzer in order to test the accuracy of the SEM spectrum imaging approach.

Results: Our FE-SEM spectrum image-based compositional analysis technique yielded ternary variation diagrams only slightly less precise that those obtained by microprobe, but with a factor of 10 to 100 higher number of spatially-resolved individual analyses. For the various 3-component permutations among the major element ternary variation diagrams, the following relations are observed for all samples: 1) The degree of scatter among the various permutations of 3-oxide variations diagrams, as a measure of glass homogeneity, shows no clear correlation with maturity (I_s/FeO) of the parent soil, 2) the mixing relations for all 3-oxide combinations, except those including Fe as FeO, are easily modeled based on varying relative contributions from model regolith plagioclase, pyroxene/olivine and ilmenite compositions, 3) the mixing trends involving FeO, such as those in MgO-FeO-TiO_2 plots (Fig. 1), require a fourth mixing component with an Fe/Mg ratio much higher than normal mare regolith pyroxene and olivine.

Discussion: The nature of the apparent "fourth" mixing component was investigated by subtracting normative plagioclase and ilmenite oxide proportions from all analyses to obtain a "residual" MgO-FeO-SiO_2 variation diagrams (Fig. 2). The diagram confirms the inability of the FeO/MgO ratio of normal lunar pyroxene and olivine compositions to explain the high FeO/MgO ratio of the fourth component. It also reveals excess SiO_2 in some of the fourth component compositions as well. Source materials in the regolith target assemblage that might account for the Fe-rich fourth component include Fe-metal from meteoroid impactors (although proportional additional Ni does not occur), and admixtures of Fe-rich pyroxene/olivine compositions from a highland source. A third contribution from vapor-deposits on the outer margins of regolith grains, that characteristically have the needed higher FeO/MgO values, is also an intriguing possibility. Although volumetrically small, such deposits may gradually contribute to adding local glass regions with high FeO/MgO over multiple cycles of regolith impact gardening.

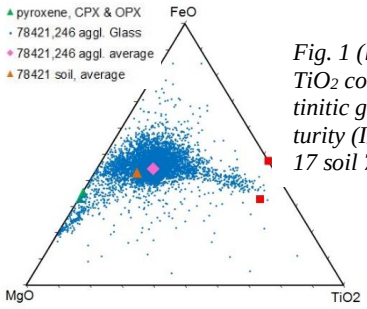

Fig. 1 (left). MgO-FeO-TiO_2 compositions of agglutinitic glass in high-maturity (I_s/FeO=92) Apollo 17 soil 78421.

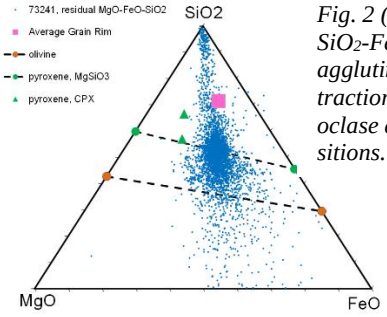

Fig. 2 (left). Residual MgO-SiO_2-FeO compositions of agglutinitic glass after subtraction of normative plagioclase and ilmenite compositions.

References: [1] Basu A. and McKay, D. S. (1985) Proc. 16th Lunar Sci. Conf, JGR, 90, D87. [2] Pieters, C. M. et al. (2000) *Meteoritics & Planet Sci., 35*, 1101-1107. [3] Taylor, L. A. et al. (2001) *JGR, 106*, 27985-27999. [4] Taylor, L. A. et al. (2000) *Meteoritics & Planet Sci., 36.*

SEEKING EVIDENCE IN UV/BLUE REFLECTANCE SPECTRA FOR DIFFERENCES IN SUBMICROSCOPIC IRON CREATED BY SPACE WEATHERING ON PARTICLES FROM S-COMPLEX ASTEROIDS AND THE MOON. F. Vilas[1] and A. R. Hendrix[1], [1]Planetary Science Institute, 1700 E. Fort Lowell Rd., Suite 106, Tucson, Arizona, 85719, fvilas@psi.edu; ahendrix@psi.edu.

In the inner Solar System, space weathering affects reflectance spectra of the Earth's moon and S-complex asteroids by spectral bluing (increasing reflectance with decreasing wavelength) of their surface materials at UV/blue wavelengths [1]. The spectral bluing is attributed to a degradation of the UV absorption seen in silicates, as a result of nanophase iron. In some cases, a spectral reversal is observed [1, 2]. Recent studies [3] show that the UV/blue is a more sensitive remote sensing indicator of the creation of submicroscopic iron on S-complex asteroid surfaces. We have demonstrated through modeling that the effect of the addition of small amounts of $npFe^0$ to particles from both a hypothetical mineral and a terrestrial basalt shows that the addition of 0.0001% $npFe^0$ affects the reflectance at UV/blue wavelengths, while the addition of 0.01% is required to see the VNIR reddening and diminution of absorption features - a factor of two orders of magnitude in amount of $npFe^0$ added to the surface material [3]. Thus, the UV/blue reflectance characteristics allow earlier detection of the onset of space weathering effects.

The structure of this weathering is evidenced in the grain coatings and rims observed in lunar fines retrieved by the Apollo missions, as well as microscopic particles retrieved from 25143 Itokawa by the Hayabusa mission [e.g., 4,5,6]. Laboratory studies of these particles show differences in the physical structure within the first ~100 nm of the weathering coatings on the surfaces of these particles. These structural differences support solar wind heavy ion irradiation and bombardment as most likely to affect the surface properties of the S-complex asteroids, and micrometeoroid bombardment as the source of weathering on the lunar surface.

At UV/blue wavelengths, surface scattering dominates over volume scattering so that reflectance is directly related to the index of refraction [7]. The index of refraction of many materials increases with decreasing wavelength, so that they become brighter at shorter wavelengths. In particular, since FUV radiation is less penetrating than visible radiation, short wavelengths are more sensitive to thin coatings on grains that may be the result of weathering processes [2].

We investigate here whether differences in the UV/blue spectral characteristics could indicate different space weathering processes. With the anticipation that remote sensing will remain the major means of studying solar system objects, thus providing a "global" context for the interpretation of samples returned by spacecraft missions, we are seeking delineators for space weathering mechanisms.

References: [1]Hendrix, A. R., & Vilas, F., (2006) AJ 132, 1396. [2]Lucke, R. L., et al. (1974) LSC 5th, 469. [3]Vilas, F. & Hendrix, A. R., (2015) AJ 150, 64. [4]Keller, L.P., & Berger, E.L., (2014) MetSoc 77th, #5088. [5]Thompson, M.S., et al., (2014) LPSC 45th, #2121. [6]Christoffersen, R., & Keller, L. P., (2014) LPSC 45th, #2084. [7]Henry, R. C., et al., (1976) Moon 15, 51.

LABORATORY INVESTIGATIONS OF ELECTROSTATIC DUST TRANSPORT ON AIRLESS BODIES AND ITS EFFECTS ON SPACE WEATHERING. X. Wang[1,2], J. Schwan[1,2], H. –W. Hsu[1,2], and M. Horányi[1,2] [1]NASA/SSERVI's Institute for Modeling Plasma, Atmospheres and Cosmic Dust, University of Colorado, Boulder, CO 80303 [2]Laboratory for Atmospheric and Space Physics, University of Colorado, Boulder, CO 80303 (e-mail: xu.wang@colorado.edu).

Introduction: Airless bodies, such as the Moon and asteroids, are covered with a layer of fine dust particles, the so-called regolith. The regolith of these bodies will experience space weathering processes due to their exposure to solar wind plasma and UV radiation. The space weathering effects can be identified from the spectral properties of their surfaces. In addition, dust particles on exposed surfaces are charged and may thus be transported due to electrostatic forces. The transport of dust particles can cause their redistribution over the surface of the airless bodies, altering the space weathering effects. The dust transport effects on the surface spectra properties have been proposed for explaining the high-albedo markers, the so-called lunar swirls, on the lunar surface in the magnetic anomaly regions [1].

Electrostatic dust transport may be related to many observed phenomena on the surfaces of airless bodies, for example the lunar horizon glow, the dust ponds on asteroid Eros, the spokes in Saturn's rings. However, its mechanisms still remain a mystery. We present new laboratory experimental results of electrostatic dust transport and its mechanisms, and discuss its possible effects on the space weathering.

Experiments and Results: The experiments were performed in a cylindrical vacuum chamber. The dust particles were loaded inside a crater of an electrically floated surface in the center of the chamber. A video camera was used to record the dust movement. Various sizes (15 – 70 microns in diameter) and shapes (irregular and spherical) of dust particles were used in the experiments.

The dust partilces were exposed to plasmas and UV light (172 nm), respectively. The plasmas were created by 140 eV primary electrons emitted from a hot filament on the top of the chamber. The dust particles were moved and lofted in both plasma and UV illumination conditions. Single dust trajectories were captured (Fig. 1), enabling novel micro-scale investigations.

A new so-called "patched charge model" has been proposed to explain our findings. We identifed the role of plasma micro-cavities that are formed in-between neighboring dust particles. The emitted secondary or photoelectrons are proposed to be absorbed inside the micro-cavities, resulting in significant charge accumulation on the surface patches of the neighboring particles. The resulting enhanced Coulomb force (repulsion) between particles is likely the dominant force to mobilize and lift them off the surface.

The hopping particles' size distributions were analyzed. In addition to single sized particles, small residues and large clumps were also lofted. The role of other properties of the dust particles, including their size, shape, surface morphology, and cohesion, will also be discussed.

Our experimental results and proposed "patched charge model" suggest that electrostatic dust transport on the surface of airless bodies is possible. The subsequent dust redistribution and migration may alter the space weathering process, change the surface mophology and cause the mixture of different types of dust grains. The surface spectral properties may therefore be different on regoliths without significant dust transport.

Figure 1: Trajectories (highlighted in green) of dust particles (Mars simulants, 38 – 48 microns) hopping off the surface that was exposed to plasma and 140 eV primary electrons. The surface morphology became smoothed after dust redistribution.

References: [1] I. Garrick-Bethell, J. W. Head III, and C. M. Pieters (2011), *Icarus*, 212, 480-492. doi:10.1016/j.icarus.2010.11.036.

ESTIMATING THE DEGREE OF SPACE WEATHERING AT THE *CHANG'E-3* LANDING SITE: RADIATIVE-TRANSFER MODELING OF NANOPHASE IRON ABUNDANCE. Zhenchao Wang[1], Yunzhao Wu[2,*], Yongchun Zheng[3], David T. Blewett[4], and Edward A. Cloutis[5]. [1]1. Institute of Surficial Geochemistry, Department of Earth Sciences, Nanjing University, Nanjing 210023, China; [2]School of Geographic and Oceanographic Sciences, Nanjing University, Nanjing, 210023, China; [3]Key Laboratory of Lunar and Deep Space Exploration, National Astronomical Observatories of Chinese Academy of Sciences, Beijing 100012, China; [4]Planetary Exploration Group, Johns Hopkins University Applied Physics Laboratory, Laurel, MD, 20723, USA; [5]Department of Geography, University of Winnipeg, 515 Portage Avenue, Winnipeg, MB R3B 2E9, Canada. (*wu@nju.edu.cn)

Introduction: On Dec. 14, 2013 the *Chang'E-3* (CE-3) spacecraft landed on the Moon in northern Mare Imbrium (340.49° E, 44.12° N) [1]. The rover *Yutu* made measurements with its four scientific instruments along a 114-m traverse (Fig. 1). Reflectance spectra (0.45 to 2.40 μm) of the surface were acquired by the Visible and Near-Infrared Spectrometer (VNIS, [2]) at four locations; these data represent the first such spectra obtained *in situ* on the Moon. We have carried out radiative-transfer modeling of the spectra with the goals of quantifying the abundance of nanophase iron ($npFe^0$) in the soil, relating the $npFe^0$ abundance to distance from the lander, and gaining insight into the cause of spectral changes in response to modification by lander rocket exhaust.

Instrument and Data: The VNIS instrument performs wavelength selection with an acousto-optic tunable filter. VNIS has two channels: an imaging spectrometer covering 0.45 to 0.95 μm (visible-near-infrared, VNIR, 100 bands), and a spot spectrometer for the wavelength range 0.90 to 2.4 μm (short-wavelength infrared, SWIR, 300 bands). A cover protects the instrument from dust contamination while it is not in use. The inside of the cover holds a Spectralon target, permitting calibration data to be obtained closely in time with the surface observations.

Surface observations were made at four locations (Fig. 1). All data are for relatively flat, smooth areas of soil; no rocks were measured. The spectra (Fig. 2) show systematic differences that are consistent with increasing maturity from Sites 5 to 8. For example, Site 5 has the deepest 1-μm band, and also the greatest (freshest) value of the OMAT optical maturity parameter [3] as computed from the VNIS spectra.

Radiative-transfer Modeling: We employ Hapke's [4] treatment to model the abundance of $npFe^0$ in the soils at each location. Preliminary results indicate that $npFe^0$ increases with distance from the lander. Therefore the brightening observed around spacecraft landing sites (Fig. 1) may relate to to maturity differences caused by removal of fine, highly mature particles by rocket blast rather than to changes in the texture of the surface (e.g., [5]).

Acknowledgements: The contribution of D.T.B. was made possible by the Chinese Academy of Sciences President's International Fellowship Initiative, Grant No. 2015VEB057.

References: [1] L. Xiao et al. (2015), *Science 347*, 1226. [2] B. Liu et al. (2014), *Res. Astron. Astrophys. 14*, 1578. [3] P. Lucey et al. (2000), *JGR-Planets 105*, 20,377. [4] B. Hapke (2001), *JGR-Planets 106*, 10,039. [5] R. Clegg et al. (2014), *Icarus 227*, 176.

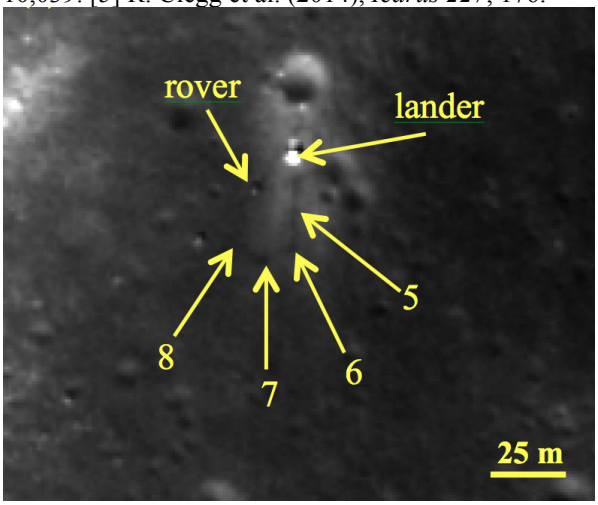

Fig. 1. LROC NAC (http://lroc.sese.asu.edu/) view of the CE-3 landing site. VNIS measurement locations 5 to 8 are labeled.

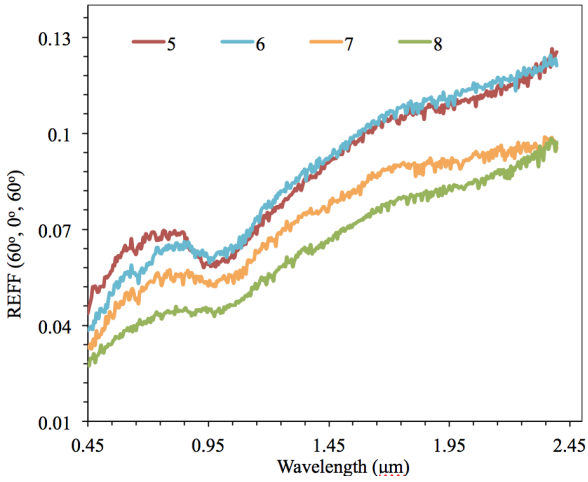

Fig. 2. CE-3 VNIS spectra for the four sites.

THE EARLIEST SPACE WEATHERING: MEGA-SOLAR-WIND EFFECTS IN EARLY SOLAR SYSTEM SILICATES. C. J. Wetteland[1] and K. E. Sickafus[2], H.Y. McSween[1], and L.A. Taylor[1]. [1] Planetary Geosciences Institute, Earth and Planetary Sciences, The University of Tennessee, Knoxville, Tennessee 37996, cjw@utk.edu. [2]Materials Science and Engineering 1508 Middle Drive Knoxville, Tennessee 37996.

Introduction: The quiescent solar wind is the result of a relatively stable Sun. However, during its evolution the Sun and other stars experience periods of instability and variably emanate particles. Young Stellar Objects (YSOs) are stars in their early stages of development, and can be classified based on total luminosity and wavelength of emitted photons. A feature of all classes of stars is mass loss, typically in the form of energetic protons and molecular hydrogen; low-rates are associated with the solar wind in main sequence stars, while high-rates are observed in T Tauri phase YSOs. T Tauri stars can experience mass loss on the order of 10^{-8}-10^{-7} solar masses ($M_{\odot}$) [1], and a factor of 10^{2}-10^{5} times greater during FU Orionis phases [2, 3, and 4]. The resulting proton flux is on the order of 10^{10} p/cm^{2}s (1 AU) and greater; this as compared to the typical solar-wind flux of $3x10^{8}$ p/cm^{2}s at 1 AU [5].

Energetic protons from YSOs can interact, or irradiate, both presolar and recently condensed nebular solids. The energy distribution from YSOs best resembles solar flares, with energies on the order of 1-10 MeV [6]. Numerous authors have incorporated protostar instabilities into early solar-system processes, and have suggested that MeV protons from bipolar outflows and magnetic recombination events could have a role in chondrule formation [7, 8, and 9]. Despite their ubiquitous nature in the early solar system, an adequate experimental investigation on the interaction of energetic particles with early solar-system solids has not been conducted [6].

Previous studies [10] have shown that high-flux protons can result in the catastrophic explosion of larger fragments, producing a distribution of smaller grains. An implication is a comminution mechanism that could exist which continuously develops the narrow size distribution and maximum diameters (~1 cm) associated with chondrules. Invoking a proton melting mechanism for chondrule formation becomes attractive when the irradiation volume is a significant volume fraction of the irradiated particle. This limits heat loss to primarily radiative, as a larger mass of mineral does not exist as a heat sink. Therefore, high-flux protons can first develop a size distribution of minerals fragments which could be later melted in similar irradiation events.

Another discovery from previous work is that significant prompt radiation is developed with relatively low-energy (< 2 MeV) protons. This finding may explain isotopic anomalies in low-Z elements (silicon and below). The production of anomalous isotopic signatures via proton capture may resemble *r-process* nucleosynthesis known to occur in supernovae. Rapid proton capture, outside of traditional nucleosynthetic stellar processes, has not been experimentally explored at the low-energies associated with solar flares.

Here we investigate and present data on how early solar system condensates (olivine) respond to the significantly higher-energy and higher-current fluxes known to occur in YSOs.

Experimental: Proton irradiations were performed using a 200 kV ion implanter and MV tandem accelerators to simulate high-flux transients, in order to explore the (i) thermal response of silicates and (ii) the production of short-term radionuclides. Irradiations were performed on slabs of San Carlos olivine, synthetic forsterite, single crystal Si wafers, fused quartz, and a 80/20 (wt.%) mixture of ball milled San Carlos olivine and Nain anorthosite pressed and sintered into a 13mm diameter pellet. Thermal effects were monitored *insitu* and examined post irradiation with optical microscopy and micro-beam x-ray diffraction. Gamma-ray signatures were collected during irradiation to determine the production rate of short –term radiation as a function of flux and energy.

Results: Presented results will indicate that for specific target thicknesses, a melt texture can be observed in synthetic forsterite. The prompt radiation observed is likely due to the $^{29}Si(p, \beta^{+})^{30}P$ reaction. The ^{30}P decays via a β^{+} particle with an approximate 2.5 minute half-life, while the anti-matter annihilation results in the production of two 511 keV γ-rays. .

References: [1] Kuhi, L. V. (1964). *The Astrophysical Journal* 140, 1409-1437. [2] Herbig, G. H. (1977) *Ibid 217*, 693-715. [3] Croswell, K. et al. (1987) *Ibid 312*, 227-242. [4] Casen, P. & Boss, A. P. (1988) *Meteorites and the Early Solar System*, ed. Kerridge J.F. Cambridge. [5] Schwenn R. (2006) *Living Reviews in Solar Physics 3*, 1-72. [6] Feigelson E.D. and Montmerle T. 1999. *Annual Review in Astronomy and Astrophysics 37*, 363–408. [7] Levy, E. H., & Araki, S. (1989) *Icarus 81*, 74-91. [8] Liffman, K., Brown, M. J. (1996). In *Chondrules and the Protoplanetary Disk* ed. Hewins R.H. et al. Cambridge. [9] Cameron, A. G. W. (1995). *Meteoritics, 30*, 133-161. [10] Wetteland C.J. et al. (2015) *METSOC 2015* Abstract #5276.

SHALLOW LUNAR HYDROGEN AND FORWARD-SCATTERED ALBEDO PROTONS. J. K. Wilson[1,2], N. Schwadron[1,2], A. P. Jordan[1,2], H. E. Spence[1,2], M. D. Looper[3], L. W. Townsend[4], [1]Space Science Center, University of New Hampshire, Durham, NH, (jody.wilson@unh.edu), [2]Solar System Exploration Research Virtual Institute, NASA Ames Research Center, CA, [3]The Aerospace Corporation, Los Angeles, CA, [4]University of Tennessee, Knoxville, TN.

Introduction. Since the launch of LRO in 2009, the CRaTER instrument has been mapping high-energy albedo protons (> 65 MeV) from the Moon [1,2]. These protons are produced by nuclear spallation, a consequence of galactic cosmic ray (GCR) bombardment of the lunar regolith. Just as spalled neutrons and gamma rays reveal elemental abundances in the lunar regolith, albedo protons may be a complimentary method for mapping compositional variations, including volatiles.

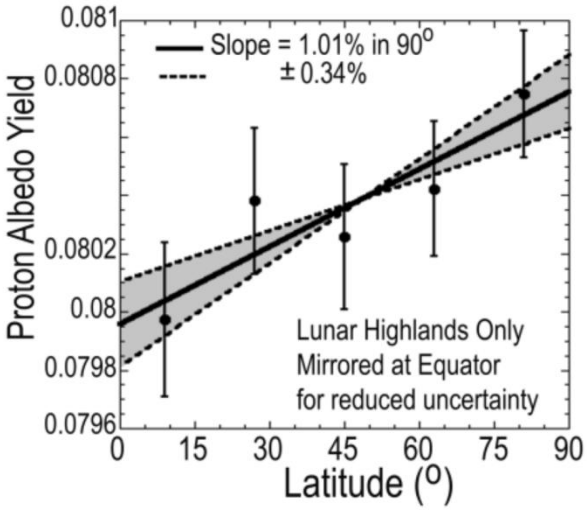

Figure 1. Albedo proton yield vs. latitude. (from [3])

Hydrogen in the regolith. We have discovered a latitudinal trend in the yield of lunar albedo protons, showing in Figure 1, that may indicate a thin (< 10 cm) hydrated layer of regolith [3]. Hydrogen atoms at these shallow depths would be forward-scattered by upwelling albedo neutrons, enhancing the total yield of protons, as illustrated in Figure 2. If true, this would constitute the first detection of volatiles in the regolith by albedo protons, and the first evidence from CRaTER of forward-directed knock-on collisions between nucleons within the regolith.

New observations. To further test the hypothesis that CRaTER can detect and distinguish forward-scattered protons, we have begun a series of targeted CRaTER observations of grazing-angle albedo protons. Any hydrogen in the top 10 cm of lunar regolith should produce a forward-scattered population of albedo protons via knock-on collisions, and result in a higher flux of grazing-angle albedo protons relative to the flux coming up from the nadir direction. In addition, intra-nuclear cascade collisions between GCRs and heavy nuclei in the regolith produce albedo particles in all directions, but preferentially in the forward direction, and thus such collisions may also contribute to higher albedo fluxes at grazing angles.

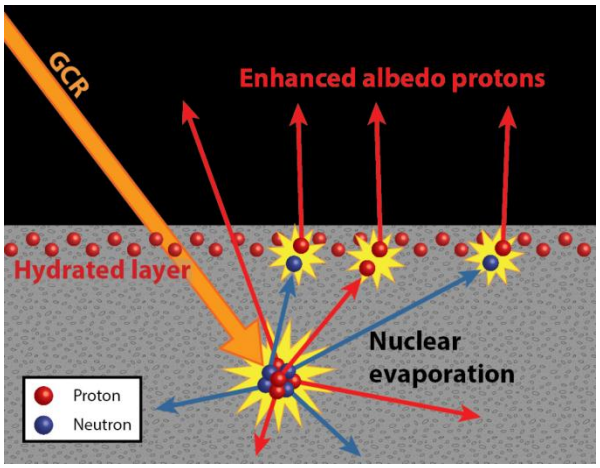

Figure 2. Illustration of enhanced albedo proton yield to due forward-scattering of hydrogen in the top layer of lunar regolith. (from [3])

Preliminary results from the first grazing-angle observations on May 26-28 show a ~40% increase in the proton yield near the horizon compared to the nadir direction, supporting our hypothesis. With additional observations we will search for spatial features (e.g.: mare vs. highlands and high-latitudes vs. low-latitudes) in the grazing-angle yield which may reveal variations in volatile (H) and other elemental abundances.

References: [1] Wilson et al. (2012), *JGR-Planets*,117, E00H23. [2] Wilson et al. (2015), *submitted to Icarus*. [3] Schwadron et al. (2015), *submitted to Icarus*.

MID-INFRARED REFLECTANCE SPECTRA OF PULSED LASER IRRADIATED OLIVINE GRAINS

Yazhou Yang[1*], Ye Yuan[1], Ziwei Wang[1], Hao Zhang[1], Weidong Jin[1], and Weibiao Hsu[2], [1] School of Earth Sciences, China University of Geosciences, Wuhan, China (yangyazhou1@gmail.com). [2] Purple Mountain Observatory, Chinese Academy of Sciences, Nanjing, China.

Introduction: Visible and near-infrared (VNIR) spectroscopy has been widely used to identify the surface mineralogy of airless bodies [1]. However, the interpretations can be severely affected by space weathering processes that may darken and redden the VNIR reflectance spectra and reduce the spectral contrast [1-4]. Both laboratory simulations and returned-sample analysis have demonstrated that the production of submicron irons (SMFe) in silicates are responsible for these optical effects, as the electronic transitions responsible for the 1 μm bands are largely affected by weathering processes [1,2]. In contrast, the absorption bands in the mid-infrared (MIR) are produced by internal lattice vibrations that are determined by lattice structures and hence should be much less susceptible to iron productions. To understand the MIR characteristics of analog materials before and after the micrometeorite bombardment, we carried out pulsed laser irradiation simulations and reflectance measurements of olivine grains.

Methods: A Nd: YAG 1064 nm nanosecond pulsed laser with pulse duration of 6-8 nanoseconds was used to irradiate olivine powders (<45 μm, 4.83 wt % FeO) placed in a vacuum chamber with a vacuum level of 10^{-3} Pa. The total irradiation energy of one irradiation in the simulation is 750 mJ/mm^2 for pulse energy of 25 mJ and 1500 mJ/mm^2 for 50 mJ, respectively. By controlling the pulse energy and irradiation durations, products with different weathering degrees can be obtained. We measured the SEM, VNIR and MIR reflectance of the samples before and after laser irradiations.

To model the optical effects of the generation of SMFe and amorphous coatings during space weathering processes, we used open-source code BART from Arturo Quirantes [8] and Mishchenko's Mie code [9] to calculate the single scattering properties of coated and un-coated grains, respectively. Single scattering quantities are then introduced into both the Hapke photometric model [10] and a strict numerical model to compute the multiple scattering contributions [11]. The particle size in the calculations was set to be 30 microns in diameter. We chose silicate glass with different Fe and Mg contents to simulate the amorphous coatings.

Results: After irradiations, VNIR spectra show the well-known reddening and darkening effect [1-4] (Fig. 1.(a), (b)). In contrast, the MIR spectra only show darkening effects but nearly all major vibrational features are retained. This implies that the crystal structure of olivines may have survived the heavy irradiation process as "over-irradiations" at 50 mJ for 5 times did not eliminate the major vibrational modes.

The MIR spectra predicted by reflectance models reveal that the MIR spectra of olivine grains are not much affected by generations of a submicroscopic iron shell or glassy shell with a thickness less than 100 nanometers. The effect of a glassy shell on VNIR spectra is negligible even when the shell thickness reaches 1 micron. The glassy shell composition effect (Fe and Mg) is also insignificant, as the refractive index difference between these two silicate glasses is much lesser than that between silicate glass and olivine crystals.

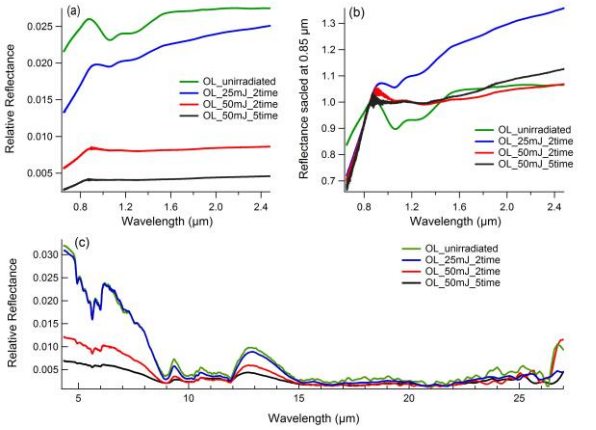

Fig. 1. VNIR and MIR spectra of olivine powders before and after irradiation with different pulse energies and times. (a) Reflectance relative to a standard Spectralon; (b) normalized at 0.85 micron; (c) MIR spectra.

References: [1] Chapman, C. R. (2004) *Ann. Rev. Planet. Sci., 32*, 539-567. [2] Sasaki, S. et al. (2002) *ASS, 29*, 783-788. [3] Yamada M. (1999) *EPS, 51*, 1255-1265.[4] Gaffey, M. J. (2010) *Icarus, 209*, 564-574. [5] Noguchi, T. et al. (2011) *Science, 333*, 1211-1125. [6] Housley R. et al. (1973), *LPSC, vol.4*, pp.2737. [7] Keller L. P. and Mckay D. S. (1997) *GCA, 61*, 2231-2341. [8] Quirantes A. and Bernard S. *(2004) JQRST, 89*, 311-321. [9] Mishchenko M. I. et al. (1999) *JQSRT, 63*, 409-432. [10] Hapke B. (2012) *Cambridge Univ. Press.* [11] Stamnes K. et al. (1988) *Appl. Opt., 27*, 2502-2509.

SIMULATION OF SPACE WEATHERING: INSTRUMENTATIONAL DEVELOPMENT. M. Yesiltas[1], J. Thieme[2], N. Simos[2], and T. D. Glotch[1],· [1]Department of Geosicenes, Stony Brook University, 255 Earth and Space Sciences Building, Stony Brook, NY, 11794-2100. (mehmet.yesiltas@stonybrook.edu), [2] Brookhaven National Laboratory, PO Box 5000 Upton, NY 11973-5000.

Introduction: Surfaces of airless bodies continuously interact with the space environment, and as a result, such surfaces are altered in various ways including chemical and physical alteration [1]. The primary agents of this alteration are solar wind and micrometeorite bombardment, each of which may break molecular bonds, form new molecules, or change elemental composition [2]. For instance, these space weathering processes create nano-phase metallic iron within amorphous silicates [3], which causes their spectral properties to be darkened and/or reddened [4], creating discrepancies between remote sensing data and spectra of laboratory analogs such as meteorites.

Methods: Here we present our experimental design for simulating space weathering in the laboratory and analyzing the spectral and chemical changes in our samples *in situ*. The experiment is being installed at the Brookhaven National Laboratory (BNL), where a sample stage will be placed in a custom-built portable vacuum chamber (Fig. 1). Once at vacuum, the sample chamber will be brought to BNL's Tandem negative ion source for H- irradiation. Each sample will be irradiated with H- ions from 10 to 100 keV to provide a range of ion penetration depths in samples. Throughout the irradiation process, we will acquire VNIR spectra between 350 - 2500 nm using an ASD Fieldspec3 Max spectrometer, which will be coupled to the vacuum chamber.

Figure 1. Model design of the vacuum chamber.

Subsequent to H- ion irradiation and spectral characterization in the infrared, our mineral and meteorite samples will be transported across the BNL campus to the National Synchrotron Light Source II (NSLSII) Sub-micron Resolution X-ray Spectroscopy beamline (SRX). At SRX, both H- irradiated and pristine samples will additionally be irradiated with a nanosecond pulsed laser which allows irradiation between 400 – 2500 nm. Compositional changes will be monitored in real time with VNIR reflectance spectroscopy and synchrotron X-ray spectroscopy. Namely, we will acquire VNIR spectra of each sample after each laser shot, after which we will also interrogate each sample using the SRX beamline to assess changes in sample structure and chemistry at sub-micron scales with high spatial resolution (~50 nm). This information will also help us map the spatial distribution of specific elements present within the samples.

Two agents of space weathering, solar wind sputtering by (and, perhaps, implantation of) hydrogen atoms and micrometeorite bombardment, lead to the maturation of the surfaces of airless bodies. While the former leads to the formation of nanophase metallic iron blobs, the latter leads to the formation of agglutinitic glass and a reduced vapor-deposited coating [3,5,6].

Our high resolution *in-situ* experiments on various minerals and meteorites will help us further understand effects of space weathering due to solar wind and micrometeorite bombardment on the exposed surfaces of airless bodies. We will be able to investigate the structural and geochemical changes associated with space weathering, as the process is occurring, using the SRX beamline of NSLSII in order to conduct detailed X-ray spectroscopy studies of samples at sub-100 nm spatial scales

Acknowledgments: This work is funded by RIS[4]E team of the SSERVI (PI T. Glotch).

References: [1] Bennett et al. (2013) *Chem. Rev.*, 113,9086–9150. [2] Loeffler et al. (2009) *Jornual of Geophy. Res.*, 114, E03003. [3] Noble et al. (2007) *Icarus*, 192, 629-642. [4] Kuhlman et al (2015 *Planetary and Space Science*, 115, 110-114. [5] Hapke, (2001) *J. Geophys. Res.*, 106, 10039-10073. [6] Keller and McKay (1993) *Science* 261, 1305-1307.